ไพรีนิลทรุกซีนสำหรับเป็นวัสดุในไดโอดอินทรีย์เปล่งแสง

นางสาวชมชนก วงศ์ศิลารัตน์

วิทยานิพนธ์นี้เป็นส่วนหนึ่งของการศึกษาตามหลักสูตรปริญญาวิทยาศาสตรมหาบัณฑิต
สาขาวิชาปิโตรเคมีและวิทยาศาสตร์พอลิเมอร์
คณะวิทยาศาสตร์ จุฬาลงกรณ์มหาวิทยาลัย
ปีการศึกษา 2558

PYRENYL TRUXENES AS MATERIALS IN ORGANIC LIGHT-EMITTING DIODES

Miss Chomchanok Wongsilarat

A Thesis Submitted in Partial Fulfillment of the Requirements

for the Degree of Master of Science Program in Petrochemistry and Polymer Science

Faculty of Science

Chulalongkorn University

Academic Year 2015

Thesis Title	PYRENYL TRUXENES AS MATERIALS IN ORGANIC LIGHT-EMITTING DIODES
By	Miss Chomchanok Wongsilarat
Field of Study	Petrochemistry and Polymer Science
Thesis Advisor	Associate Professor Paitoon Rashatasakhon, Ph.D.
Thesis Co-Advisor	Professor Vinich Promarak, Ph.D.

Accepted by the Faculty of Science, Chulalongkorn University in Partial Fulfillment of the Requirements for the Master's Degree

.....Dean of the Faculty of Science
(Associate Professor Polkit Sangvanich, Ph.D.)

THESIS COMMITTEE

.....Chairman
(Assistant Professor Warinthorn Chavasiri, Ph.D.)

.....Thesis Advisor
(Associate Professor Paitoon Rashatasakhon, Ph.D.)

.....Thesis Co-Advisor
(Professor Vinich Promarak, Ph.D.)

.....Examiner
(Associate Professor Nuanphun Chantarasiri, Ph.D.)

.....External Examiner
(Nakorn Niamnont, Ph.D.)

ชมชนก วงศ์ศิลารัตน์ : ไพรีนิลทรุกซีนสำหรับเป็นวัสดุในไดโอดอินทรีย์เปล่งแสง (PYRENYL TRUXENES AS MATERIALS IN ORGANIC LIGHT-EMITTING DIODES) อ.ที่ปรึกษาวิทยานิพนธ์หลัก: รศ. ดร. ไพฑูรย์ รัชตะสาคร, อ.ที่ปรึกษาวิทยานิพนธ์ร่วม: ศ. ดร. วินิช พรมอารักษ์, 72 หน้า.

อนุพันธ์ทรุกซีนชนิดใหม่ที่มีจำนวนหมู่แทนที่ของไดไพรีนิลคาร์บาโซลต่างกันได้ถูกสังเคราะห์ขึ้นโดยปฏิกิริยา C-N ครอสคัปปลิงระหว่างแกนกลางไอโอโดทรุกซีน และไดไพรีนิลคาร์บาโซล โมเลกุลเป้าหมาย (1-3) ที่สังเคราะห์ได้พิสูจน์ทราบเอกลักษณ์ด้วยเทคนิค ^{1}H-NMR, ^{13}C-NMR และ MALDI-TOF mass spectroscopy สารประกอบเหล่านี้คายแสงในช่วงสีฟ้า (ความยาวคลื่นของการคายพลังงานแสงสูงสุด 421 ถึง 423 นาโนเมตร) และมีความเสถียรทางความร้อนที่ดีเยี่ยม (อุณหภูมิการสลายตัวที่ 10% สูงกว่า 440 องศาเซลเซียส) เหมาะสำหรับการประยุกต์ใช้ในอุปกรณ์ทางอิเล็กทรอนิกส์ สารประกอบทั้งหมดถูกนำไปใช้เป็นชั้นสารเรืองแสงและใช้ BCP เป็นชั้นสารบล็อกประจุบวกในอุปกรณ์ไดโอดเรืองแสงอินทรีย์ที่มีโครงสร้างเป็น ITO/PEDOT:PSS/1–3/BCP/LiF:Al อุปกรณ์ที่ได้ทั้งหมดเปล่งแสงในช่วงสีน้ำเงิน ตามมาตรฐานการส่องสว่าง CIE (CIE, x= 0.15, y= 0.10 ถึง 0.19) ด้วยประสิทธิภาพความสว่างสูงเมื่อเทียบกับอุปกรณ์อ้างอิงที่ใช้ NPB ระหว่างโมเลกุลทั้งสาม พบว่าอุปกรณ์ที่ใช้สาร 2 แสดงประสิทธิภาพที่ดีสุด โดยให้ค่าความสว่างสูงสุดอยู่ที่ 8,001 แคนเดลาต่อตารางเมตร ที่ 9.6 โวลต์ และค่าศักย์ไฟฟ้าเริ่มต้นที่ 3.4 โวลต์ นอกจากนี้ยังมีการศึกษาสมบัติการส่งผ่านประจุบวกของสารประกอบเหล่านี้เทียบกับสารมาตรฐานเชิงการค้าNBP ได้ถูกตรวจสอบโดยใช้ Alq_3 เป็นชั้นเปล่งแสงที่มีโครงสร้างเป็น ITO/PEDOT:PSS/1–3/Alq_3/LiF:Al อุปกรณ์ทั้งหมดเปล่งแสงในช่วงสีเขียวของ Alq_3 (ความยาวคลื่นของการคายพลังงานแสงสูงสุด = 512 ถึง 517 นาโนเมตร, CIE 0.26, 0.50) ความสามารถในการส่งผ่านประจุบวกของสารเหล่านี้เทียบเท่ากับ NPB โดยอุปกรณ์ที่ใช้สาร 2 แสดงประสิทธิภาพที่ดีที่สุด ให้ค่าความสว่างสูงสุดอยู่ที่ 44,773 แคนเดลาต่อตารางเมตร ที่ 10.8 โวลต์ และค่าศักย์ไฟฟ้าเริ่มต้น 2.8 โวลต์

สาขาวิชา ปิโตรเคมีและวิทยาศาสตร์พอลิเมอร์ ลายมือชื่อนิสิต .....

ปีการศึกษา 2558 ลายมือชื่อ อ.ที่ปรึกษาหลัก .....

ลายมือชื่อ อ.ที่ปรึกษาร่วม .....

5572244523 : MAJOR PETROCHEMISTRY AND POLYMER SCIENCE
KEYWORDS: TRUXENE / PYRENE / CARBAZOLE / OLED / ELECTROLUMINESCENT

CHOMCHANOK WONGSILARAT: PYRENYL TRUXENES AS MATERIALS IN ORGANIC LIGHT-EMITTING DIODES. ADVISOR: ASSOC. PROF. PAITOON RASHATASAKHON, Ph.D., CO-ADVISOR: PROF. VINICH PROMARAK, Ph.D., 72 pp.

A new series of truxene derivatives with different numbers of dipyrenylcarbazole substituents have been synthesized via C-N cross-coupling. The Cu-catalyzed C-N coupling between the iodinated truxene core and dipyrenylcarbazole thus provides the target molecules (1-3) which are characterized by ^{1}H-NMR, ^{13}C-NMR and MALDI-TOF mass spectroscopy. These compounds emitted in the blue region (l_{em}= 421 to 423 nm) and showed excellent thermal stabilities ($T_d^{10\%}$ above 440°C) suitable for application in optoelectronic devices. All compounds were used as hole-transporting non-doped emitters and BCP as a hole blocking layer in the OLEDs with the structure of ITO/PEDOT:PSS/1–3/BCP/LiF:Al. All devices emitted deep blue color according to the CIE coordinates (CIE, x= 0.15, y= 0.10 to 0.19) with high luminance efficiencies as compared to the reference device using NPB. Among the three materials, compound 2 could give lead to the best device performance with high maximum brightness of 8,001 cd/m^2 at 9.6 V and turn-on voltage (V_{on}) at 3.4 V. In addition, the hole-transport properties of these compounds compared with the commercial standard NPB were investigated using devices configuration of ITO/PEDOT:PSS/1–3/Alq_3/LiF:Al. All devices displayed a bright green emission of Alq_3 (l_{em}= 512 to 517 nm, CIE 0.26, 0.50). Their ability as HTL for green OLEDs was comparable to a common hole-transporter NPB. The device based on 2 exhibited the best performance with highest maximum brightness of 44,773 cd/m^2 at 10.8 V and turn-on voltage (V_{on}) at 2.8 V.

Field of Study:	Petrochemistry and Polymer Science	Student's Signature .....
		Advisor's Signature .....
Academic Year:	2015	Co-Advisor's Signature .....

ACKNOWLEDGEMENTS

First of all, I would like to express my sincere gratitude to my advisor, Associate Professor Dr. Paitoon Rashatasakhon for giving me opportunities, invaluable assistance, excellent guidance and constant encouragement throughout this research. Sincere thanks are also extended to Professor Dr. Vinich Promarak (co-advisor), Professor Mongkol Sukwattanasinitt, Assistant Professor Dr. Anawat Ajavakom, Assistant Professor Dr. Sumrit Wacharasindhu and Dr. Sakulsuk Unarunotai for their generous advice, invaluable guidance and encouragement. Additionally, I am also greatly grateful to Assistant Professor Taweesak Sudyoadsuk and Dr. Narid Prachumrak very much for valuable suggestion on OLED work.

My appreciation is also given to the committee, Assistance Professor Dr. Warinthorn Chavasiri, Associate Professor Dr. Nuanphun Chantarasiri, Dr. Nakorn Niamnont for their kindness, valuable suggestion and recommendations.

I also thank Ms. Pornpat Sam-ang, Ms. Kanokthorn Boonkitpatarakul, Ms. Rungthiwa Arunchai and Mr. Thanachart Techajaroonjit for their traning, helps and suggestions. Moreover, I would like to thank everyone in MAPS group for a great friendship, smile, spirit and their helps.

Finally, I would like to express my thankfulness to my family and my friends for all their support throughout the period of this research.

CONTENTS

Page

Page

Page

LIST OF FIGURES

LIST OF SCHEME

LIST OF TABLES

LIST OF ABBREVIATIONS

A	Ampere
Å	Angstrom
Alq_3	Tris(8-hydroxyquinoline)aluminium
Al	Aluminium
BuBr	Butylbromide
^{o}C	Degree of celsius
cm^2	Square centimeter (s)
Ca	Calcium
Cd	Candela
$CDCl_3$	Dueterated chloroform
$CHCl_3$	Chloroform
CH_2Cl_2	Dichloromethane
CH_3COOH	Acetic acid
CuI	Copper iodide
CV	Cyclic voltammetry
d	Doublet
DMF	Dimethylformamide
DMSO-d_6	Dueterated dimethyl sulfoxide
DSC	Differential scanning colorimeter
EL	Electroluminescent
Em	Emission
EMMs	Emitting materials
EML	Emitting layer
EtOAc	Ethyl acetate
eV	Electron volt
g	Gram (s)
h	Hour (h)
HCl	Hydrochloric acid

HNO_3	Nitric acid
HOMO	Highest occupied molecular orbital
H_2SO_4	Sulfuric acid
HTL	Hole-transporting layer
HBL	Hole-blocking layer
HTMs	Hole-transporting materials
Hz	Hertz
ITO	Indium tin oxide
J	Coupling constant
K_2CO_3	Potassium carbonate
KI	Potassium iodide
KIO_3	Potassium iodate
K_3PO_4	Tripotassium phosphate
LED	Light-emitting diode
lm	Lumen
LiF	Lithium fluoride
LUMO	Lowest unoccupied molecular orbital
Mg	Magnesium
m^2	Square meter (s)
m	Multiplet
mg	Milligram (s)
$MgSO_4$	Magnesium sulfate
min	Minute (s)
mL	Milliliter (s)
mmol	Millimole (s)
M	Molar
MS	Mass spectroscopy
NaH	Sodium hydride
NaOH	Sodium hydroxide
nm	Nanometer (s)
NMR	Nuclear magnetic resonance

OLED	Organic light-emitting diode
$Pd(PPh_3)_4$	Tetrakis(triphenylphosphine) palladium(0)
PL	Photoluminescent
rpm	Revolutions per minute
s	Singlet
sec	second (s)
t	Triplet
Tg	Glass transition temperature
TGA	Thermo gravimetric analysis
TLC	Thin layer chromatography
V	Volt (s)
W	Watt (s)
%	Percent (s)
δ	Chemical shift
ε	Molar absorptivity
λ	Wavelength
μM	Micromolar (s)
°C	Degree Celsius
Φ	Fluorescence quantum yield

CHAPTER I

INTRODUCTION

1.1 Introduction to OLED

An organic light emitting diode (OLED) is a light-emitting diode (LED) in which the emissive electroluminescent layer is a film of organic compounds which emits light under application of an external voltage. This layer of organic semiconductor material is situated between a transparent conducting anode and metallic cathode [1, 2]. When voltage is applied to the device, holes are injected from the anode and electrons from the cathode; transport and radiative recombination of electron hole pairs at the emissive layer result in electroluminescence (EL). OLEDs are used in television screens, computer monitors, small, portable system screens such as mobile phones and PDAs, watches, advertising, information and indication; they can also be used in light sources for general space illumination and in large-area light-emitting elements. Due to their comparatively early stage of development, they typically emit less light per unit area than inorganic solid-state based LED point-light sources.

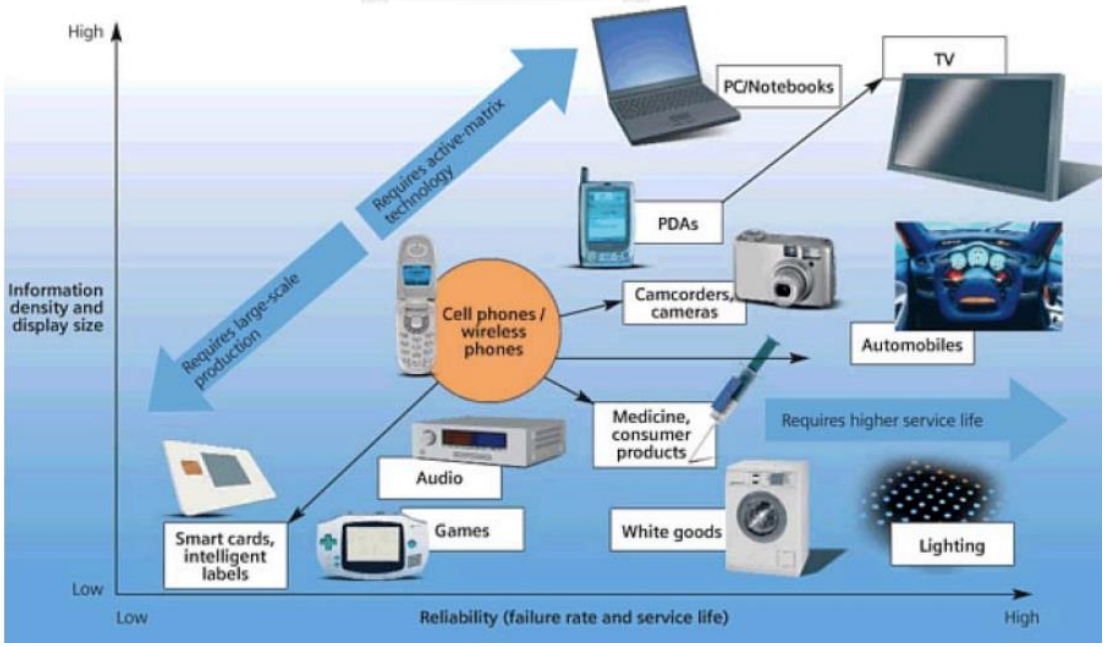

Figure 1.1 OLED Overview

1.2 Advantage and disadvantage of OLEDs

OLEDs are already commercialized for display markets. Currently OLEDs are used to create digital displays with limited size such as mobile phones, MP3 players, PDAs and some digital cameras since they have various advantageous features.

Advantage :

- Self-emission and fast response: Without the use of backlight, light generated
- High resolution: <5um pixel size
- High brightness: ~100,000 cd/m^2 (30,000 ft-L)
- Low voltage: ~3-10 V
- Color-tunable selectivity: Many organic materials to make blue to red light
- Lightweight, thin and flexible devices
- Wide-viewing angle: More than 160 deg.
- Low cost materials and substrates
- Easy fabrication

However, OLEDs have some **disadvantages** due to organic materials are very sensitive to oxygen and water molecules which can degrade the device very fast [3]. Moreover, for small molecular devices have low glass transition temperature (T_g) which affect to the operating temperature cannot exceed the glass transition temperature. Some organic molecules also have low mobility due to amorphous nature [4, 5].

1.3 OLED structure and operation

OLEDs structure and operation are shown in **Figure 1.2**. For the basic structure of OLED is a single-layer, which is consisted of a conductive layer and an emissive layer sandwiched between a transparent conducting anode and metallic cathode.

The typical OLEDs mostly use indium tin oxide (ITO) as the anode due to its relatively high work function and high transparency (90%) to visible light, a wide band gap (Eg = 3.5-4.3 eV) semiconductor. The conductance and transparency of ITO are mostly dependent on the film thickness and composition ratio of two components. When the thickness of ITO increased, the conductance increases but the transparency decreases. So very important parameter is its work function relative to the organic materials [6, 7].

For the cathode, The widely OLEDs use material which low work function metal alloy such as Ca, Mg, Al are used to minimize the energy barrier for electrons injection from low work function of the cathode to the lowest unoccupied molecular orbital (LUMO) level of organic materials. The problem of many low work function metals is extreme reactivity to oxygen and water, hence Ca and Mg should be protected by an additional layer.

During operation, a voltage is applied across the OLED such that electrons are injected from the cathode and the holes are injected from the anode. These injected carriers recombine, form excitons and some of them decay radiatively to give the electroluminescence (EL). Thus, for injection EL the fundamental physical processes include carrier injection, transport, recombination and radiative exciton decay [8]. The color of the light depends on the type of organic molecule and the energy difference of HOMO and LUMO of the emitting organic material.

The way to increase performance of OLED device is to control the recombination of electrons and holes by inserting hole-transporting or/and electron transporting layer between the electrodes to reduce the energy barrier between the electrodes and organic layer for injection of charge to balance the amount of holes and electrons that inject into the emitting layer, called the Multi-layer OLED [1].

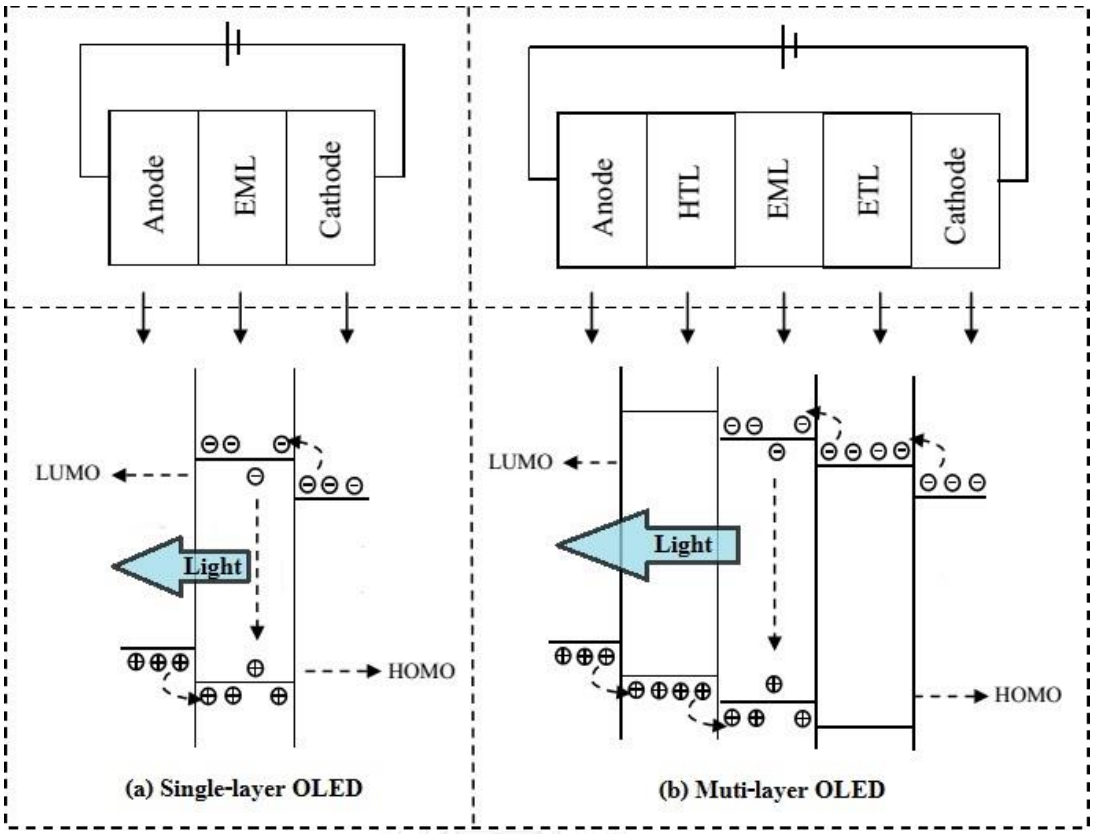

Figure 1.2 Structure (top) and mechanism diagram (bottom) of (a) Single layer OLED and (b) Multi-layer OLED.

1.4 Organic electroluminescent materials

1.4.1 Light-emitting molecular material

First, efficient OLEDs using small molecules were developed by Dr. Ching W. Tang *et al.* at Eastman Kodak.[1] The low molecular weight materials commonly used in OLEDs include organometallic chelates (for example Alq_3, used in the organic light-emitting device reported by Tang *et al.*), fluorescent and phosphorescent dyes and conjugated dendrimers. A number of materials are used for their charge transport properties, for example triphenylamine and derivatives are normally used as hole transport materials [9]. Fluorescent materials can be chosen to get light emission depend on different wavelengths of compounds such as pyrene [10], perylene [11], rubrene [12, 13] and Alq_3 [14, 15] are often used.

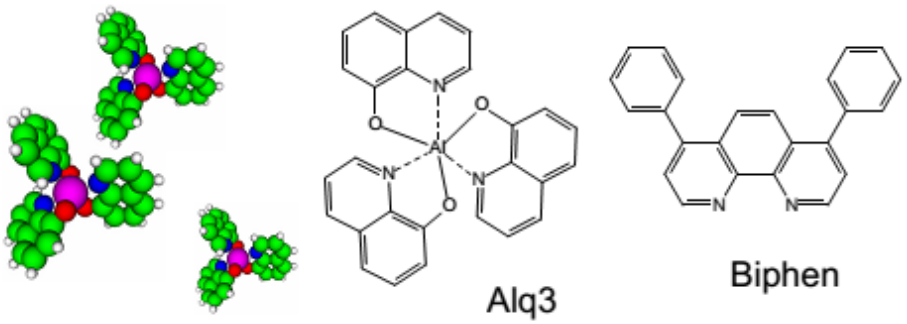

Figure 1.3 Small molecule OLEDs by Tang, van Slyke (Kodak) [16].

1.4.2 Light-emitting polymer

Polymer light-emitting diodes (PLED) or light-emitting polymers (LEP) are an electroluminescent conductive polymer that emits light when connected to an external voltage [17]. One example was the first light-emitting device synthesised by J. H. Burroughes *et al.*, which involved a single layer of poly(p-phenylene vinylene) [18]. They are used as a thin film for full-spectrum color displays. Vacuum deposition is not a suitable technique for forming thin films of polymers. However, polymers can be used solution processing techniques, and spin coating is a common technique of depositing thin polymer films [15, 19]. This technique is more suited to forming large-area films than thermal evaporation. No vacuum is required, and the emissive materials can also be applied on the substrate by a commercial inkjet printing techniques [20].

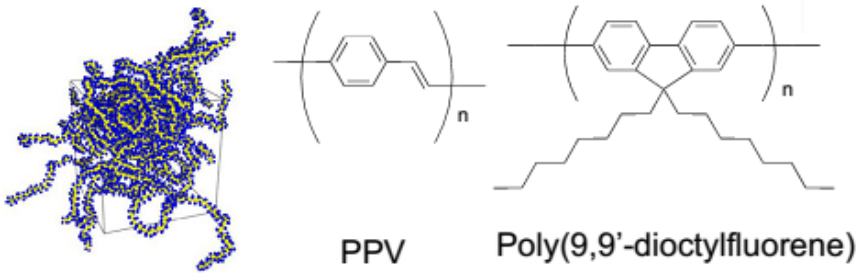

Figure 1.4 Polymer OLEDs by Burroughes, Friend and Bradley (Cambridge) [16].

1.5 Hole-transporting materials (HTMs)

The key functions of HTM are transports holes into EML and trap electron its coming from the cathode inside EML for increasing performance emit light of OLED.

The HTMs should be have an excellent hole-transporting properties or high hole mobility. The typical used p-type materials for HTM are *N,N'*-diphenyl-*N,N'*-bis(3-methyl)-1,1'-biphenyl-4,4'-diamine (TPD) and 4,4'-bis-[*N*-(1-naphthayl)-*N*-phenyl-amino]-biphenyl (NPB) [21, 22] as shown in **Figure 1.5**

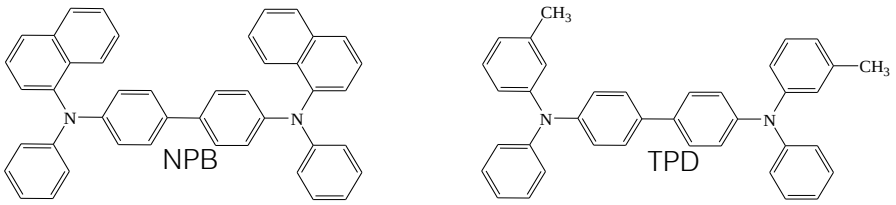

Figure 1.5 Chemical structures of NPB and TPD.

1.6 Emitting materials (EMMs)

The emissive layer materials are made up of organic molecules. Generally, holes are more travel than electrons in organic semiconductors. The decay of the excited state results in a relaxation of the energy levels of the electron, accompanied by emission of radiation whose frequency is in the visible region. The frequency of this radiation depends on the band gap of the material, in this case the difference in energy between the HOMO and the LUMO. The color of the light produced can be varied according to the type of organic molecule used for its process. To obtain color displays, a number of organic layers are used. Another factor of the light produced is its intensity. If more current is applied to the OLED, the brighter the light appears.

Recent development in emissive materials have focused on the blue electroluminescence (EL) as a number of new fluorescent blue light-emitting materials, such as anthracene [23], triphenylfluoranthene [24], fluorene [10], triarylamine [25, 26] and pyrene derivatives [27, 28]. However, pyrene derivatives are more attractive to several their excellent properties, such as high quantum efficiency, charge-transfer ability, and hole-transporting ability [28, 29]. On the other hand, it is well-known that carbazole is a good hole-transporting and electroluminescent group, and many LED materials contain carbazole moieties as the key constructing block

[30]. The exceptional hole-transporting ability of the carbazole-containing derivatives is attributed to the electron donating capabilities of carbazole moieties. Furthermore, the chemical and thermal stabilities of carbazole derivatives are extremely high and the carbazole ring can be easily functionalized at the 3-, 6-, and 9-positions [31-33]. On the other hand, truxene or 10,15-dihydro-5H-diindenol[1, 2-a:10, 20-c]-fluorene is a planar heptacyclic polyarene. It can be formally regarded to as a C3-symmetrically fused fluorene trimer. Because its unique three-dimensional topology which could be comfortably functionalized by different substituents at C-2, -7, -12 positions and at C-5, -10, -15 positions, truxene has been thoroughly developed as an attractive building block and starting material for numerous functional organic materials such as OLEDs [34, 35], fluorescence proves [36, 37], organic solar cells [38] as well as large p-conjugation dendrimer macromolecular [23, 39, 40].

For these reasons, the objectives of this work are following:

(1) To synthesize three novel compounds by a combination of 3,6-Dipyrenylcarbazole units with truxene core as both blue-emitting and hole-transporting materials for OLED.

(2) To characterize and study the electronic, photophysical, electrochemical and thermal properties of target molecules.

(3) To investigate their potential application as both blue-emitting and hole-transporting materials for OLED.

1.7 Literature reviews

This part will survey about applications of carbazole, pyrene and truxene derivatives as the HTMs and EMMs for OLED.

In 2007, Yang et. al. [41], synthesized pyrene derivatives (DP, DPB) as the EMLs for highly efficient OLEDs. The multi-layer devices were fabricated with pyrene derivatives with the structure of ITO/NPB (50 nm)/DP or DPB (30 nm)/BCP (10 nm)/Alq_3 (30 nm)/LiF (1 nm)/Al). The devices created the blue EL emissions with 1931 CIE chromaticity (x = 0.21, y = 0.35) and (x = 0.19, y = 0.25), respectively. The

device base on DPB displays a maximum luminance of 42,445 cd/m^2 at 400 mA/cm^2 and the luminance efficiency of 8.57 cd/A and 5.18 lm/W at 20 mA/cm^2.

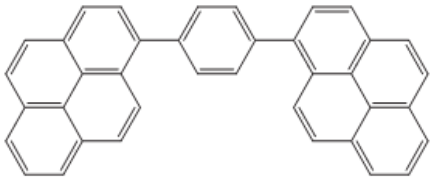

Figure 1.6 Chemical structures of DBD

In the same year, Moorthy and coworkers [42], synthesized the tetraarylpyrenes derivatives **1**-**3** (**Figure 1.7**) as emitting materials in OLEDs. The results indicatied that the attached arene units provide thermal stability and noncrystalline property. After that, they have studied electroluminescence properties of compounds. The devices were fabricated with the structure of ITO/NPB (400 Å)/**1** or **2** or **3** (100 Å)/TPBI (400 Å)/LiF (10 Å)/Al (1500 Å). All devices lead to pure blue electroluminescence according to the CIE coordinates. The device base on **3** showed the best performance, resulting a maximum brightness of 4730 cd/m^2. The maximum brightness efficiency was achieved 2.7 cd/A at a current density of 5.25 mA/cm^2 (6.5 V).

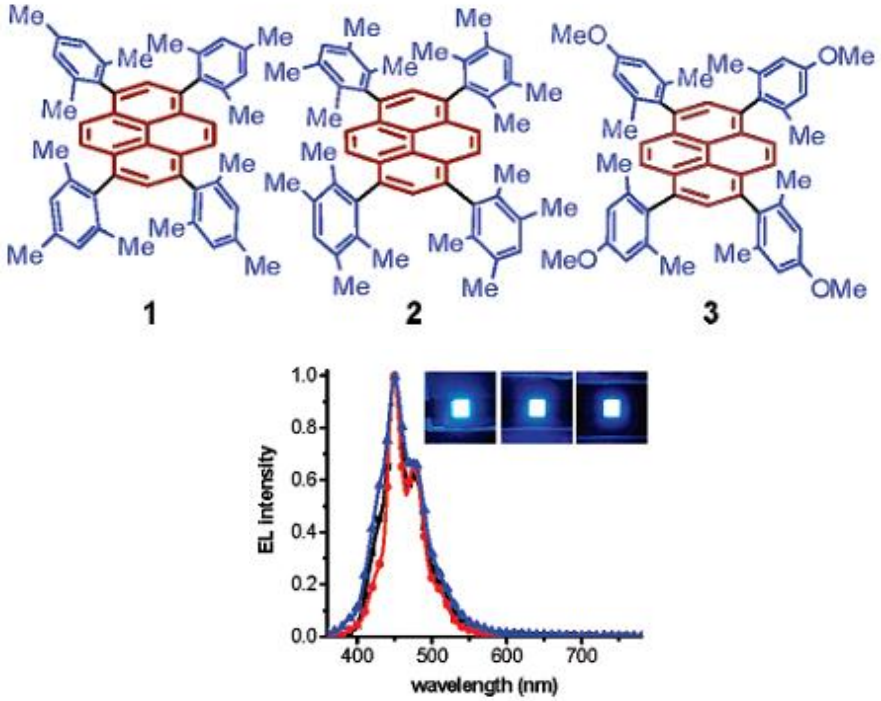

Figure 1.7 Chemical structures of the tetraarylpyrenes derivatives **1**-**3** (Top), EL spectra of OLEDs and their emission colors under applied voltage (Bottom).

In 2009, Yang and his research group [43], synthesized two solution-processable triphenylamine-based dendrimers with truxene core as hole-transporting materials for organic light-emitting diodes; Tr-TPA3 and Tr-TPA9 (**Figure 1.8**). The dendrimers showed excellent solubility in organic solvents, high thermal stability with high *Tg* above 110 $^{\circ}$C and good film forming. Then, they fabricated devices which used these dendrimers as hole-transporting layer and Alq_3 as emitting layer. The device base on Tr-TPA9 exhibited the turn-on voltage of 2.5 V, the maximum luminance of about 11,058 cd/m^2 and the maximum current efficiency of 4.01 cd/A.

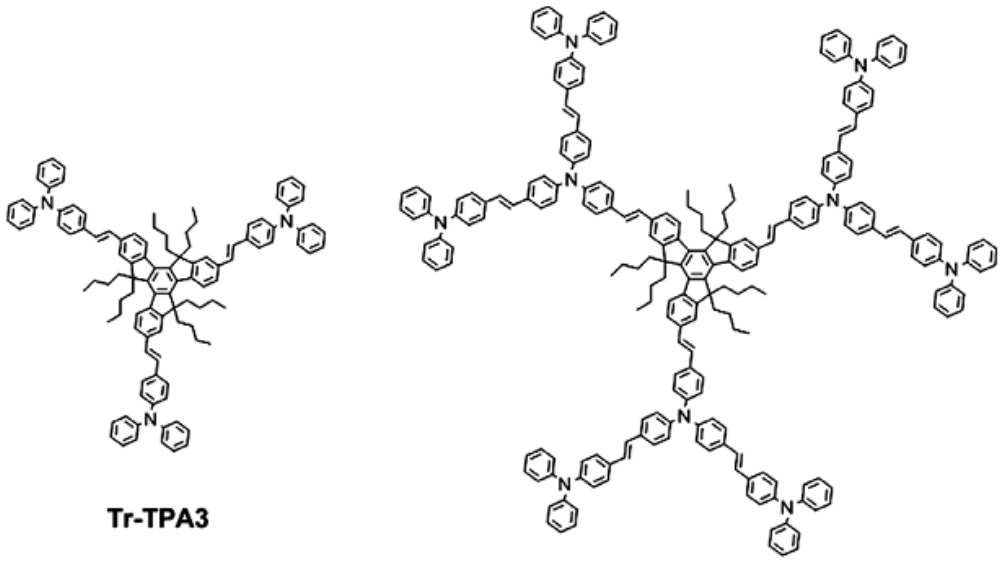

Figure 1.8 Chemical structures of dendrimers.

In 2010, Kumchoo and coworkers [28]. successfully synthesized three derivatives of 3,6-dipyrenylcarbazole (**1**-**3**) as blue light emitting and hole-transporting materials. All compounds displayed the maximum wavelengths absorption at around 345-347 nm. They have excellent thermal stability, showing *Tg* above 160^{o}C. These compounds were used as emissive material in a single-layer OLEDs. Devices base on compound **3** exhibited the best performance, it showed the bright blue emission with maximum brightness (L_{max}) 1,600 cd/m^2 at 8.8 V and a turn-on voltage (V_{on}) of 3.8 V. Then, The devices with the structure of ITO/HTM/Alq_3/LiF/Al were fabricated using compound **1**-**3** as HTL and Alq_3 as EML. This device showed the maximum brightness (L_{max}) of 9,300 cd/m^2 at 8.8 V with a turn-on voltage (V_{on}) of 4.2 V for green OLED.

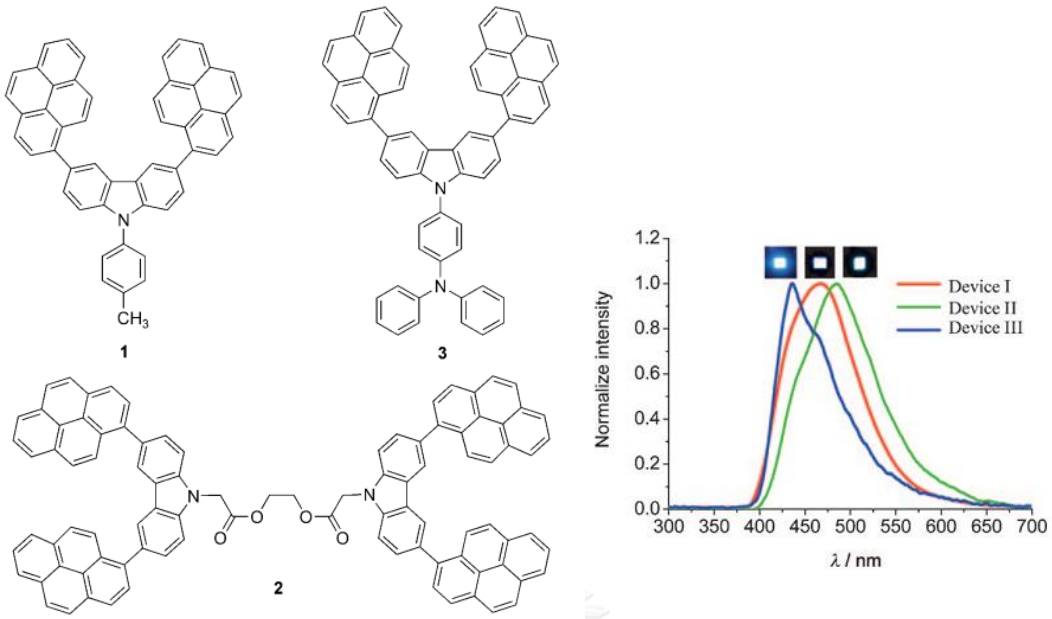

Figure 1.9 Chemical structures of dipyrenylcarbazole derivatives (**1-3**), EL spectra of OLEDs and their emission colors under applied voltage (**1-3** as EMLs).

In 2014, Promarak and coworkers [44], synthesized carbazole dendrimers containing oligoarylfluorene cores as non-doped solution processed "RGB" light-emitters for OLEDs. These dendrimers showed excellent morphologically stable thin films with T_g above 273 ^{o}C. The double-layer OLEDs using these dendrimers as hole-transporting non-doped emitters and BCP as hole-blocking layer (ITO/PEDOT:PSS/1a-ac/BCP/LiF:Al) emit pure RGB colour (EL_{max} = 415, 521 and 622 nm) with high luminance efficiencies (up to 9.21 cd/A).

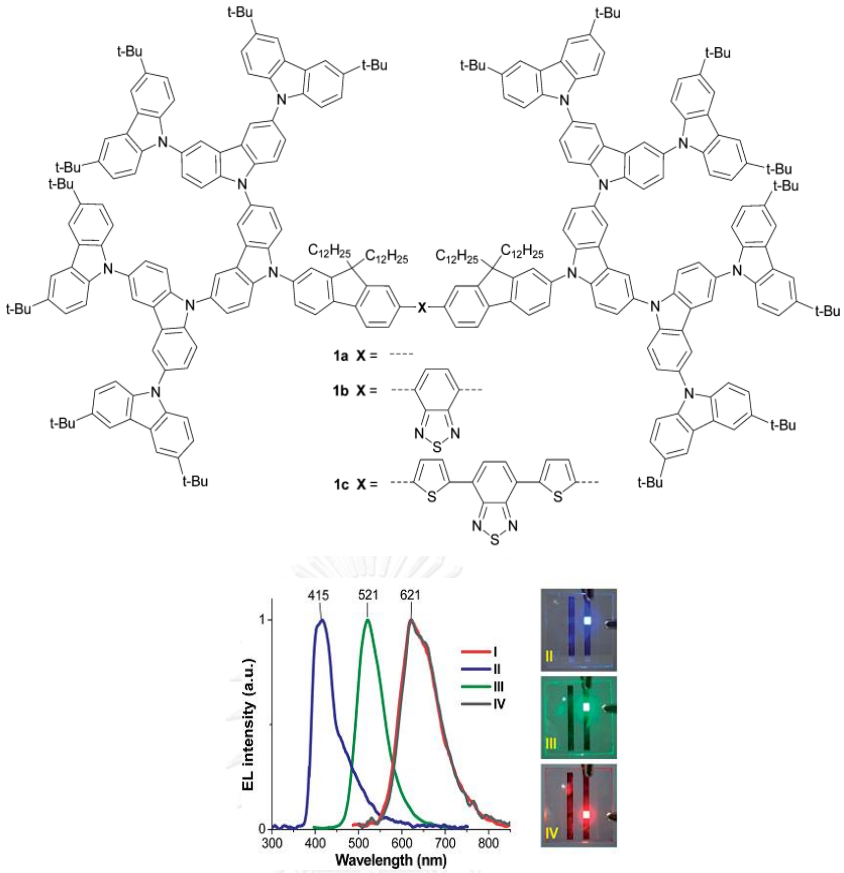

Figure 1.10 Chemical structures of carbazole dendrimers (Top), EL spectra of OLEDs and their emission colors under applied voltage (Bottom).

In 2014, Nguyen and colleagues [45], reported a series of novel HTMs (**3a**–**c**) based on 4-(9*H*-carbazol-9-yl)triphenylamine conjugated with different carbazole or triphenylamine derivatives. The resulting compounds exhibited good morphological and thermal stabilities with high T_g and T_d values. For devices performance, HTM 3c was found to be the best, showing good performance with a low V_{on} of 3.1 V, current and power efficiencies of 39.2 cd/A and 29.3 lm/W, respectively.

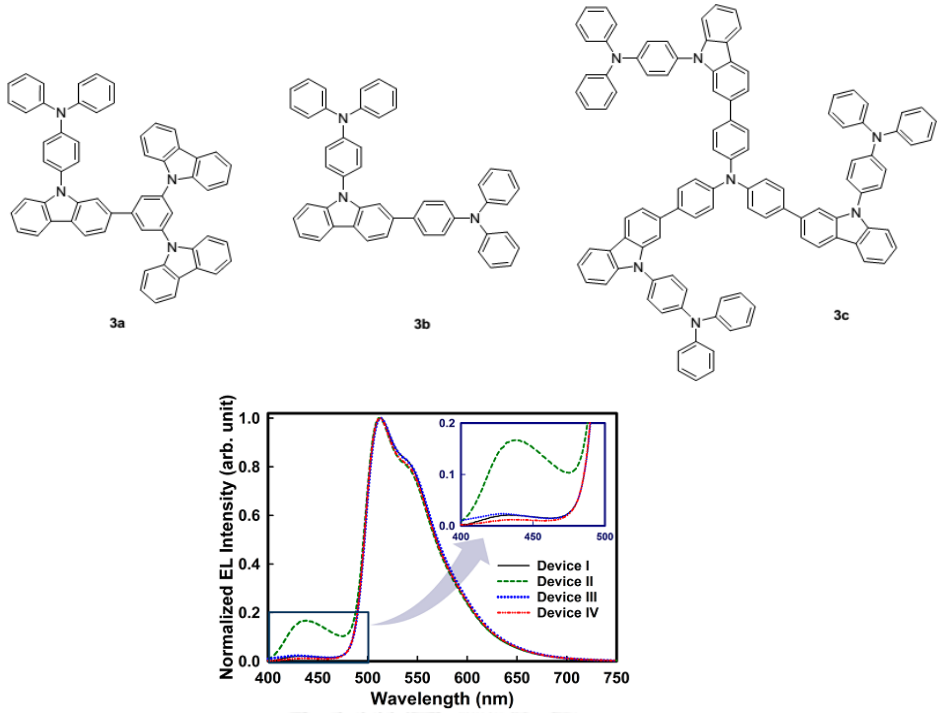

Figure 1.11 Chemical structures of HTMs (Top), EL spectra of OLEDs (Bottom).

In the same year, Chercka et. al. [46], developed a new pyrene based emitter material (**Figure 1.12**) for highly efficient OLEDs. They prepare OLEDs with a doped matrix emissive layer (EL) by using mCPPO1 (9-(3-(9H-carbazole-9-yl) phenyl)-3-(dibromophenylphosphoryl)-9H-carbazole) as host material. The device displays an exceptional deep blue photoluminescence (CIE: x = 0.16, y = 0.024) and good external quantum efficiency (EQE) of 3.1%.

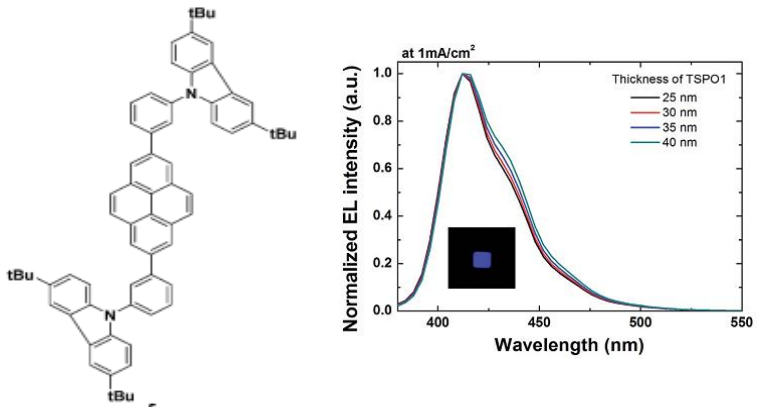

Figure 1.12 Chemical structures of 2,7-functionalized pyrene-based (left), EL spectra of OLEDs (right).

In 2015, Raksasorn and coworkers [40], successfully synthesized two star-shaped carbazolyl truxene derivatives (1 and 2) *via* Cu catalyzed C–N coupling reaction. Both compounds display good thermal stabilities with high T_g at 249 and 293 ^{o}C and the decomposition temperature at 5% weight loss around 392 and 371 ^{o}C, respectively. The devices base on both compounds exhibit good hole-transporting properties as the structure of ITO/PEDOT:PSS/**1** or **2**/Alq3/LiF:Al could provide maximum brightness of 12,000 cd/m^2 with turn-on voltages of 3.1–4.1 V, and maximum external quantum efficiency of 0.89–1.13%

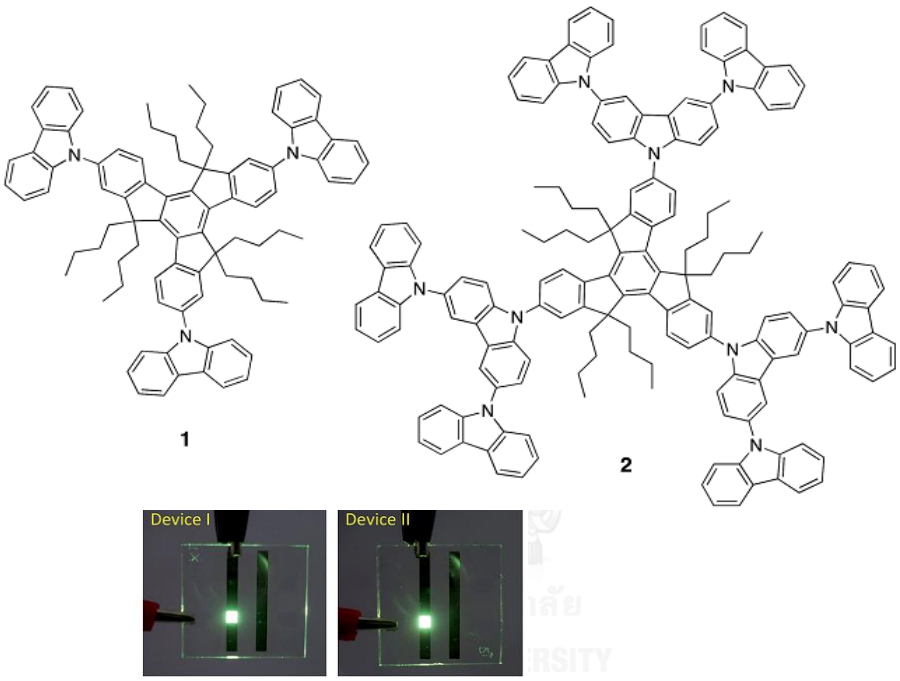

Figure 1.13 Chemical structures of two star-shaped carbazolyl truxene derivatives (**1** and **2**), photographic images of working Device I and II

CHAPTER II

EXPERIMENTAL

2.1 Synthesis

2.1.1 Instruments and Equipment

Thin layer chromatography (TLC) was performed on aluminium sheets precoated with silica gel (Merck Kiesegel 60 F_{254}) (Merck KgaA, Darmstadt, Germany). Column chromatography was performed on silica gel (Merck Kieselgel 60G) (Merck KGaA, Darmstadt, Germany). All ^{1}H-NMR spectra were determined on Varian Mercury NMR spectrophotometer (Varian, USA) at 400 MHz with chemical shifts reported as ppm in $CDCl_3$. The ^{13}C-NMR spectra were measured on Bruker Mercury NMR spectrophotometer (Bruker, Germany) which equipped at 100 MHz with chemical shifts reported as ppm in $CDCl_3$. Mass spectra were recorded on a Microflex MALDI-TOF mass spectrometer (BrukerDaltonics) using doubly recrystallized α- cyano-4-hydroxy cinnamic acid (CCA) as a matrix. Absorption spectra were measured by a ShimadzuUV-2550 UV-Vis spectrophotometer. Fluorescence spectra were obtained from an Agilent technologies Cary Eclipse spectrofluorometer.

The fluorescence quantum yields (Φ) were determined by comparison with a standard of known fluorescence quantum yield according to the following equation [47].

$$\Phi_{\mathrm{x}} = \Phi_{\mathrm{ST}} \left(\frac{Slope_x}{Slope_{ST}}\right)\left(\frac{\eta_x^2}{\eta_{ST}^2}\right)$$

Where the subscripts X refer to the unknown samples and ST refers to the standard quinine sulfate solution in 0.01 M H_2SO_4, which fluorescence quantum yield is known to be 0.54 [47], Ø is the fluorescence quantum yield, *Slope* is the slope from the plot of integrated fluorescence intensity versus absorbance, and η is the refractive index of the solvent. The refractive indexes of $CHCl_3$ and 0.01 M H_2SO_4 were 1.445 and 1.333, respectively. The maximum absorbance of all samples should never exceed 0.1. The fluorescence emission spectra of the same solutions using

appropriate excitation wavelengths selected were recorded based on the maximum absorption wavelength (λ_{max}) of each compound.

The electrochemical analysis by cyclic voltammetry was performed using an AUTOLAB spectrometer. All measurements were made at room temperature on sample solutions in freshly distilled dichloromethane with 0.1 M tetrabutylammomium hexafluorophosphate ($TBAPF_6$) as electrolyte. A platinum working electrode, a platinum wire counter electrode and a $Ag/AgNO_3$ (Sat.) reference electrode were used in all cyclic voltammetry experiments.

Thermal properties, Differential Scanning Calorimeter (DSC) results were performed on NETZSCH DSC 204F1 and Thermogravimetric Analysis (TGA) results were studied using NETZSCH TG 209F3.

2.1.2 Synthetic procedures

3,6-Diiodo-9H-carbazole (4)

A stirred solution of carbazole (5.0 g, 29.90 mmol) in acetic acid was added potassium iodide (6.7 g, 40.36 mmol). Then, potassium iodate (9.7 g, 45.32 mmol) was added in small portions over a period of 5 min and the resulting mixture was refluxed for 20 min. The reaction was allowed to cool to room temperature and diluted with EtOAc. The combined organic layer was dried over $MgSO_4$ filtered, and concentrated under reduced pressure to give a brown solid residue. The crude product was purified by recrystallization from acetone and hexane to yield **4** as light brown crystals (12.38 g, 98.8%).^{1}H NMR (400 MHz, DMSO) δ 11.57 (s, 1H), 8.57 (s, 2H), 7.66 (d, *J* = 7.6 Hz, 2H), 7.36 (d, *J* = 7.3 Hz, 2H) ppm. [28, 40]

3,6-Di(pyren-1-yl)-9H-carbazole (5)

A mixture of **4** (1.4 g, 3.3 mmol), pyrene-1-boronic acid (2.0 g, 8.1 mmol), $Pd(PPh_3)_4$, 2 M K_2CO_3 aqueous solution was heated refluxing in THF conditions for 24 h. After the reaction was cooled to room temperature, the resulting brown solution was extracted with CH_2Cl_2 (3 x 50 ml). The combined organic layer was dried over $MgSO_4$, filtered, and concentrated under reduced pressure. The crude product was purified by flash chromatography using hexane: CH_2Cl_2 (75:25) as the eluent to yield

5 as pale green solid (1.23 g, 66%). ^{1}H NMR (400 MHz, DMSO) δ 11.72 (s, 1H), 8.50 (s, 2H), 8.36 (d, *J* = 8.3 Hz, 2H), 8.30 – 8.12 (m, 14H), 8.06 (t, *J* = 8.0 Hz, 2H), 7.80 (d, *J* = 7.8 Hz, 2H), 7.70 (d, *J* = 7.7 Hz, 2H) ppm. MALDI-TOF MS: $C_{44}H_{25}N$ found 567.004 ($[M]^+$ calcd: 567.198). [28]

10,15dihyhro-5H-diindeno[1,2-a:1',2'-c] fluorene (Truxene) (6)

3-Phenylpropionic acid (10.02 g, 66.72 mmol) was mixed with polyphosphoric acid (50 g) and heated at 60 °C for 30-40 min in nitrogen atmosphere. Then, water (5 mL) was added to the reaction and temperature was raised to 160 °C for 3 h. After the reaction was cooled to room temperature, the mixture was poured into ice water and grey powder was filtered off under suction and washed with water. The residue was recrystallized from toluene to yield **6** as light-yellow power (11.12 g, 49%). ^{1}H NMR (400 MHz, $CDCl_3$) δ 7.93 (d, *J* = 7.9 Hz, 1H), 7.68 (d, *J* = 7.6 Hz, 1H), 7.49 (d, *J* = 7.5 Hz, 1H), 7.40 (d, *J* = 7.4 Hz, 1H), 4.22 (s, 2H) ppm. [39, 40, 48]

5,5,10,10,15,15-Hexabutyl-truxene (7)

A solution of truxene (**6**) (1.00 g, 2.92 mmol) in DMF (50 mL) at 0 °C under nitrogen, NaH (1.19 g, 29.8 mmol) was added and the solution was allowed to warm to room temperature and stirred for 30 min, then n-butyl bromide (3.2 mL) was added for 24 h. The mixture was poured into water and extracted with EtOAc. The combined organic layer was dried over $MgSO_4$, filtered, and concentrated under reduce pressure. The crude product was purified by silica gel column chromatography using hexane as the eluent to yield **7** as white solid (1.48 g, 75%). ^{1}H NMR (400 MHz, $CDCl_3$) δ 8.38 (d, *J* = 7.3 Hz, 1H), 7.46 (m, 2H), 7.38 (m, 2H), 3.04 – 2.91 (m, 2H), 2.15 – 2.04 (m, 2H), 0.96 – 0.79 (m, 4H), 0.62 – 0.36 (m, 10H) ppm. [37]

General synthesis and characterization of compound 8, 9 and 10

A mixture of truxene (**7**) and solvent (CH_3COOH:H_2SO_4:H_2O:CCl_4) = 100:5:20:8) was heated to 40 °C. After adding KIO_3 and I_2 to the mixture, the mixture was heated to 80 °C and stirred for 4 h at this temperature. After the reaction was completed, the mixture was cooled to room temperature and filtered off under suction, washed with water. Then the residue refluxed in methanol for 2h and followed by cooling to room temperature, filtered off under suction [48, 49].

5,5,10,10,15,15-Hexabutyl-2-iodo-truxene (8)

According to above general procedure, **8** was synthesized from **7** (0.50 g, 0.73 mmol), KIO_3 (0.05 g, 0.24 mmol) and I_2 (0.06 g, 0.24 mmol) to provide **8** (0.41 g, 68% yield) as white solid. ^{1}H NMR (400 MHz, $CDCl_3$) δ 8.4-8.3 (m, 2H), 8.14 - 8.04 (d, *J* = 8.5 Hz, 1H), 7.77 (s, 1H), 7.75 - 7.68 (d, *J* = 8.2 Hz, 1H), 7.49 - 7.42 (m, 2H), 7.43 - 7.32 (m, 4H), 3.05 - 2.78 (m, 6H), 2.1 - 1.95 (m, 6H), 0.98 - 0.8 (m, 12H), 0.62 - 0.34 (m, 30H) ppm.

5,5,10,10,15,15-Hexabutyl-2,7-diiodo-truxene (9)

According to above general procedure, **9** was synthesized from **7** (0.20 g, 0.294 mmol), KIO_3 (0.04 g, 0.19 mmol) and I_2 (0.05 g, 0.19 mmol) to provide **9** (0.17 g, 64% yield) as white solid. ^{1}H NMR (400 MHz, $CDCl_3$) δ 8.4-8.3 (m, 1H), 8.14-7.97 (d, *J* = 8.5 Hz, 2H), 7.77 (s, 2H), 7.73 - 7.61 (d, *J* = 8.2 Hz, 2H), 7.50 - 7.42 (m, 1H), 7.43 - 7.29 (m, 2H), 3.03 - 2.28 (m, 6H), 2.13 - 1.90 (m, 6H), 1.03 - 0.68 (m, 12H), 0.61 - 0.20 (m, 30H) ppm.

5,5,10,10,15,15-hexabutyl-2,7,12-triiodo-truxene(10)

According to above general procedure, **10** was synthesized from **7** (0.5 g, 0.73 mmol), KIO_3 (0.16 g, 0.75 mmol) and I_2 (0.55 g, 2.16 mmol) to provide **10** (93% yield) as white solid. ^{1}H NMR ($CDCl_3$): δ 8.07 (d, *J* = 8.4 Hz, 1H), 7.76 (s, 1H), 7.71 (d, *J* = 8.4 Hz, 1H), 2.91 – 2.77 (m, 2H), 2.08 – 1.95 (m, 2H), 0.99 – 0.78 (m, 4H), 0.59 – 0.30 (m, 10H) ppm.

General synthesis and characterization of compound 1, 2 and 3

The iodinated truxene, dipyrenylcarbazole, 1 mol% CuI, 10 mol% diamine ligand and K_3PO_4 in dioxane (1 M) at 110°C for 24 h. The resulting light yellowish green mixture was allowed to cool to room temperature and extracted with CH_2Cl_2 (3 × 50 mL). The combined organic layer was dried over $MgSO_4$, filtered, and concentrated under reduce pressure. The crude product was purified by column chromatography on silica gel, eluting with hexane/CH_2Cl_2 to provide the products [50].

Compound 1

According to above general procedure, **1** was synthesized from **8** (0.15 g, 0.18 mmol) and **5** (0.13 g, 0.22 mmol) purified by column chromatography using hexane:CH_2Cl_2 (90:10) as the eluent to obatain **1** as white solid (0.96 g 43% yield). ^{1}H NMR (400 MHz, $CDCl_3$) δ 8.72 - 8.67 (d, *J* = 8.7 Hz, 1H), 8.53 - 8.50 (s, 2H), 8.45 – 8.39 (m, 2H), 8.39 – 8.35 (d, *J* = 8.4 Hz, 2H), 8.30 – 8.25 (d, *J* = 8.3 Hz, 2H), 8.22 – 8.19 (s, 2H), 8.19 – 7.97 (m, 14H), 7.93 – 7.87 (s, 1H), 7.85-7.79 (m, 5H), 7.55 – 7.40 (m, 6H), 3.20 – 2.90 (m, 6H), 2.29 - 2.00 (m, 6H), 1.15 - 0.82 (m, 18H), 0.70 - 0.50 (m, 24H) ppm. ^{13}C NMR (100 MHz, $CDCl_3$) δ 158.8, 155.8, 153.6, 153.4, 145.4, 145.0, 144.9, 140.7, 140.13, 140.09, 140.04, 139.96, 139.7, 138.7, 138.5, 138.3, 137.54, 137.51, 135.7, 133.2, 131.4, 130.9, 130.3, 129.0, 128.8, 128.0, 127.34, 127.26, 127.1, 126.5, 126.0, 125.8, 125.5, 125.0, 124.8, 124.7, 124.6, 124.5, 124.4, 123.6, 122.3, 122.2, 120.6, 109.8, 55.9, 55.5, 36.7, 36.5, 29.5, 26.6, 26.5, 26.4, 22.8, 22.7, 13.72, 13.66 ppm. MALDI-TOF MS: $C_{95}H_{89}N$ found 1244.909 ($[M]^+$ calcd: 1244.702)

Compound 2

According to above general procedure, **2** was synthesized from **9** (0.15 g, 0.16 mmol) and **5** (0.27 g, 0.48 mmol) purified by column chromatography using hexane:CH_2Cl_2 (85:15) as the eluent to obatain **2** as white solid (0.109 g, 38% yield). ^{1}H NMR (400 MHz, $CDCl_3$) δ 8.75 - 8.69 (m, 2H), 8.55 - 8.50 (s, 4H), 8.50 – 8.45 (d, *J* = 8.4 Hz, 1H), 8.40 -8.35 (m, 4H), 8.30 – 8.25 (d, *J* = 8.3 Hz, 4H), 8.23 - 8.19 (s, 2H), 8.19 – 7.98 (m,

28H), 7.97 – 7.93 (d, *J* = 7.9 Hz, 2H), 7.90 - 7.81 (m, 10H), 7.59 – 7.43 (m, 3H), 3.25 – 3.06 (m, 6H), 2.43 – 2.28 (m, 6H), 1.12 – 0.80 (m, 18H), 0.70 – 0.55 (m, 24H) ppm. ^{13}C NMR (100 MHz, $CDCl_3$) δ 156.2, 156.0, 153.7, 145.9, 145.8, 145.5, 141.0, 140.2, 139.8, 139.7, 139.3, 138.6, 138.2, 138.1, 136.3, 133.7, 133.6, 131.8, 131.3, 130.6, 129.3, 129.1, 128.3, 127.7, 127.6, 127.4, 127.0, 126.5, 126.3, 126.1, 125.8, 125.3, 125.2, 124.9, 124.8, 124.0, 122.7, 121.0, 110.1, 56.31, 56.27, 56.0, 37.0, 36.8, 32.1, 29.9, 29.5, 27.0, 26.9, 26.8, 23.2, 23.1, 22.8, 14.3, 14.2, 14.1 ppm. MALDI-TOF MS: $C_{139}H_{112}N_2$ found 1809.868 ($[M]^+$ calcd: 1809.885)

Compound 3

According to above general procedure, **3** was synthesized from **10** (0.15 g, 0.14 mmol) and **5** (0.6 g, 0.99 mmol) purified by column chromatography using hexane:CH_2Cl_2 (75:25) as the eluent to obatain **3** as white solid (0.079 g, 24% yield). ^{1}H NMR (400 MHz, $CDCl_3$) δ 8.80 - 8.75 (d, *J* = 8.7 Hz, 3H), 8.55 - 8.50 (s, 6H), 8.40 – 8.35 (d, *J* = 8.3 Hz, 6H), 8.32 - 8.25 (d, *J* = 8.2 Hz, 6H), 8.22 – 8.19 (s, 3H), 8.19 – 7.98 (m, 42H), 7.90 – 7.87 (d, *J* = 7.9 Hz, 3H), 7.83 -7.79 (m, 12H), 3.30 – 3.15 (m, 6H), 2.45 – 2.35 (m, 6H), 1.20 – 1.15 (m, 18H), 0.95 – 0.55 (m, 24H) ppm. ^{13}C NMR (100 MHz, $CDCl_3$) δ 156.1, 146.0, 141.0, 139.6, 138.6, 136.5, 133.7, 131.7, 131.3, 130.6, 129.3, 129.1, 128.3, 127.7, 127.6, 127.5, 126.2, 125.8, 125.3, 125.2, 124.9, 124.8, 124.1, 122.7, 110.1, 56.4, 37.0, 27.1, 23.2, 14.2 ppm. MALDI-TOF MS: $C_{183}H_{135}N_3$ found 2377.723 ($[M]^+$ calcd: 2375.069)

2.2 OLED device fabrication section

2.2.1 Commercially available materials

The commercial sources and purities of materials used in these experiments are shown in **Table 2.1**. All materials were analytical grade and used without further purification, unless indicated.

Table 2.1 Commercially available materials for OLED device fabrication

Materials	Purity (%)	Company
1″ × 1″ Indium oxide doped tin oxide (99.3 wt % In_2O_3:0.7 wt % SnO_2)-coated glasses (5-15 Ω/sq)	99.5	Kintec
Poly(3,4-ethylenedioxythiophene)–poly(styrene) (0.5 wt % PEDOT: 0.5 wt % PSS)	1.3	Baytron
2,9-dimethyl-4,7-diphenyl-1,10-phenanthroline (BCP)	99.99	Sigma-Aldrich
Tris(8-hydroxyl-quinoline) aluminum (Alq_3)	98	Sigma-Aldrich
N,N-diphenyl-*N,N'*-bis(1-naphthyl)-(1,1'-biphenyl)-4,4'-diamine (NPB)	99	Sigma-Aldrich
Lithium fluoride (LiF)	99.98	ACROS
Aluminium (Al) wire	99.97	BDH

2.2.2 Reagents

The reagents were obtained from various suppliers as shown in **Table 2.2**. All reagents were analytical grade and used without further purification, unless indicated.

Table 2.2. List of reagents.

Reagents	Purity (%)	Company
Hydrochloric acid (HCl) 37%	36.5	Carlo Erba
Nitric acid (HNO_3) 69%	68.5-69.5	BDH
Sodium hydroxide (NaOH)	99.99	Carlo Erba
Acetone	99.5	BDH

2.2.3 Instruments

The following instruments were used in this study:

(1) Photoluminescence (PL) spectrophotometer (Perkin–Elmer, Model LS 50B)

(2) Spin-coater (Chemat Technology, Model KW-4A)

(3) Thermal evaporator (ANS Technology, Model ES280)

(4) Digital source meter (Keithley, Model 2400)

(5) Multifunction optical meter (Newport, Model 1835-C)

(6) Calibrated photodiode (Newport, Model 818 UVCM)

(7) USB Spectrofluorometer (Ocean Optics, Model USB4000FL)

2.2.4 Organic thin film preparation and characterization

The preparation process of organic thin films is described in **Figure 2.1**.

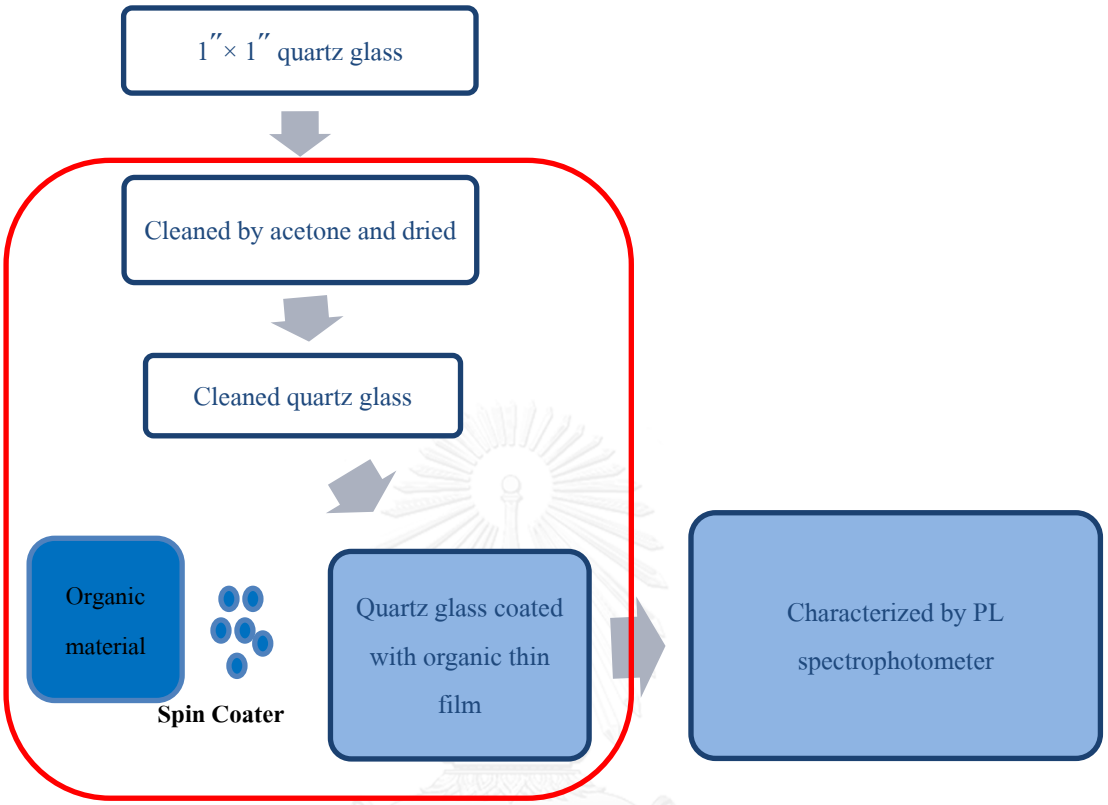

Figure 2.1 Preparation and characterization of organic thin film

2.2.5 Thermal evaporation of the organic thin film

In order to study the photophysical properties of solid state materials, organic thin films coating on quartz glass substrates (1” x 1”) were prepared by spin coater. Prior to film deposition, the substrates were cleaned with acetone in ultrasonic bath followed by drying on a hotplate. The organic material was dissolved in the solution of $CHCl_3$:toluene (2:1 %v/v) and then filtered through a 0.45 μm pore size nylon filter (Orange scientific) and spin-coated onto a cleaned quartz glass surface at 2500 rpm for 30 sec. Finally, the quartz glass coated with the organic film was baked at 100 °C for 10 min.

2.2.6 OLED device fabrication

The OLEDs fabrication process is described in **Figure 2.2**.

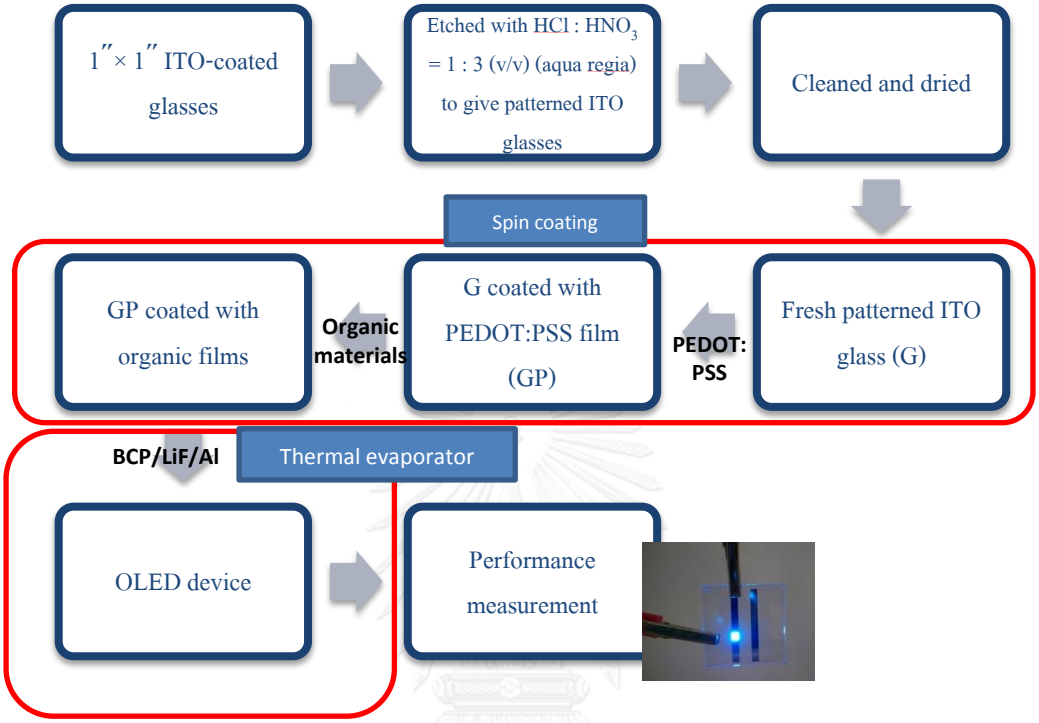

Figure 2.2 Fabrication and measurement of OLED

2.2.7 Patterning process for ITO-coated glasses

The ITO-coated glasses (**Figure 2.3a**) were firstly etched to give a pattern of ITO sheet on glass. Prior to the patterning process, the ITO sheet on glass was covered with a 2 x 10 mm of negative dry film photo resist. The covered ITO glass (**Figure 2.3b**) was immersed in the solution of $HCl:HNO_3$ (1:3 v/v) (aqua regia) for 10 min, with stirring during the etching process. The etched ITO glass was cleaned by thoroughly rinsing with water and subsequently soaking in 0.5 M NaOH for 10 min to remove the negative dry film from an ITO-coated glass surface. Finally, these substrates were thoroughly rinsed with water to give the patterned ITO glasses as shown in **Figure 2.3c**.

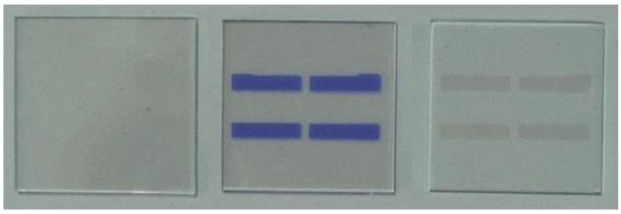

Figure 2.3 (a) ITO-coated glass, (b) ITO-coated glass covered with 2 x 10 mm of negative dry film photo resist and (c) patterned ITO glass

2.2.8 Cleaning process for the patterned ITO glasses

The cleanliness of the ITO surface was an important factor in the performance of the OLEDs devices. The patterned ITO glasses were cleaned for 10 min with detergent in ultrasonic bath followed by a thorough rinse with DI water and then ultra-sonicated in acetone for 10 min. Finally, the substrates were dried in vacuum oven at 100 $^{\circ}$C to give fresh patterned ITO glasses.

2.2.9 Spin-coating method of PEDOT:PSS

A PEDOT:PSS solution was diluted with DI water and stirred for 1 day. The spin-coating method was performed on a spin coater as shown in **Figure 2.4**. The diluted PEDOT:PSS solution was filtered through a 0.45 μm pore size nylon filter (Orange scientific) and spin-coated onto a fresh patterned ITO glass surface at 3000 rpm for 30 second. Finally, the patterned ITO glass coated with the PEDOT:PSS film was baked at 120°C for 15 min for curing.

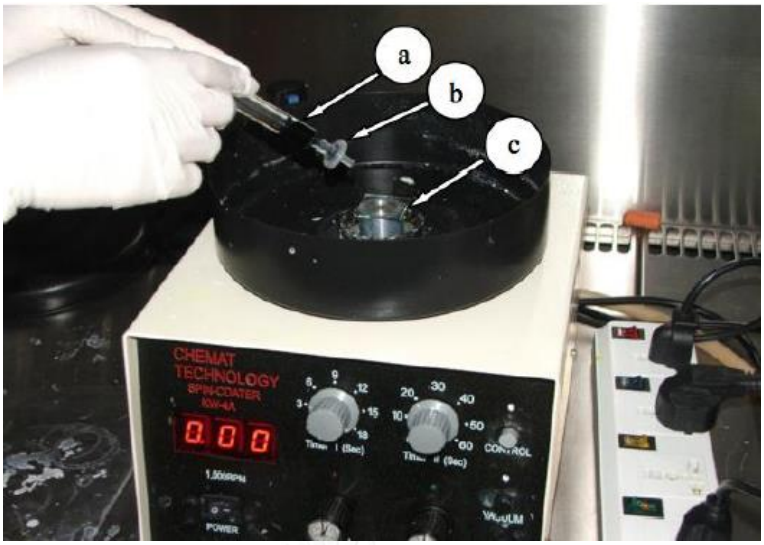

Figure 2.4 Spin-coating method by using a spin coater. (a) PEDOT:PSS solution in the syringe, (b) nylon filter, and (c) fresh patterned ITO glass.

2.2.10 Organic thin film deposition

The deposition of other organic layers was the next step in the fabrication of OLEDs. The organic layers were deposited using spin coating method (**Figure 2.4**) with the same procedure described in section 2.2.5. Prior to the deposition, the patterned ITO glass coated with PEDOT:PSS film was placed on a substrate holder. The organic material was dissolved in the solution of $CHCl_3$:toluene (2:1) and then filtered through a 0.45 μm pore size nylon filter (Orange scientific) and spin-coated onto a patterned ITO glass coated with PEDOT:PSS film surface at 3000 rpm for 30 sec. Finally, the ITO glass coated with the organic film was baked at 100°C for 10 min.

2.2.11 Hole-blocking and cathode deposition**.**

After organic thin film deposition by the technique of spin coating, the next step is increasing hole-blocking layer before closing with cathode deposition. 2,9-dimethyl-4,7-diphenyl-1,10-phenanthroline (BCP) was evaporated from a tungsten boat to deposit at the device. Finally, an ultra thin LiF layer and Al cathode contact were sequentially co-evaporated from two tungsten boats through a shadow mask (**Figure 2.5**) with 2 mm wide slits arranged perpendicularly to the ITO fingers, to

obtain the OLED with an active area of 2 × 2 mm^2 (**Figure 2.6**). The operating vacuum for evaporation of this cathode was under 1 × 10^{-5} mbar at high evaporation rates of 5 – 10 Å/sec. The thickness of LiF and Al of all devices were 0.5 and 150 nm, respectively.

Figure 2.5 Instrument for cathode deposition. (a) tungsten boats and (b) 2 mm wide fingers of a shadow mask.

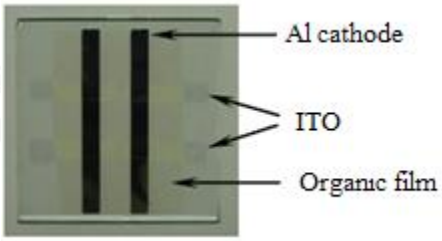

Figure 2.6 OLED device with 4 pixels. A pixel active area of a device is 2 x 2 mm^2.

2.2.12 Device measurement

The instruments for OLED device measurements are shown in **Figure 2.7**. The computer was used for controlling of the digital source meter, the multifunction optical meter and the USB spectrofluorometer as well as recording the data. The digital source meter applied the voltages to the device and measured the resulting currents. The multifunction optical meter connected with the calibrated photodiode

served in the measurement of the luminance (brightness). The USB spectrofluorometer was used for the EL spectra acquisition.

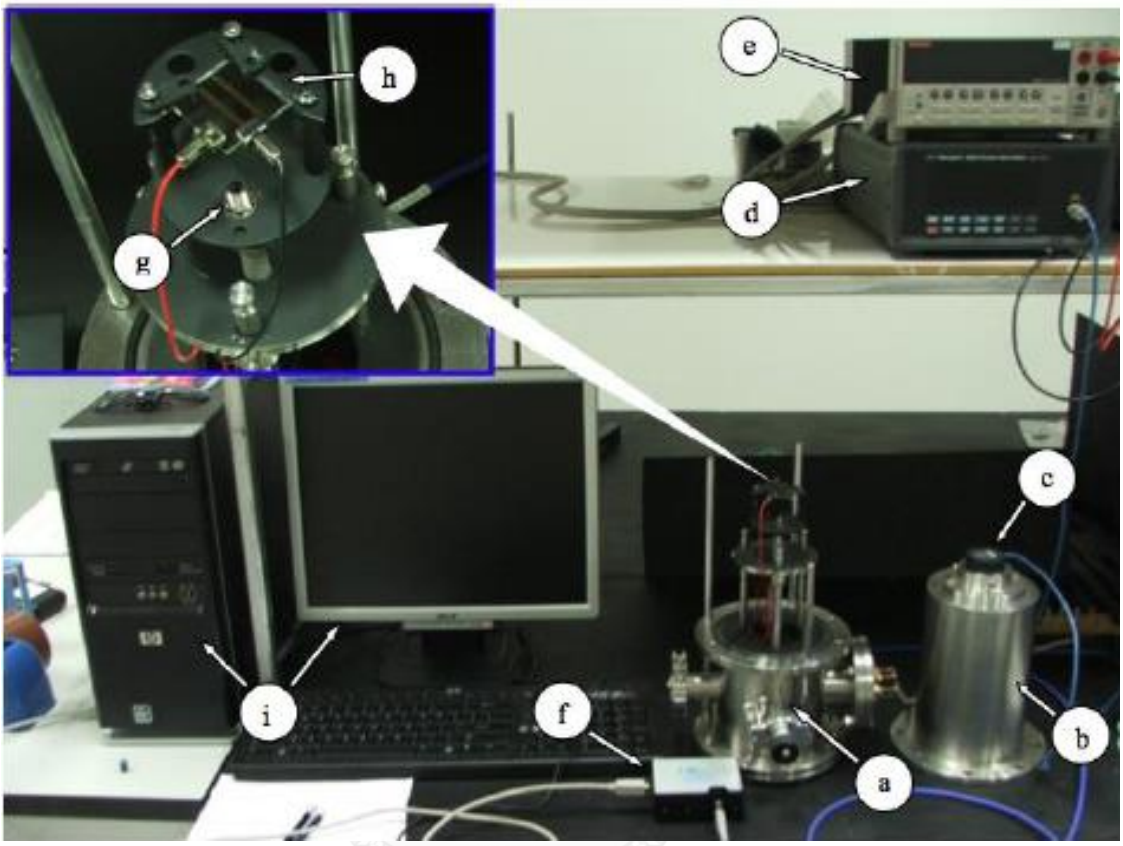

Figure 2.7 Instruments for determination of OLED device performance: (a) OLED test box, (b) lid of OLED test box, (c) calibrated photodiode, (d) multifunction optical meter, (e) digital source meter, (f) USB spectrofluorometer, (g) probe of USB spectrofluorometer, (h) OLED device holder, (i) computer controller and recorder for digital source meter, multifunction optical meter and USB spectrofluorometer.

All device measurements were performed in an OLED test box by blocking the incident light at room temperature under ambient atmosphere. When voltages were applied, the currents, brightness, and EL spectra were recorded at the same time to give the current density–voltage–luminance (*J-V-L*) characteristics and EL spectra. The turn-on voltage was defined at the brightness of 1 cd/m^2. The current density was calculated as the following formula (1):

$$J = \frac{I}{A} \quad (1)$$

Here, I (mA) is the current and *A* (cm^2) is the pixel active area of the device. The luminous efficiency of the device was calculated as the following formula (2):

$$\eta_{lum} = \frac{L}{J} \quad (2)$$

Here, L (cd/m^2) is the luminance and *J* (mA/cm^2) is the current density..

Power Efficiency

The luminous efficacy or power efficiency is the lumen output per input electrical power of the device. It is measured in lumen per watt (lm/W) or candela per ampere (cd/A). It is represented by η_p.

The coordinate value calculation of Commission Internationale de l'Eclairage 1931 (CIE 1931)

The coordinate value of CIE 1931 was calculated from the EL spectrum. In the study of the perception of color, one of the first mathematically defind color space was the CIE 1931 XYZ color space, crated by the International Commission on Illumination (CIE) in 1931 [51, 52]. The CIE XYZ color space was derived from a series of experiments done in the late 1920s by Wright [53] and Guild [54]. Their experimental results were combined into the specification of the CIE RGB color space, from which the CIE XYZ color space was derived. Firstly, the tristimulus value was calculated as the following formula (3):

$$X = 683\int_{360}^{830} S(\lambda)\,\bar{x}(\lambda)\Delta(\lambda), Y = 683\int_{360}^{830} S(\lambda)\,\bar{y}(\lambda)\Delta(\lambda), Z = 683\int_{360}^{830} S(\lambda)\,\bar{z}(\lambda)\Delta(\lambda) \quad (3)$$

Here, S(λ) is the spectral data; Z, Y, and Z are the tristimulus values; and $\bar{x}$, $\bar{y}$, $\bar{z}$ $\bar{x}$are the tyistimulus functions.

The coordinate value of CIE 1931 was calculated from formula (4):

$$\text{CIE 1931 } x = \frac{X}{X+Y+Z}, \text{CIE 1931 } y = \frac{Y}{X+Y+Z} \quad (4)$$

The CIE 1931 chromaticity is shown in **Figure 2.8**

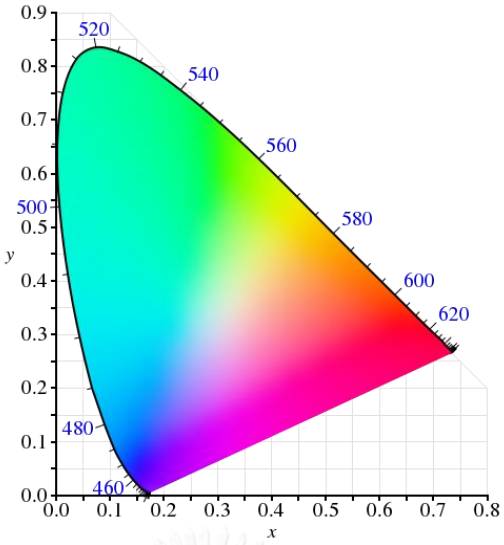

Figure 2.8 CIE 1931 xy Chromaticity Diagram

Note; the parameters used to evaporate all materials are the parameters of Al only, such as density of Al= 2.7. Thus, to evaluate the real thickness of the organic layers deposited by thermal evaporator and the thickness of PEDOT:PSS layer deposited by spin coating method, in the future, the glass substrate will be measured by scanning electron microscope (SEM) or/and the atomic force microscope (AFM). The real calculation of the CIE coordinate was obtained by the Microsoft office excel 2007 with the calculated formula of CIE 1931.

CHAPTER III
RESULTS AND DISCUSSION

3.1 Synthesis

A new series of truxene derivatives with different numbers of dipyrenylcarbazole substituents (**1-3**) are proved in **Figure 3.1**. They were synthesized from hexabutyl truxene as core and then coupling with dipyrenylcarbazole branch via C-N coupling reaction (Ullmann coupling). The synthetic route employed for preparing them is shown in **Scheme 1**.

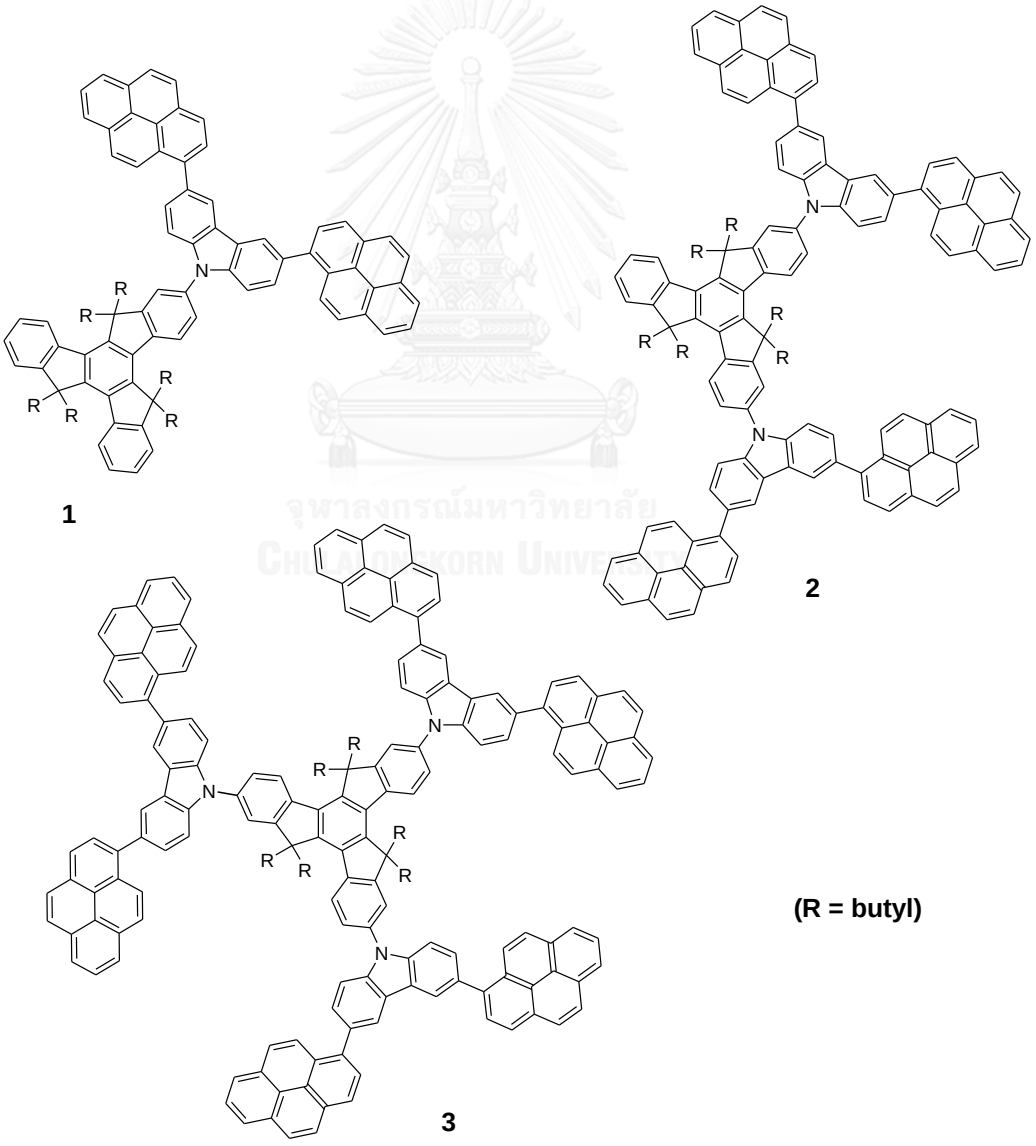

Figure 3.1 Structures of compounds (**1-3**)

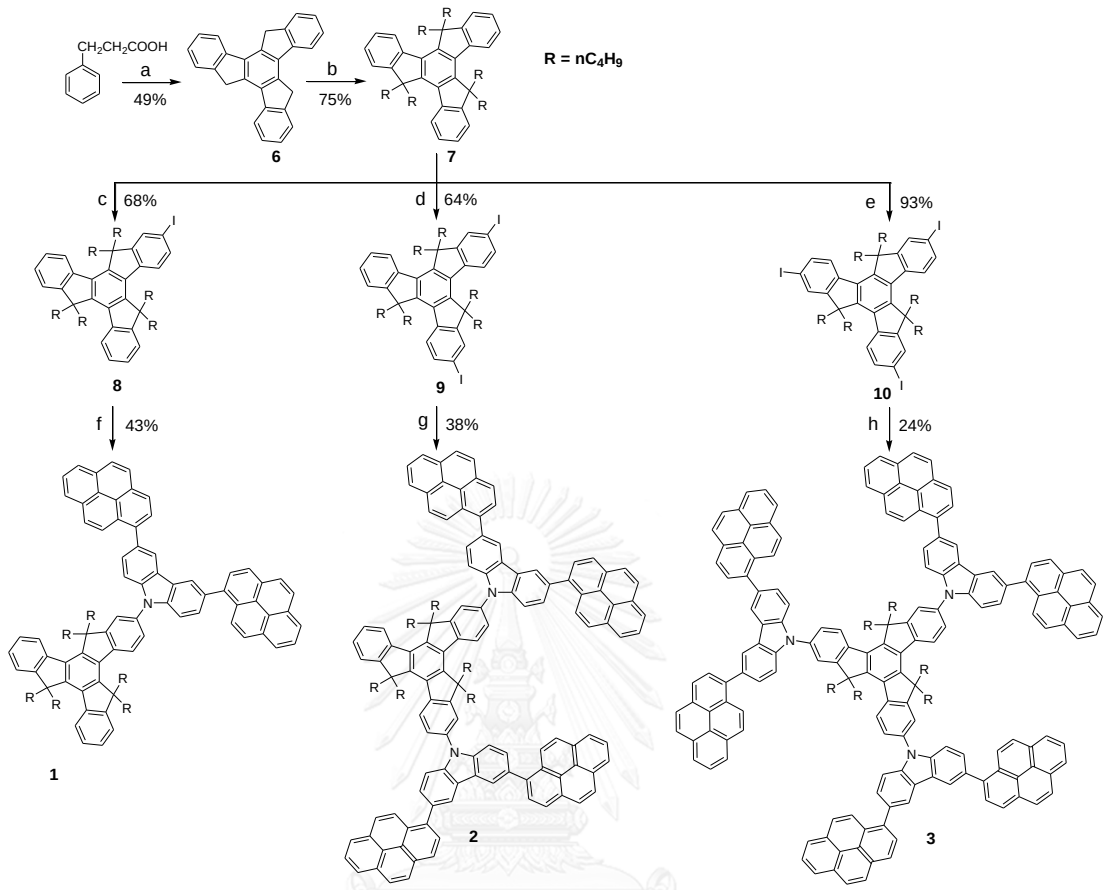

Key: (a) PPA, 160°C, 3 h; (b) n-BuBr, NaH, DMF, RT, 24 h; (c)(d)(e) KIO_3 and I_2, CH_3COOH:H_2SO_4:H_2O:CCl_4, 80°C, 4 h; (f)(g)(h) Dipyrenylcarbazole, 1 mol% CuI, 10 mol% Diamine ligand, K_3PO_4, Dioxane (1 M), 110°C for 24 h.

Scheme 2.1 Synthetic Pathway Used for the Preparation of the Compounds **1-3**

The required 3,6-dipyrenyl carbazole (**5**) for this study has been synthesized by two-step protocol (**Figure 3.2**) involving Suzuki cross coupling of pyrene with iodinated carbazole. In the first step, carbazole was iodinated at 3- and 6- position using KI/KIO_3 in refluxing acetic acid for 20 minutes to give brown solid residue after that recrystallization to afford 3,6-Diiodo-9H-carbazole (**4**) as light brown crystals in 98% yield confirmed by ^{1}H-NMR and ^{13}C-NMR, which were in good agreement with the literature reports [28]**.**

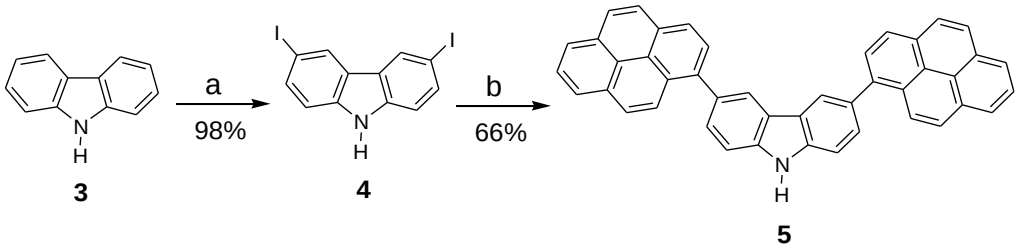

Figure 3.2 Key: (a) KI, KIO_3, AcOH, refluxing, 20 min;
(b) Pyrene-1-boronic acid, [$Pd(PPh_3)_4$], 2M K_2CO_3, THF refluxing, 24 h.

The second step involved the coupling of **4** with the commercially available pyrene-1-boronic acid via Suzuki cross coupling reaction using $Pd(PPh_3)_4$ as a catalyst and the K_2CO_3 as a base in THF to obtain dipyrenylcarbazole (**5**) as pale green in 66% yield [28].

For the synthesis core of target molecules, the first step, 3-phenylpropionic acid was converted to truxene (**6**) dehydro-cyclotrimerization by step-heating to 160 ℃ in polyphosphoric acid in nitrogen atmosphere. Compound **6** as light-yellow power, in 49% yield confirmed by ^{1}H and ^{13}C-NMR, which was in good agreement with the literature reports [37].

Then, to enhance the solubility in organic solvents and also prevent the aggregation by pi-stacking, full alkylation was carried out at 5-, 10-, and 15-position, obtaining **7** as white crystalline in 75% yield confirmed by ^{1}H and ^{13}C-NMR, which were in good agreement with the literature reports [37, 40].

The controlled iodination of **7** using KIO_3 and I_2 could be accomplished by using various molar equivalent of KIO_3-I_2 in mixed solvent (CH_3COOH:H_2SO_4:H_2O:CCl_4) = 100:5:20:8). Then the residue was refluxed in methanol followed by vacuum filtration to afford mono- (**8),** di- **(9)** or tri-iodinated product (**10)** in 68, 64 or 93% yield, respectively, as white powders. The ^{1}H NMR of **8, 9** and **10** in $CDCl_3$ are compared as shown in **Figure 3.3**.

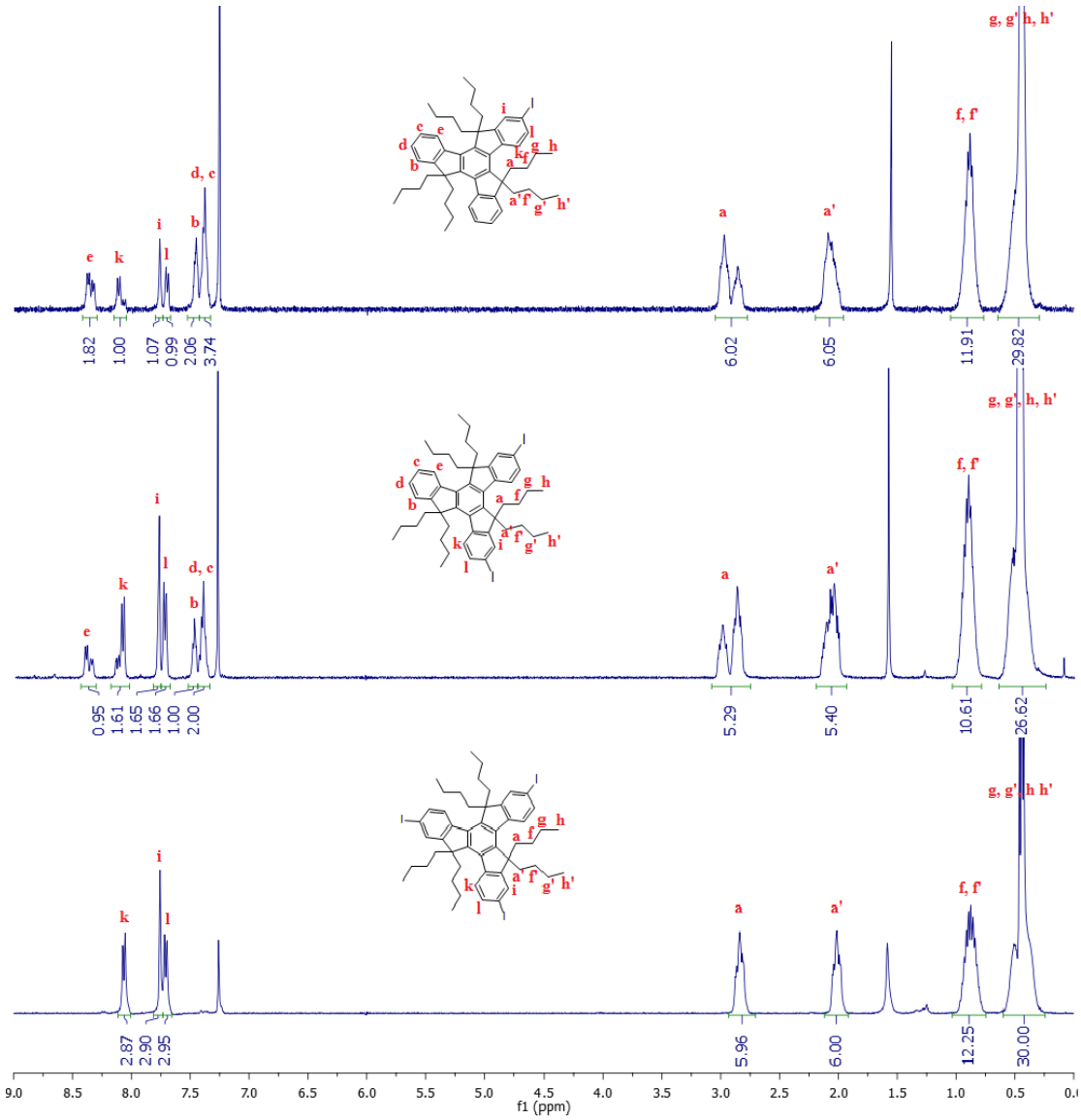

Figure 3.3 ^{1}H- NMR of 5,5,10,10,15,15-hexabutyl-2-iodo-truxene (**8**), 5,5,10,10,15,15-Hexabutyl-2,7-diiodo-truxene (**9**) and 5,5,10,10,15,15-Hexabutyl-2,7,12-triiodo-truxene (**10**) in $CDCl_3$

The final steps were the Ullmann coupling reactions between the iodinated truxene core and dipyrenylcarbazole branch catalyzed by CuI/K_3PO_4/±trans-1,2-diaminocyclohexane in 1,4-dioxane. The crude product was purified by column chromatography on silica gel using hexane:CH_2Cl_2 to give compounds **1, 2** and **3** in 43, 38 and 24% yield, respectively, as white solids.

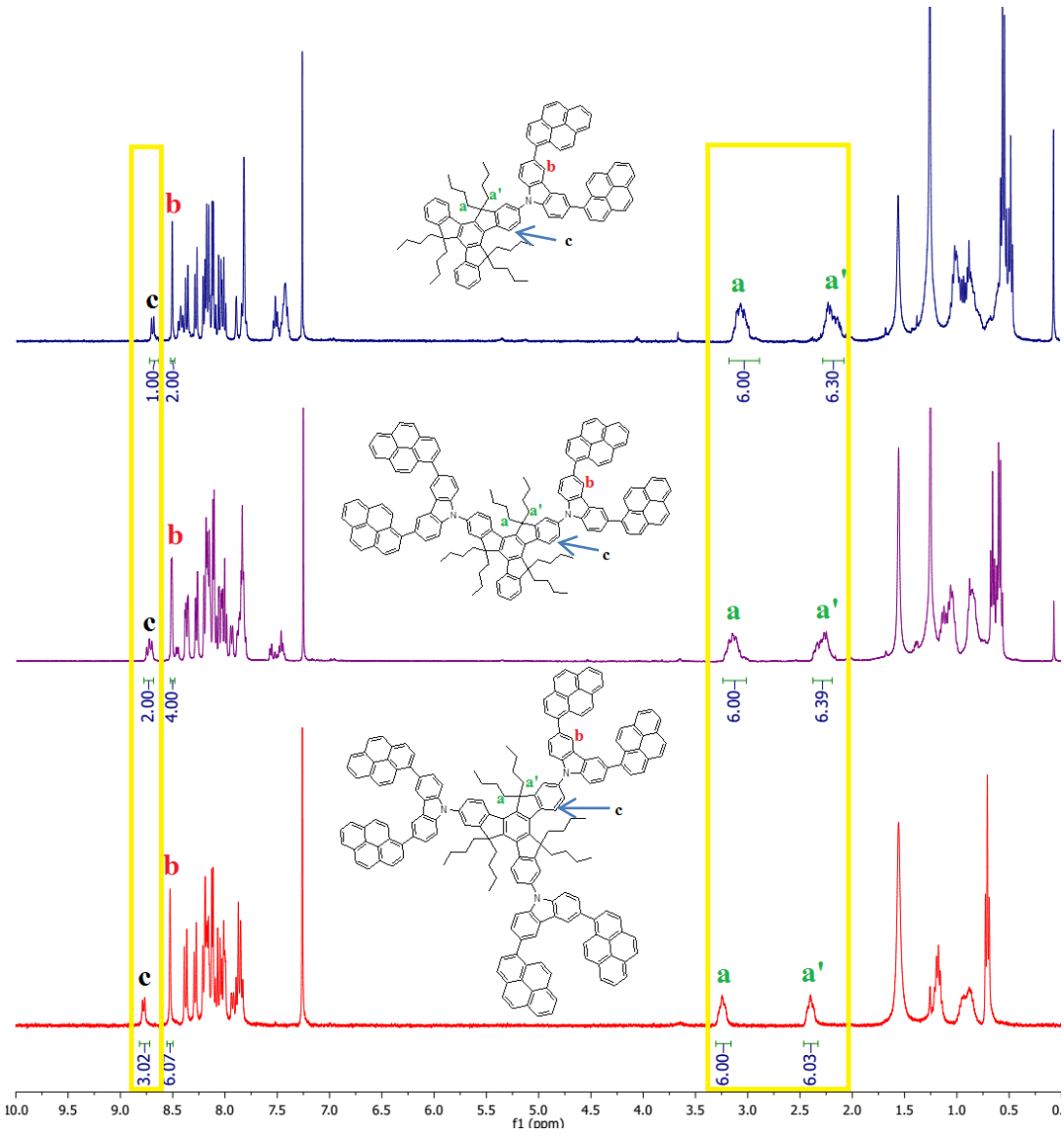

Figure 3.4 ^{1}H NMR of **1, 2** and **3** in $CDCl_3$

Stacked ^{1}H NMR spectra of **1-3** shown in **Figure 3.4** consist of three parts, which correspond to the truxene core, dipyrenylcarbazole branches and butyl chains. All molecules comprise of major characterictic peak, two multiple signals of methylene protons of butyl chain H_a and $H_{a'}$, singlet signal of aromatic protons in carbazole branch H_b, doublet signal of aromatic protons in truxene core H_c. The increasing ratio of H_a**:** H_b**:** H_c are 6: 2 : 1 for **1**, 6: 4: 2 for **2**, 6: 6: 3 for **3** respectively, corresponding to increasing of dipyrenylcarbazole unit. In Addition, H_a and H_c

positions of **2** and **3** exhibited gradually deshield shift compared to **1,** relative to the increment of the dipyrenylcarbazole branches.

3.2 Optical properties

The photophysical properties of **1-3** were all measured in $CHCl_3$ solution and thin films coated on quartz substrate. The results are summarized in **Table 3.1**. The solution UV–visible absorption spectra of all compounds exhibited absorption maxima (λ_{max}) around 348 - 350 nm. The compound **1** displays four absorption bands at 242 nm, 281 nm, 309 nm and 348 nm, which are attributed to the absorption of pyrene, carbazole, truxene moieties and π-π^* transitions of the overall conjugated aromatic systems, respectively. As the number of dipyrenylcarbazole units increased, the intensity of carbazole and truxene bands at 281 nm and 310 nm of **2** and **3** decrease in comparison with that of **1** (**Figure3.5**).

For the emission properties, all compounds exhibited similar spectra featuring emission maxima around 421 to 423 nm which are in the blue region (**Figure 3.6**). The fluorescence quantum yield ($\emptyset_f$) of **1**-**3** measured in $CHCl_3$ are 0.72, 0.59 and 0.55, respectively. The decrease in quantum yield may be due to the two-photon absorption (TPA) process as reported in a relatively similar aromatic systems [21, 55, 56]. The thin film PL spectra of **1**-**3** exhibit also featureless emission bands with a red-shift compared to their spectra in solution as shown in **Figure 3.6**

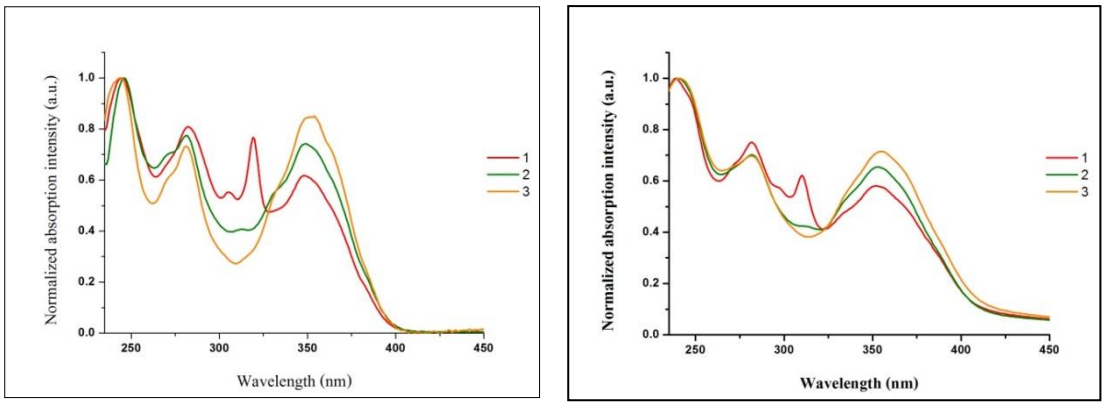

Figure 3.5 Normalized absorption spectra of **1**-**3** in $CHCl_3$ solution (left) and thin film (right).

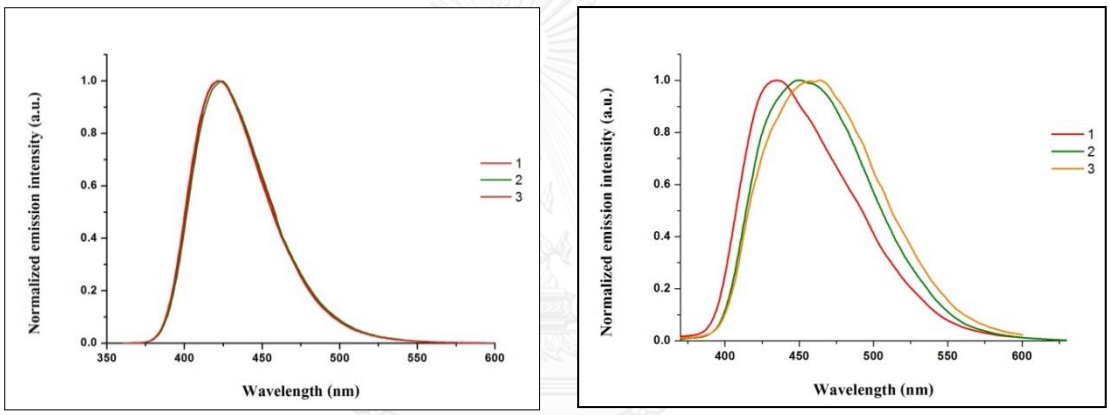

Figure 3.6 Normalized emission spectra of **1**-**3** in $CHCl_3$ solution (left) and thin film (right).

Table 3.1 Optical Data for Compounds**1-3**

Cmpd	Absorption-λ_{max} (nm)/ log ε (M^1cm^1)		Emission-λ_{max} (nm)		Ø[e]
	Solution[a]	Thin film[b]	Solution[c]	Thin film[d]	
1	242 (4.67), 281 (4.56), 309 (4.45), **348** (4.45)	352	421	435	0.72
2	244 (4.79), 281 (4.65), **349** (4.61)	353	423	449	0.59
3	244 (5.05), 281 (4.89), **350** (4.92)	356	421	457	0.55

[a] Measured for $CHCl_3$ solutions.

[b] Measured for spin-cast thin film.

[c] The PL emission excited at the absorption maxima in dilute $CHCl_3$ solution.

[d] The PL emission excited at the absorption maxima in thin film.

[e] Relative quantum yield was obtained by comparing with standards quinine sulfate solution in 0.01 M H_2SO_4 ($\emptyset_F$ = 0.54) PL quantum yield determined in $CHCl_3$ solution (A<0.1) at room temperature.

3.3 Electrochemical properties

The hole-transporting ability and electrochemical properties of all compounds were investigated by cyclic voltammetry (CV). In addition, the HOMO-LUMO energy levels were calculated from CV resulting data.

The cyclic voltammetry (CV) experiments were operated using an AUTOLAB spectrometer with a three-electrode assembly comprising in dichloromethane in the presence of tetrabutylammonium hexafluorophosphate ($TBAPF_6$ 0.10 M) as supporting electrolyte with a scanning rate of 0.05 V/s at room temperature and the resulting data are summarized in **Table 3.2**. A platinum working electrode, a platinum wire counter electrode, and a $Ag/AgNO_3$ (Sat.) reference electrode were used in all cyclic voltammetry experiments.

As shown in **Figure 3.7**, the onset oxidation potentials (E_{onset}) of all compounds are presented around 0.75- 0.80V. The HOMO-LUMO energy levels can be calculated following equations:

HOMO (eV) = - (4.44 eV + E_{onset}). (5)

E_g (eV) = 1240/λ_{onset} (6)

|LUMO| = |HOMO| - E_g (7)

Where E_{onset} are the onset oxidation potentials coherent to Ag/Ag^+. The energy band gab (E_g) was estimated from the absorption beginning from UV-Vis absorption spectra of the dyes.

The onset absorption of dyes (**1**, **2** and **3**) are observed around 397- 400 nm relating to the energy gaps around 3.10-3.12 eV.

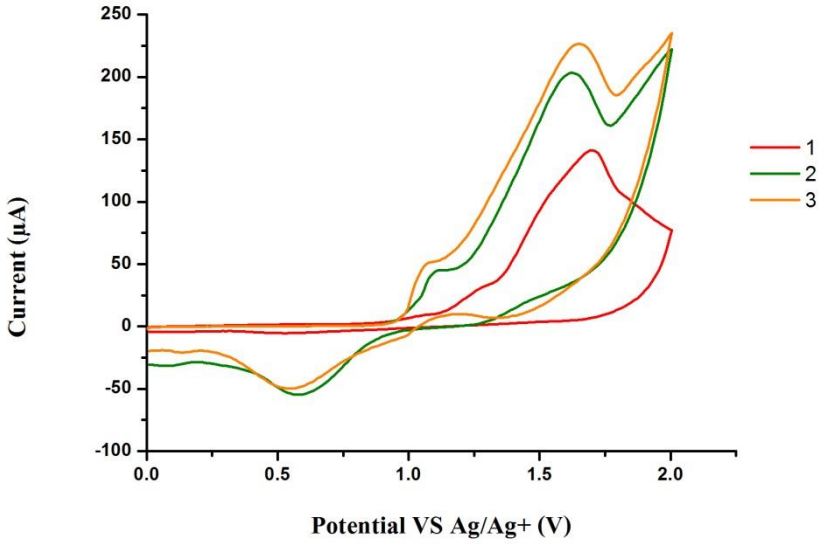

Figure 3.7 CV curves of componds (**1**-**3**) measured in 0.1 M tetrabutylammomium hexafluorophosphate ($TBAPF_6$) versus $Ag/AgNO_3$ in dichloromethane.

Table 3.2 The experimental and calculated electrochemical properties of **1**-**3**.

Cmpd	Experimental data				Calculated data[e]		
	E_g (eV)[a]	E_{onset} (V)[b]	HOMO (eV)[c]	LUMO (eV)[d]	E_g (eV)	HOMO (eV)	LUMO (eV)
1	3.12	0.75	-5.19	-2.07	3.49	-5.13	-1.64
2	3.10	0.80	-5.24	-2.14	3.48	-5.13	-1.65
3	3.11	0.80	-5.24	-2.13	3.50	-5.15	-1.65

[a] The optical band gap estimated from the onset of the absorption spectra (E_g = 1240/λ_{onset}).

[b] Onset oxidation potential estimated from the cyclic voltammogram.

[c] Estimated by the empirical equation: HOMO = -(4.44+ E_{onset}).

[d] Estimated from LUMO = HOMO + E_g.

[e] All calculations were performed by Gaussian 09 code and geometry optimizations were done by B3LYP/6-31G(d,p) in $CHCl_3$ solution modelled by the Polarizable Continuum Model (PCM) method.

Quantum chemical calculation: To study an information about the geometry and electronic structure of all compounds as shown in **Figure 3.8**. The three compounds were optimized using B3LYP/6-31G(d,p) in $CHCl_3$ solution modeled by the Polarizable Continuum Model (PCM) method (**Figure 3.9**). All computations were performed by GAUSSIAN 09 [57]. The results revealed that the substituted branches were twisted to the core of the compounds with the dihedral angles around 55-56 degrees. These large twisting of the dihedrals may reduce the conjugation of electrons along the molecules which directly influences the electronic and photophysical properties of these compounds. For the one-branched analog (**1**), HOMO and LUMO show that the electron densities are delocalized over the branch in which bonding and anti-bonding are occupied. This implies that the lowest excitation of electron in this molecule is attributed to π-π^* transition. For the compounds **2** and **3,** the HOMOs show that the contributions of electron density are

very similar in which only two branches (first and second) are occupied. The third branch of analog (**3**) is not involved in the delocalization of electron. However, electron density in the second branch of the both compounds are significantly less than the first branch. This suggest that increase degree of the branch does not significantly alter the photophysical properties of the compounds. The LUMO of all compounds are also very similar. The electron density in the LUMO of all compounds are delocalized on the anti-bonding region of the first branch. The HOMO and LUMO suggest that electron transition at the lowest excitation is mainly from the π-π^* transition for all the compounds.

The calculated energy difference between HOMO and LUMO ($\Delta_{H\text{-}L}$) of the three compounds are similar at around 3.48-3.49 eV. This confirmed the large dihedral angles between the truxene core and the associating dipyrenylcarbazole branches. Due to the transition of electron mainly come from π-π^* transition in the first branch while the second and third branches are almost not contributing. Therefore, the $\Delta_{H\text{-}L}$ values and the photophysical properties of all compounds are very similar. The values from the calculation are in good agreement with the experimental data.

Due to these HOMO energy levels are similar (-5.19 to – 5.24 eV) and suitable with the work functions of typically used ITO anode (-4.80 eV) and the commercially available PEDOT:PSS (-5.0 eV) as hole injection layer whereas the LUMO energy levels of all compounds (-2.07 to -2.14 eV) are nearly with the work function of LiF:Al cathode (-4.20 eV) and the commercially available BCP (-3.0 eV) as hole-blocking layer. So these materials are appropriate for OLED application by using as the hole-transporting layer.

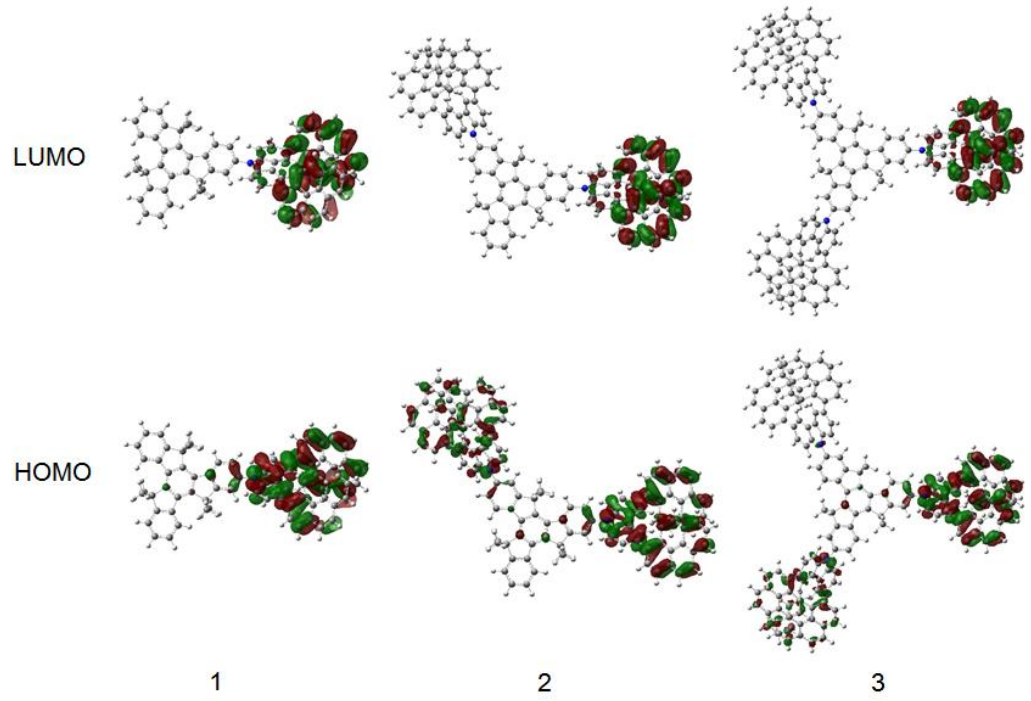

Figure 3.8 The HOMO and LUMO orbitals of the compounds (**1**-**3**) calculated by B3LYP/6-31G(d,p) method.

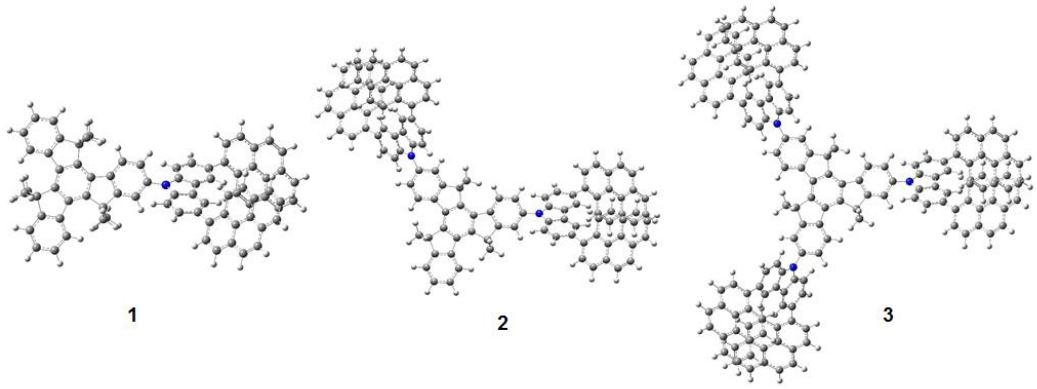

Figure 3.9 Optimized structure of the compounds (**1**-**3**).

3.4 Thermal properties

For OLED applications, the critical for device stability and lifetime are depend on the thermal stability of organic materials. Due to, heat is generated during device operation which can change the organic layer morphology leading to the degradation

of OLEDs. The thermal properties of **1**-**3** were investigated by the thermo gravimetric analysis (TGA) and differential scanning calorimetry (DSC).

The thermal properties of all compounds are illustrated as **Figure 3.10** and concluded in **Table 3.3**. The TGA curves show that all three compounds are thermally stable with the decomposition temperature at 10% weight loss ($T_d^{10\%}$) excellent above 440°C. From DSC measurement, there was one sharp endothermic peak for **1** at 313°C due to melting temperature (T_m) and there was no endothermic baseline shift due to glass transition temperature (T_g); it revealed that **1** has high crystalline. For **2** and **3** reveal an endothermic baseline shift owing to glass transition (T_g) above 165°C with no crystallization and melting were detected at higher temperature, indicating highly stable amorphous material.

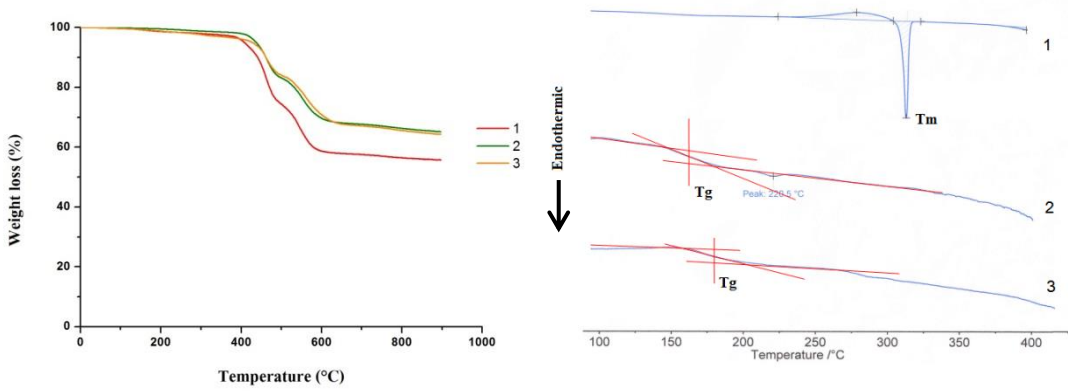

Figure 3.10 TGA thermograms of **1**-**3** measured at a heating rate of 10 °C/min^{-1} (left) and DSC (1st heating scan) (right).

Table 3.3 Thermal properties of **1**-**3**

Compounds	T_g[a] (°C)	T_m[a] (°C)	T_d[b] (°C)
1	-	313	441
2	165	-	461
3	180	-	461

[a] Obtained from DSC measured at heating rate of 10°C/min under N_2.

[b] The decomposition temperature at 10% weight loss obtained from TGA measured at heating rate of 10°C/min under N_2.

3.5 Electroluminescent (EL)

3.5.1 Investigation of the light-emitting properties

Overall to study their electroluminescent properties, muti-layer OLEDs device was fabricated using (1-3) as emitting layers (EMLs) by spin-coating and comparing with the commercial standard NPB which emitted blue light region.

In the first step, to optimal condition spin-coated thin film from compound 1 in device (I - III) of structure ITO / PEDOT:PSS / **1**(spin-coating)(40 nm)/ BCP (30 nm) / LiF (1.0 nm):Al (100 nm) as shown in **Figure 3.11**

Device I 0.5 %w/v of compound **1**

Device II 1.0 %w/v of compound **1**

Device III 1.5 %w/v of compound **1**

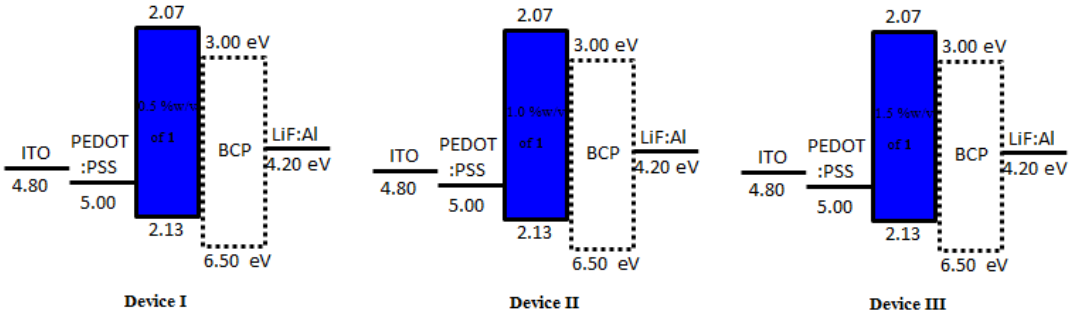

Figure 3.11 Energy level diagrams of device (I - III)

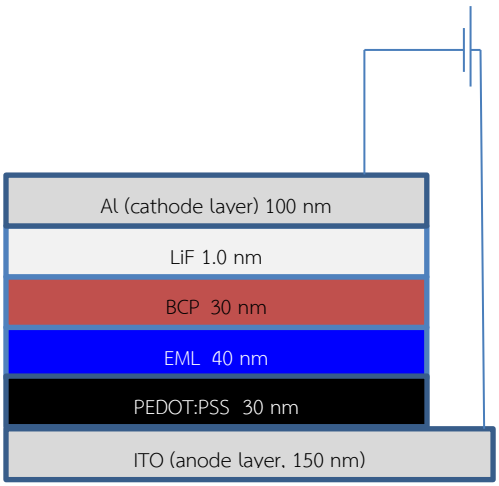

Figure 3.12 Configuration of Device

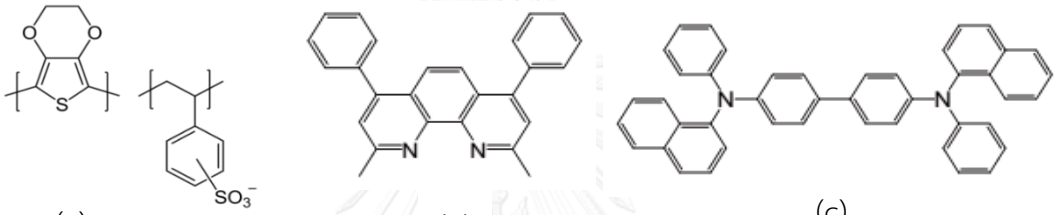

Figure 3.13 Chemical structure of PEDOT:PSS (a), and BCP (b) and NPB (c)

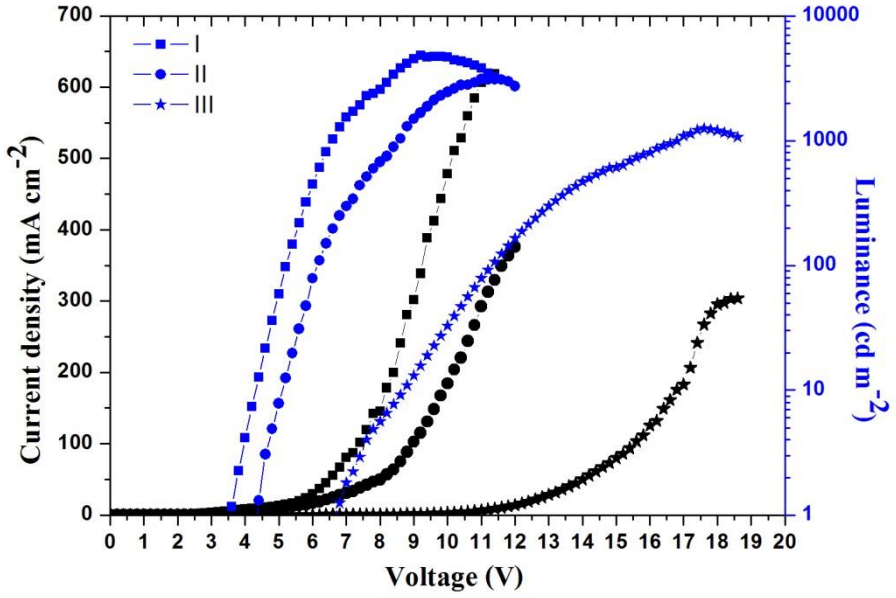

Figure 3.14 Current density-voltage-luminance (J-V-L) characteristics of the OLEDs (device I - III).

Under applied voltage, the devices (I - III) emit a pure deep blue emission with peak centred at 424 nm, CIE coordinates of (0.15, 0.10) and summarized in **Table 3.4**, the results reveal that device (I) showed the highest performances of the device with a maximum luminance (L_{max}) of 4,811 cd/m^2 at 9.2 V, a low turn-on voltage (V_{on}) at 3.6 V, maximum luminance efficiency (η_{lum}) at 1.97 cd/A at the voltage 7.2 V (**Figure 3.14**), Indicating that at the low concentration molecule might be rearrangement in thin film well than high concentration. So we choose this condition for preparing to fabricate devices (IV- VI) with compound **2**, **3** and standard NPB respectively as shown in **Figure 3.15**.

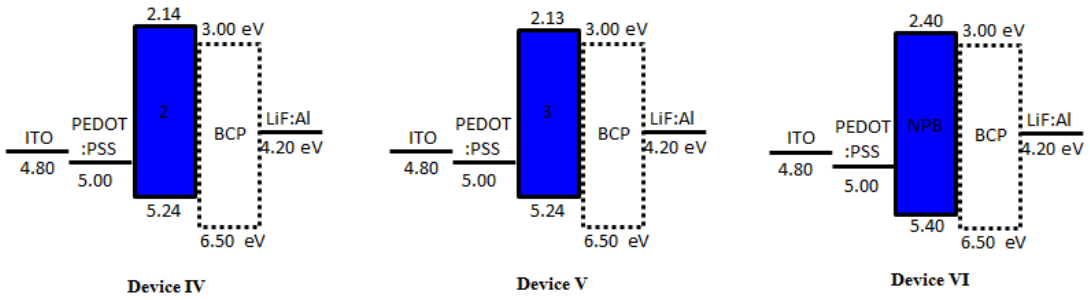

Figure 3.15 Energy level diagrams of device (IV - VI)

The results are summarized in **Table 3.4**. Under applied voltage, all devices exhibited blue emission. The EL spectra of all devices match with their solid film (spin-coated) PL spectra. The voltage-luminance and voltage-current density characteristics (*J-V-L*) of the devices appear promising in term of brightness and efficiency. The device fabricated with compound **3** as EML (Device V) exhibits highest brightness with L_{max} of 8,115 cd/m^2 at 10.8 V, a turn-on voltage (V_{on}) at 3.8 V. However, device IV which has compound 2 as EML displayed the best performance in terms of high maximum brightness at 8,001 cd/m2 at 9.6 V, a low turn-on voltage (V_{on}) at 3.4 V and maximum luminance efficiency (η_{lum}) at 2.33 cd/A at the voltage 6.6 V (**Figure 3.16**).

Table 3.4 Device characteristics of OLEDs fabricated with 1 – 3 as the EMLs (device I – VI)

Device	EML	λ_{em}^{EL}	V_{on}[e]	L_{max}[f]	J_{max}[g] (mA cm^{-2})	η_{lum}[h] (cd A^{-1}) (at the voltage (V))	CIE[i] **(x,y)**
I[a]	1	424	3.6	4,811/9.2V	338	1.97/7.2V	0.15, 0.10
II[b]	1	424	4.4	3,099/11V	293	1.48/8.8V	0.15, 0.10
III[c]	1	424	6.6	1,248/17.6V	267	1.29/10.8V	0.16, 0.11
IV[d]	2	463	3.4	8,001/9.6V	660	2.33/6.6V	0.15, 0.14
V[d]	3	468	3.8	8,115/10.8V	670	1.99/8.0V	0.16, 0.19
VI[d]	NPB	427	2.8	2,685/8.8V	719	0.71/4.2V	0.15, 0.07

[a] ITO/PEDOT:PSS/**1** (0.5 %w/v)/BCP/LiF:Al

[b] ITO/PEDOT:PSS/**1** (1.0 %w/v)/BCP/LiF:Al

[c] ITO/PEDOT:PSS/**1** (1.5 %w/v)/BCP/LiF:Al

[d] ITO/PEDOT:PSS/**EML**/BCP/LiF:Al

[e] Turn-on voltage (V).

[f] Maximum luminance (cd/m^2) (at applied potential V).

[g] Current density (mA/m^2).

[h] Luminance efficiency (cd/A).

[i] Commission International d'Eclairage coordinates (*x*, *y*).

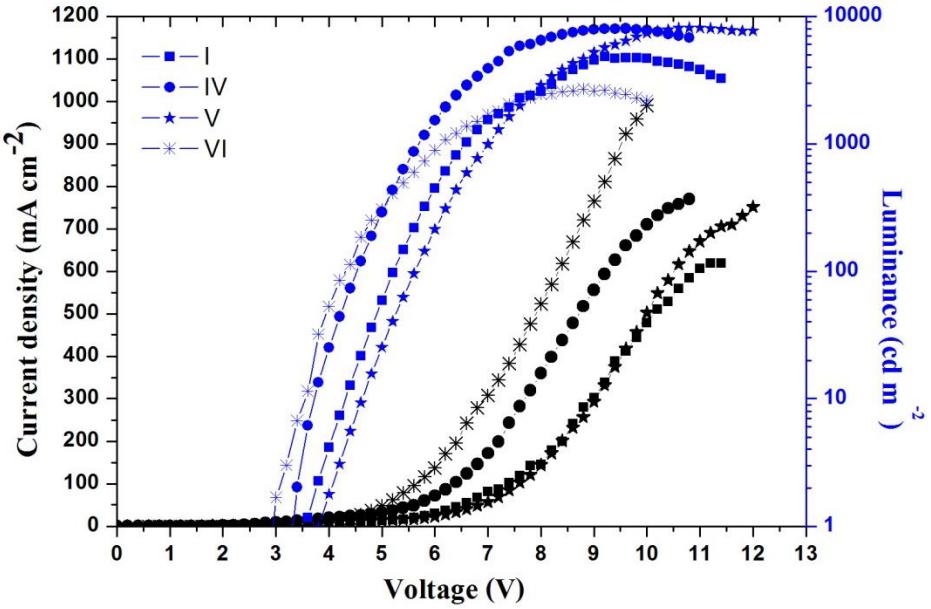

Figure 3.16 Current density-voltage-luminance (J-V-L) characteristics of the OLEDs (device I, IV - VI).

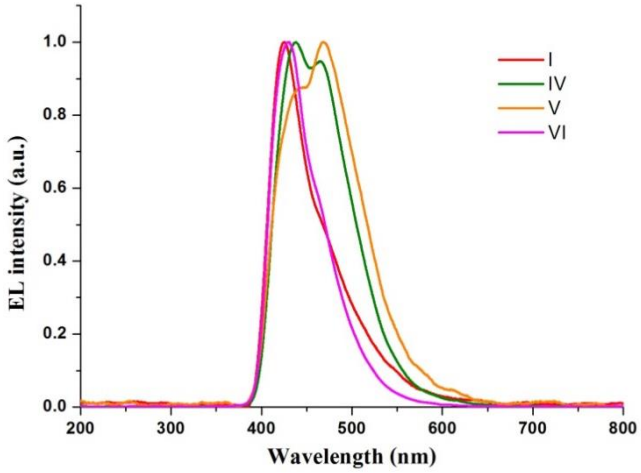

Figure 3.17 EL spectra plot of OLEDs (devices I, IV – VI).

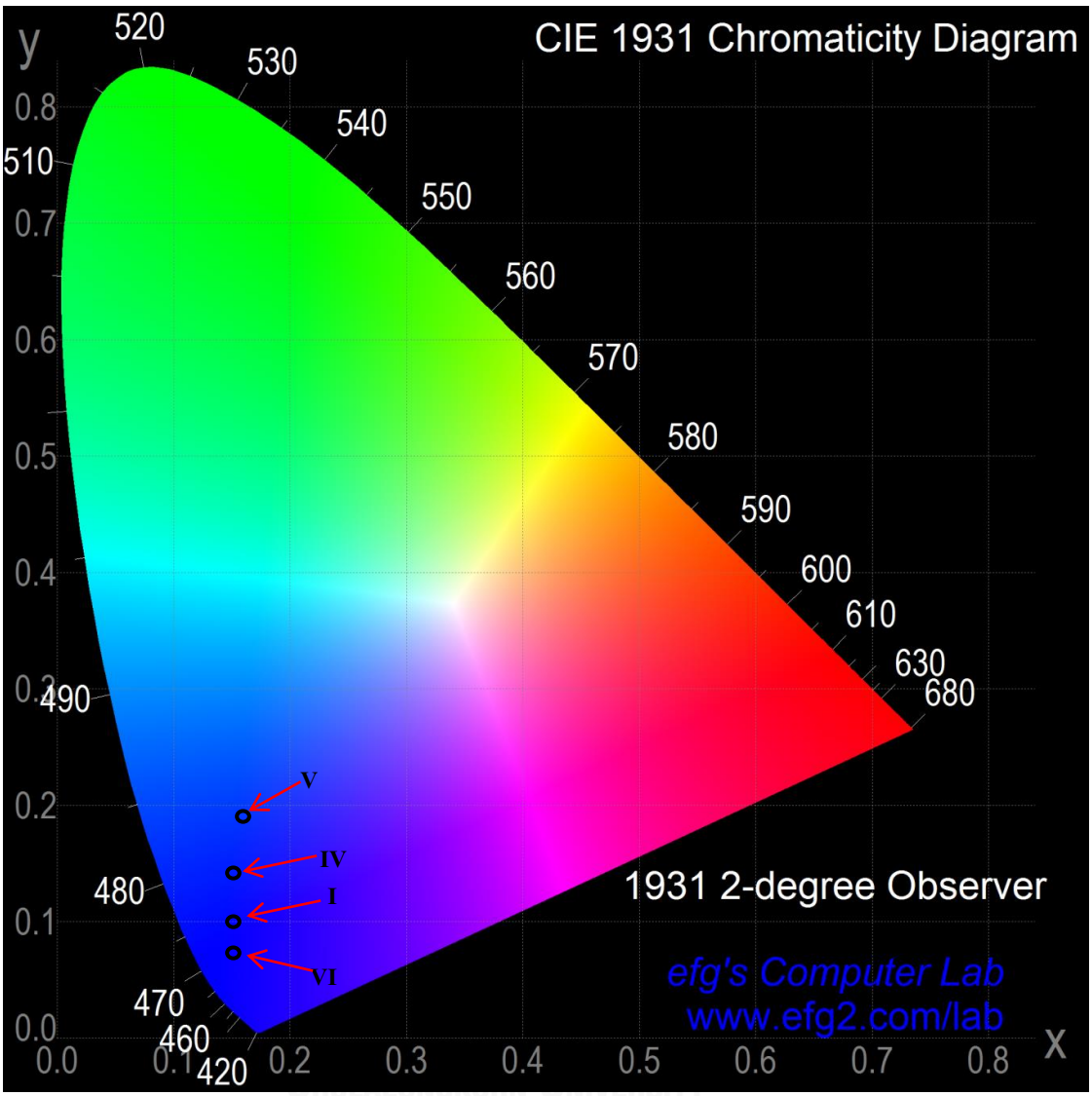

Figure 3.18 A CIE chromaticity diagram showing the positions of devices.

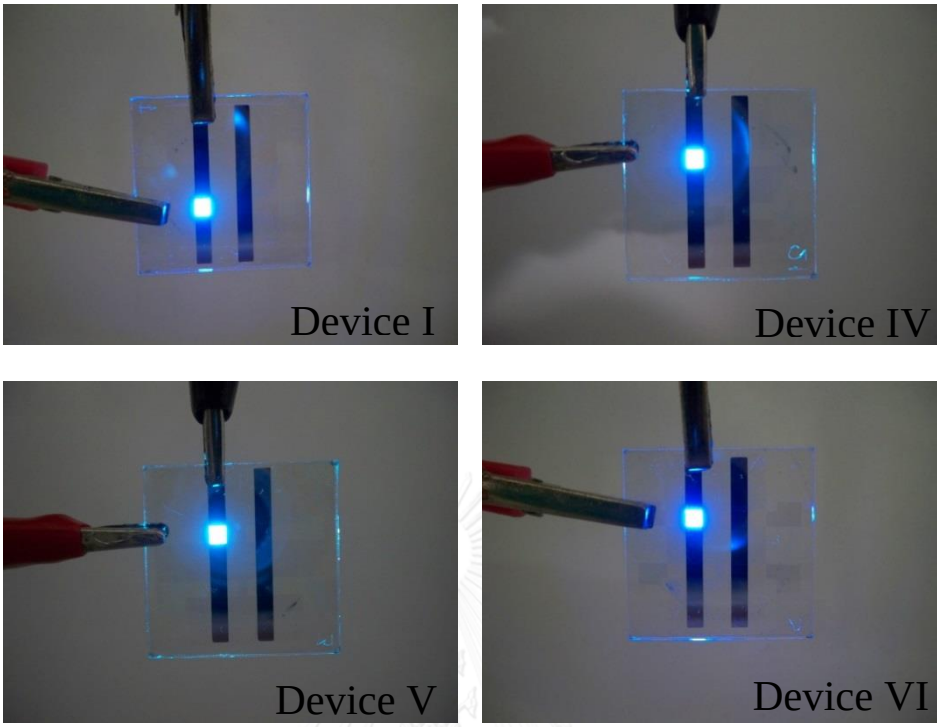

Figure 3.19 Emission color of OLEDs (devices I, IV – VI)**.**

3.5.2 Investigation of the hole-transporting properties

As mentioned above, the HOMO energy level of all compounds are around at -5.19 to -5.24 (eV) which are suitable for the work function of ITO anode (4.80 eV). Since the HOMO energy level of the emissive layer Alq_3 is at 5.80 eV, it is also possible that our compounds can be appropriate for application as hole-transporting materials (HTM) in OLEDs. To test this hypothesis, a number of multi-layer OLED devices were fabricated with structure of ITO/PEDOT:PSS/**HTL**[spin-coated **1**-**3** 30nm]/Alq_3[50nm]/LiF[1.0nm]/Al[100nm] (Device VII - IX). For device X – XI, the commercially available NPB is used as HTL in order to compare with our compounds. Moreover, the reference device XII also fabricated without an HTL was compared with all devices as shown in **Figure 3.20**

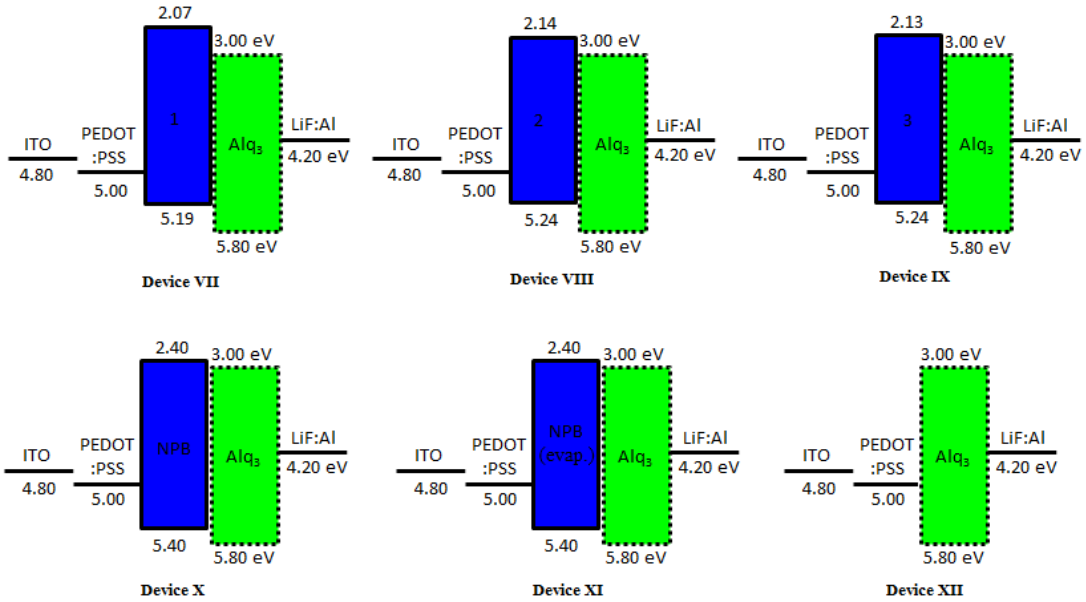

Figure 3.20 Energy level diagrams of device (VII - XII)

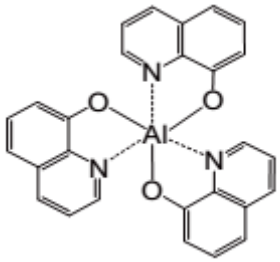

Figure 3.21 Chemical structure of Alq_3

All devices VII to XII emit bright green color of Alq_3 (512 - 517 nm and CIE 0.26, 0.50) as shown in **Figure 3.23**, indicating that **1**-**3** acted only as the hole-transporting layer like NPB. The summarized data in **Table 3.5** indicated that all devices with HTL exhibited better performance compared to the reference device without HTL. The device (VIII) utilizing compound **2** displayed the best performance with highest maximum brightness of 44,773 cd/m^2 at 10.8 V, a low turn-on voltage (V_{on}) at 2.8 V and maximum luminance efficiency (η_{lum}) at 7.39 cd/A at the voltage 6.6 V.

Table 3.5 Device characteristics of OLEDs fabricated with 1 – 3 as the HTL (device VII – XII)

Device	HTL	λ_{em} EL	V_{on}[b]	L_{max}[c]	J_{max}[d] (mA cm^{-2})	η_{lum}[e] (cd A^{-1}) (at the voltage (V))	CIE[f] **(x,y)**
VII[a]	1	512	3.0	35,593/11.6V	1,058	6.03/7.4V	0.26, 0.50
VIII[a]	2	512	2.8	44,773/10.8V	1,057	7.39/7.4V	0.26, 0.49
IX[a]	3	512	3.2	37,953/10.8V	1,020	6.06/7.4V	0.27, 0.52
X[a]	NPB	517	2.4	31,857/9.4V	1,598	4.45/4.6V	0.29, 0.54
XI[a]	NPB (evap.)	515	3.0	36,958/11.0V	1,423	5.15/5.6V	0.27, 0.53
XII[a]	-	517	4.0	4,633/9.6V	794	1.01/7.0V	0.29, 0.53

[a] ITO/PEDOT:PSS/**HTL**/Alq_3/LiF:Al

[b] Turn-on voltage (V).

[c] Maximum luminance (cd/m^2) (at applied potential V).

[d] Current density (mA/m^2).

[e] Luminance efficiency (cd/A).

[f] Commission International d'Eclairage coordinates (*x*, *y*).

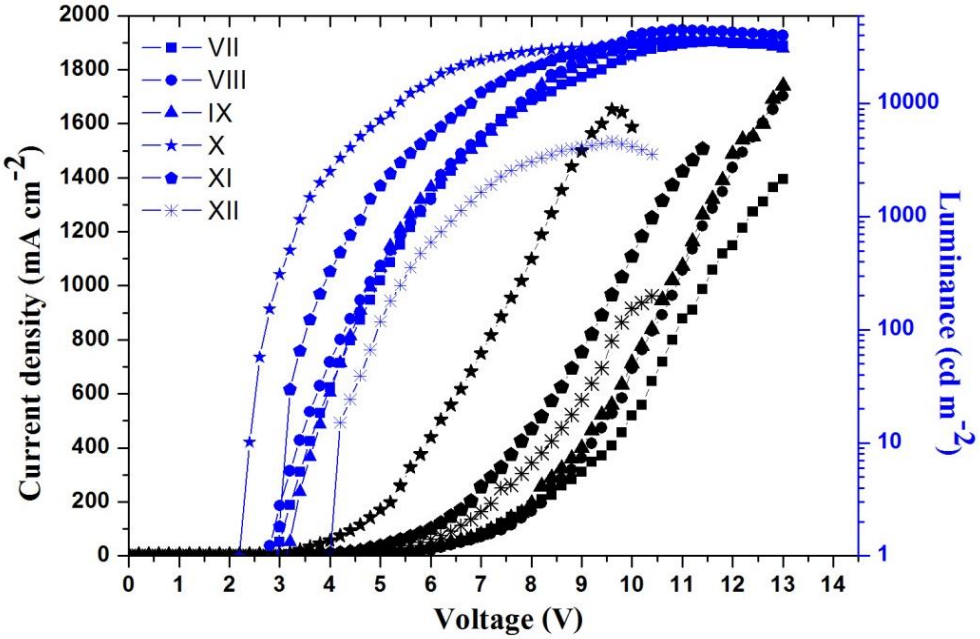

Figure 3.22 Current density-voltage-luminance (J-V-L) characteristics of the OLEDs (device VII – XII).

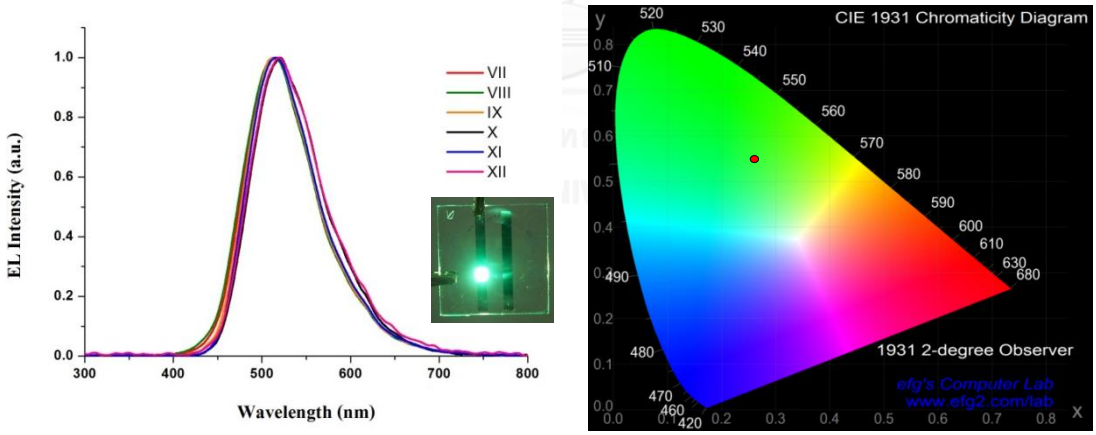

Figure 3.23 Plots of EL spectra and emission color of Alq_3-based OLEDs (devices VII – XII) (left) and A CIE chromaticity diagram showing the positions of devices (VII – XII) (right).

The morphology of the spin-casting films (**1**-**3**), which may contribute to the OLED device performances, was examined by atomic force microscopy (AFM). The AFM images of all thin films spin-coated from the $CHCl_3$-toluene (2:1) solution show excellent film-forming properties (**Figure 3.24**). The films are highly uniform with smooth surface. This homogeneous morphology was necessary for OLEDs with reduce leak currents and improved thermal stability during device operation.

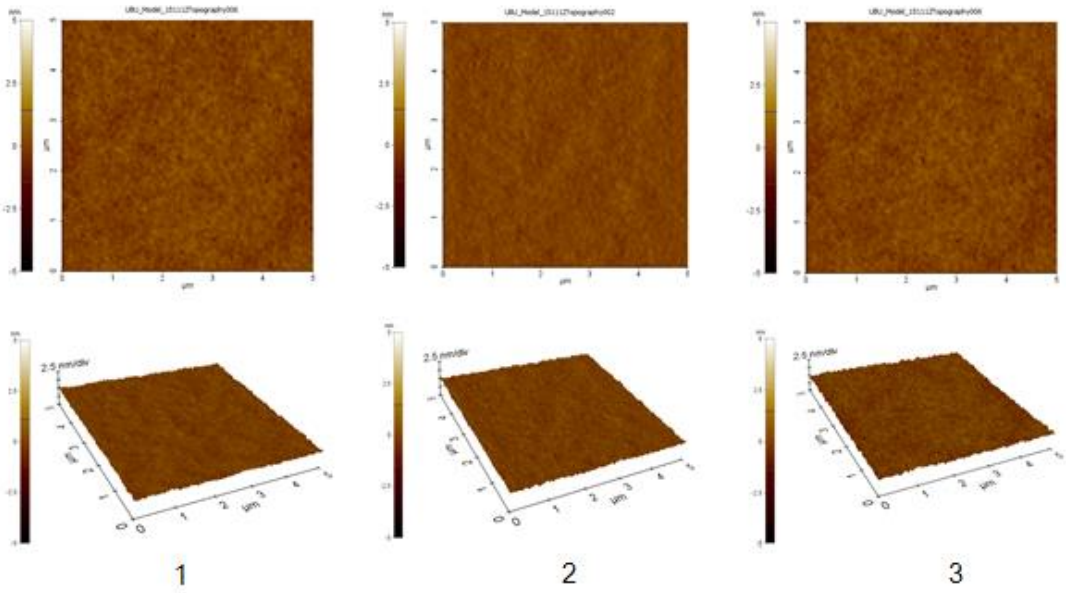

Figure 3.24 AFM images of the spin-coated films of **1**-**3**

CHAPTER IV
CONCLUSION

A series of novel compounds based on truxene derivatives with different numbers of dipyrenylcarbazole pendants have been synthesized via C-N coupling. The solution UV–visible absorption spectra of all compounds exhibited absorption maxima (λ_{max}) around 348 - 350 nm and emission maxima around 421 - 423 nm which are in the blue region. The resulting these compounds showed good morphological thin film with high *Tg* above 165°C and thermal stabilities at 10% weight loss ($T_d^{10\%}$) excellent above 440°C, indicating that these compounds are suitable for application as OLED materials.

The multi-layer OLEDs using these compounds as hole-transporting non-doped emitters and BCP as a hole-blocking layer (ITO/PEDOT:PSS/**1–3**/BCP/LiF:Al) emit deep blue color according to the CIE coordinates with high luminance efficiencies as compared to the reference device using NPB. Among three materials, the **2**-base blue OLED was found to be the best device performance with high maximum brightness of 8,001 cd/m^2 at 9.6 V, a low turn-on voltage (V_{on}) at 3.4 V and maximum luminance efficiency η) at 2.33 cd/A at 6.6 V.

As a hole-transporting properties, spin-coated OLEDs with a structure of ITO/PEDOT:PSS/**1–3**/Alq_3/LiF:Al. All device display a bright green emission of Alq_3 (EL_{max} 512 - 517 nm, CIE 0.26, 0.50). Their ability as HTL for green OLEDs was comparable to a common hole-transporter NPB. The device **VIII** (**2**-base) exhibited the best performance with highest maximum brightness of 44,773 cd/m^2 at 10.8 V, a low turn-on voltage (V_{on}) at 2.8 V and maximum luminance efficiency (η_{lum}) 7.39 cd/A at 7.4 V.

REFERENCES

[1] Tang, C.W. and VanSlyke, S.A. Organic electroluminescent diodes. Applied Physics Letters 51(12) (1987): 913-915.

[2] Tang, C.W., VanSlyke, S.A., and Chen, C.H. Electroluminescence of doped organic thin films. Journal of Applied Physics 65(9) (1989): 3610-3616.

[3] Sugiyama, K., Ishii, H., Ouchi, Y., and Seki, K. Dependence of indium–tin–oxide work function on surface cleaning method as studied by ultraviolet and x-ray photoemission spectroscopies. Journal of Applied Physics 87(1) (2000): 295-298.

[4] Coropceanu, V., Cornil, J., da Silva Filho, D.A., Olivier, Y., Silbey, R., and Brédas, J.-L. Charge Transport in Organic Semiconductors. Chemical Reviews 107(4) (2007): 926-952.

[5] Kanemitsu, Y. Proceedings of the Fifteenth International Conference on Amorphous Semiconductors-Science and Technology Microscopic nature of hopping charge transport in disordered molecular solids. Journal of Non-Crystalline Solids 164 (1993): 1271-1274.

[6] Wang, P.-W., Liu, Y.-J., Devadoss, C., Bharathi, P., and Moore, J.S. Electroluminescent diodes from a single component emitting layer of dendritic macromolecules. Advanced Materials 8(3) (1996): 237-241.

[7] Hung, L.S. and Chen, C.H. Recent progress of molecular organic electroluminescent materials and devices. Materials Science and Engineering: R: Reports 39(5–6) (2002): 143-222.

[8] Jen, A.K.-Y., Liu, Y., Hu, Q.-S., and Pu, L. Efficient light-emitting diodes based on a binaphthalene-containing polymer. Applied Physics Letters 75(24) (1999): 3745-3747.

[9] Bellmann, E., Shaheen, S.E., Thayumanavan, S., Barlow, S., Grubbs, R.H., Marder, S.R., Kippelen, B., and Peyghambarian, N. New Triarylamine-Containing Polymers as Hole Transport Materials in Organic Light-Emitting Diodes: Effect of Polymer Structure and Cross-Linking on Device Characteristics. Chemistry of Materials 10(6) (1998): 1668-1676.

[10] Thomas, K.R.J., Kapoor, N., Bolisetty, M.N.K.P., Jou, J.-H., Chen, Y.-L., and Jou, Y.-C. Pyrene-Fluorene Hybrids Containing Acetylene Linkage as Color-Tunable Emitting Materials for Organic Light-Emitting Diodes. The Journal of Organic Chemistry 77(8) (2012): 3921-3932.

[11] Li, G., Zhao, Y., Li, J., Cao, J., Zhu, J., Sun, X.W., and Zhang, Q. Synthesis, Characterization, Physical Properties, and OLED Application of Single BN-Fused Perylene Diimide. The Journal of Organic Chemistry 80(1) (2015): 196-203.

[12] Okumoto, K., Kanno, H., Hamada, Y., Takahashi, H., and Shibata, K. High efficiency red organic light-emitting devices using tetraphenyldibenzoperiflanthene-doped rubrene as an emitting layer. Applied Physics Letters 89(1) (2006): 013502.

[13] Saxena, K., Mehta, D.S., Rai, V.K., Srivastava, R., Chauhan, G., Kamalasanan, M.N., and Jain, V.K. Studies on organic light-emitting diodes based on rubrene-doped zinc quinolate. physica status solidi (a) 206(7) (2009): 1660-1663.

[14] Li, W., Jones, R.A., Allen, S.C., Heikenfeld, J.C., and Steckl, A.J. Maximizing Alq3 OLED Internal and External Efficiencies: Charge Balanced Device Structure and Color Conversion Outcoupling Lenses. Journal of Display Technology 2(2) (2006): 143-152.

[15] Chizu, S., Yoshiaki, T., Takeshi, Y., Makoto, K., and Shuji, D. Recent progress of high performance polymer OLED and OPV materials for organic printed electronics. Science and Technology of Advanced Materials 15(3) (2014): 034203.

[16] Doust, A. Polymer OLED Materials and Device Operation. 2011.

[17] Trattnig, G., Pogantsch, A., Langer, G., Kern, W., and Zojer, E. Polymer-based red, green, and blue emitting devices fabricated by reductive photopatterning. Applied Physics Letters 81(22) (2002): 4269.

[18] Burroughes, J.H., Bradley, D.D.C., Brown, A.R., Marks, R.N., Mackay, K., Friend, R.H., Burns, P.L., and Holmes, A.B. Light-emitting diodes based on conjugated polymers. Nature 347(6293) (1990): 539-541.

[19] Muller, C.D., Falcou, A., Reckefuss, N., Rojahn, M., Wiederhirn, V., Rudati, P., Frohne, H., Nuyken, O., Becker, H., and Meerholz, K. Multi-colour organic light-emitting displays by solution processing. Nature 421(6925) (2003): 829-833.

[20] Sato, Y., Ichinosawa, S., and Kanai, H. Operation characteristics and degradation of organic electroluminescent devices. Selected Topics in Quantum Electronics, IEEE Journal of 4(1) (1998): 40-48.

[21] Xu, C. and Webb, W.W. Measurement of two-photon excitation cross sections of molecular fluorophores with data from 690 to 1050 nm. Journal of the Optical Society of America B: Optical Physics 13(3) (1996): 481-491.

[22] Tong, Q.-X., Lai, S.-L., Chan, M.-Y., Lai, K.-H., Tang, J.-X., Kwong, H.-L., Lee, C.-S., and Lee, S.-T. High Tg Triphenylamine-Based Starburst Hole-Transporting Material for Organic Light-Emitting Devices. Chemistry of Materials 19(24) (2007): 5851-5855.

[23] Huang, J., Xu, B., Su, J.-H., Chen, C.H., and Tian, H. Efficient blue lighting materials based on truxene-cored anthracene derivatives for electroluminescent devices. Tetrahedron 66(38) (2010): 7577-7582.

[24] Chiechi, R.C., Tseng, R.J., Marchioni, F., Yang, Y., and Wudl, F. Efficient Blue-Light-Emitting Electroluminescent Devices with a Robust Fluorophore: 7,8,10-Triphenylfluoranthene. Advanced Materials 18(3) (2006): 325-328.

[25] Fu, H.-Y., Sun, X.-Y., Gao, X.-d., Xiao, F., and Shao, B.-X. Synthesis and characterization of benzothiazole derivatives for blue electroluminescent devices. Synthetic Metals 159(3–4) (2009): 254-259.

[26] Lu, J., Xia, P.F., Lo, P.K., Tao, Y., and Wong, M.S. Synthesis and properties of multi-triarylamme-substituted carbazole-based dendrimers with an

oligothiophene core for potential applications in organic solar cells and light-emitting diodes. Chemistry of Materials 18(26) (2006): 6194-6203.

[27] Lee, H., Park, Y.I.L., Kim, B., Lee, J.-H., and Park, J. Highly efficient blue emitting materials based on indenopyrazine derivatives for OLEDs [Invited]. Optical Materials Express 4(5) (2014): 924-933.

[28] Kumchoo, T., Promarak, V., Sudyoadsuk, T., Sukwattanasinitt, M., and Rashatasakhon, P. Dipyrenylcarbazole Derivatives for Blue Organic Light-Emitting Diodes. Chemistry – An Asian Journal 5(10) (2010): 2162-2167.

[29] Tang, C., Liu, F., Xia, Y.-J., Lin, J., Xie, L.-H., Zhong, G.-Y., Fan, Q.-L., and Huang, W. Fluorene-substituted pyrenes—Novel pyrene derivatives as emitters in nondoped blue OLEDs. Organic Electronics 7(3) (2006): 155-162.

[30] Harismah, K. Development of New Carbazole Polymers for LED Applications. University of Sheffield, Department of Chemistry, 2008.

[31] Li, J., Liu, D., Li, Y., Lee, C.-S., Kwong, H.-L., and Lee, S. A High Tg Carbazole-Based Hole-Transporting Material for Organic Light-Emitting Devices. Chemistry of Materials 17(5) (2005): 1208-1212.

[32] Kochapradist, P., Prachumrak, N., Tarsang, R., Keawin, T., Jungsuttiwong, S., Sudyoadsuk, T., and Promarak, V. Multi-triphenylamine-substituted carbazoles: synthesis, characterization, properties, and applications as hole-transporting materials. Tetrahedron Letters 54(28) (2013): 3683-3687.

[33] Justin Thomas, K.R., Lin, J.T., Tao, Y.-T., and Ko, C.-W. Light-Emitting Carbazole Derivatives: Potential Electroluminescent Materials. Journal of the American Chemical Society 123(38) (2001): 9404-9411.

[34] Lei, T., Luo, J., Wang, L., Ma, Y., Wang, J., Cao, Y., and Pei, J. Highly stable blue light-emitting materials with a three-dimensional architecture: Improvement of charge injection and electroluminescence performance. New Journal of Chemistry 34(4) (2010): 699-707.

[35] Cao, X.Y., Liu, X.H., Zhou, X.H., Zhang, Y., Jiang, Y., Cao, Y., Cui, Y.X., and Pei, J. Giant extended π-conjugated dendrimers containing the 10,15-dihydro-5H-diindeno[1,2-a;1′,2′-c]fluorene chromophore: Synthesis, NMR behaviors, optical properties, and electroluminescence. Journal of Organic Chemistry 69(18) (2004): 6050-6058.

[36] Yuan, M.S., Liu, Z.Q., and Fang, Q. Donor-and-acceptor substituted truxenes as multifunctional fluorescent probes. Journal of Organic Chemistry 72(21) (2007): 7915-7922.

[37] Sam-ang, P., Raksasorn, D., Sukwattanasinitt, M., and Rashatasakhon, P. A nitroaromatic fluorescence sensor from a novel tripyrenyl truxene. RSC Advances 4(101) (2014): 58077-58082.

[38] Ning, Z., Zhang, Q., Pei, H., Luan, J., Lu, C., Cui, Y., and Tian, H. Photovoltage improvement for dye-sensitized solar cells via cone-shaped structural design. Journal of Physical Chemistry C 113(23) (2009): 10307-10313.

[39] Earmrattana, N., Sukwattanasinitt, M., and Rashatasakhon, P. Water-soluble anionic fluorophores from truxene. Dyes and Pigments 93(1–3) (2012): 1428-1433.

[40] Raksasorn, D., Namuangruk, S., Prachumrak, N., Sudyoadsuk, T., Promarak, V., Sukwattanasinitt, M., and Rashatasakhon, P. Synthesis and characterization of hole-transporting star-shaped carbazolyl truxene derivatives. RSC Advances 5(89) (2015): 72841-72848.

[41] Yang, C.-H., Guo, T.-F., and Sun, I.W. Highly efficient greenish blue-emitting organic diodes based on pyrene derivatives. Journal of Luminescence 124(1) (2007): 93-98.

[42] Moorthy, J.N., Natarajan, P., Venkatakrishnan, P., Huang, D.-F., and Chow, T.J. Steric Inhibition of π-Stacking: 1,3,6,8-Tetraarylpyrenes as Efficient Blue Emitters in Organic Light Emitting Diodes (OLEDs). Organic Letters 9(25) (2007): 5215-5218.

[43] Yang, Z., Xu, B., He, J., Xue, L., Guo, Q., Xia, H., and Tian, W. Solution-processable and thermal-stable triphenylamine-based dendrimers with truxene cores as hole-transporting materials for organic light-emitting devices. Organic Electronics 10(5) (2009): 954-959.

[44] Sudyoadsuk, T., Moonsin, P., Prachumrak, N., Namuangruk, S., Jungsuttiwong, S., Keawin, T., and Promarak, V. Carbazole dendrimers containing oligoarylfluorene cores as solution-processed hole-transporting non-doped emitters for efficient pure red, green, blue and white organic light-emitting diodes. Polymer Chemistry 5(13) (2014): 3982-3993.

[45] Nguyen, Q.P., Baek, S.J., Kim, M.J., Shin, N.Y., Kim, G.W., Choe, D.C., Kwon, J.H., and Chai, K.Y. Novel hole transporting materials based on 4-(9H-carbazol-9-yl)triphenylamine derivatives for OLEDs. Molecules 19(9) (2014): 14247-56.

[46] Chercka, D., Yoo, S.-J., Baumgarten, M., Kim, J.-J., and Mullen, K. Pyrene based materials for exceptionally deep blue OLEDs. Journal of Materials Chemistry C 2(43) (2014): 9083-9086.

[47] Williams, A.T.R., Winfield, S.A., and Miller, J.N. Relative fluorescence quantum yields using a computer-controlled luminescence spectrometer. Analyst 108(1290) (1983): 1067-1071.

[48] Yuan, M.-S., Fang, Q., Liu, Z.-Q., Guo, J.-P., Chen, H.-Y., Yu, W.-T., Xue, G., and Liu, D.-S. Acceptor or Donor (Diaryl B or N) Substituted Octupolar Truxene: Synthesis, Structure, and Charge-Transfer-Enhanced Fluorescence. The Journal of Organic Chemistry 71(20) (2006): 7858-7861.

[49] Goubard, F. and Dumur, F. Truxene: a promising scaffold for future materials. RSC Advances 5(5) (2015): 3521-3551.

[50] Kunz, K., Scholz, U., and Ganzer, D. Renaissance of Ullmann and Goldberg Reactions - Progress in Copper Catalyzed CN, CO and C-S-Coupling. Synlett (15) (2003): 2428-2439.

[51] Thornton, W.A. Spectral sensitivities of the normal human visual system, color-matching functions and their principles, and how and why the two sets should coincide. Color Research & Application 24(2) (1999): 139-156.

[52] Poynton, C.A. Digital Video and HDTV: Algorithms and Interfaces. Morgan Kaufmann Publishers, 2003.

[53] Wright, W.D. A re-determination of the trichromatic coefficients of the spectral colours. Transactions of the Optical Society 30(4) (1929): 141.

[54] Guild, J. The Colorimetric Properties of the Spectrum. Philosophical Transactions of the Royal Society of London A: Mathematical, Physical and Engineering Sciences 230(681-693) (1932): 149-187.

[55] Yuan, M.-S., Fang, Q., Zhang, Y.-R., and Wang, Q. Synthesis and photophysical properties of three (multi)branched planar molecules. Spectrochimica Acta Part A: Molecular and Biomolecular Spectroscopy 79(5) (2011): 1112-1115.

[56] Albota, M., Beljonne, D., Brédas, J.-L., Ehrlich, J.E., Fu, J.-Y., Heikal, A.A., Hess, S.E., Kogej, T., Levin, M.D., Marder, S.R., McCord-Maughon, D., Perry, J.W., Röckel, H., Rumi, M., Subramaniam, G., Webb, W.W., Wu, X.-L., and Xu, C. Design of Organic Molecules with Large Two-Photon Absorption Cross Sections. Science 281(5383) (1998): 1653-1656.

[57] Frisch, M.J., Trucks, G.W., Schlegel, H.B., Scuseria, G.E., Robb, M.A., Cheeseman, J.R., Scalmani, G., Barone, V., Mennucci, B., Petersson, G.A., Nakatsuji, H., Caricato, M., Li, X., Hratchian, H.P., Izmaylov, A.F., Bloino, J., Zheng, G., Sonnenberg, J.L., Hada, M., Ehara, M., Toyota, K., Fukuda, R., Hasegawa, J., Ishida, M., Nakajima, T., Honda, Y., Kitao, O., Nakai, H., Vreven, T., Montgomery Jr., J.A., Peralta, J.E., Ogliaro, F., Bearpark, M.J., Heyd, J., Brothers, E.N., Kudin, K.N., Staroverov, V.N., Kobayashi, R., Normand, J., Raghavachari, K., Rendell, A.P., Burant, J.C., Iyengar, S.S., Tomasi, J., Cossi, M., Rega, N., Millam, N.J., Klene, M., Knox, J.E., Cross, J.B., Bakken, V., Adamo, C., Jaramillo, J., Gomperts, R., Stratmann, R.E., Yazyev, O., Austin, A.J., Cammi, R., Pomelli, C., Ochterski, J.W., Martin, R.L., Morokuma, K., Zakrzewski, V.G., Voth, G.A., Salvador, P., Dannenberg, J.J., Dapprich, S., Daniels, A.D., Farkas, Ö., Foresman, J.B., Ortiz, J.V., Cioslowski, J., and Fox, D.J. Gaussian 09. 2009, Gaussian, Inc.: Wallingford, CT, USA.

APPENDIX

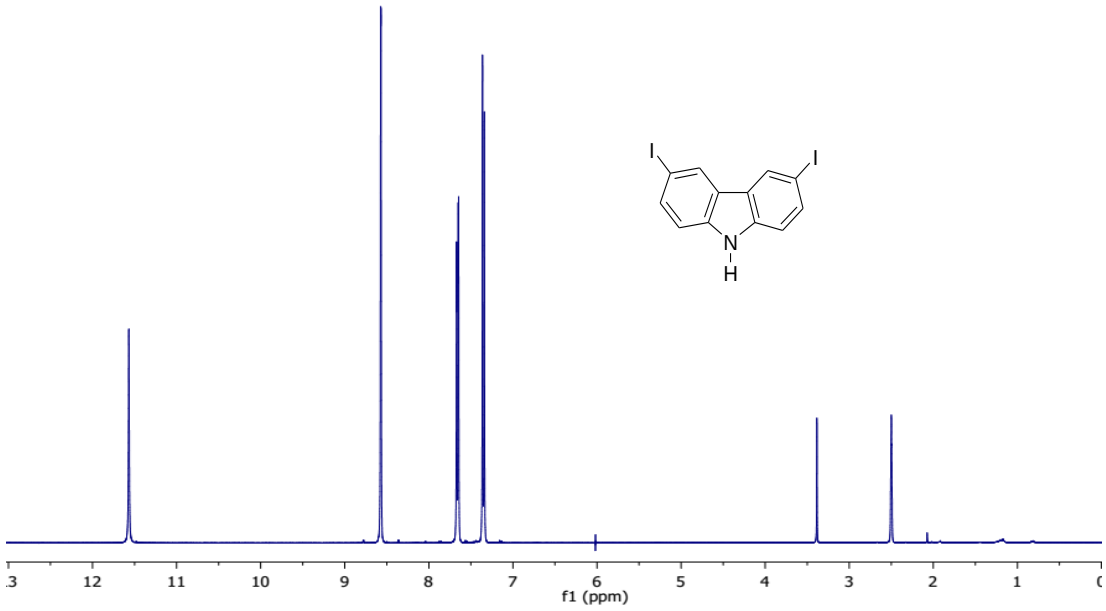

Figure A1. ^{1}H-NMR spectrum of 3,6-diiodo-9*H*-carbazole(**4**) in DMSO-d_6

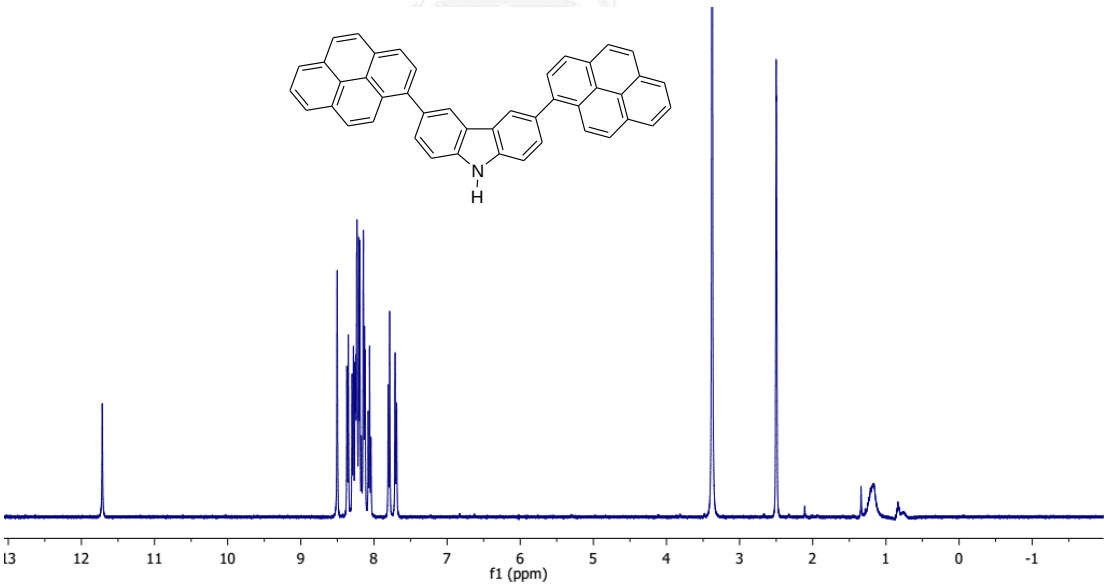

Figure A2. ^{1}H-NMR spectrum of 3,6-Di(pyren-1-yl)-9H-carbazole (**5**) in DMSO-d_6

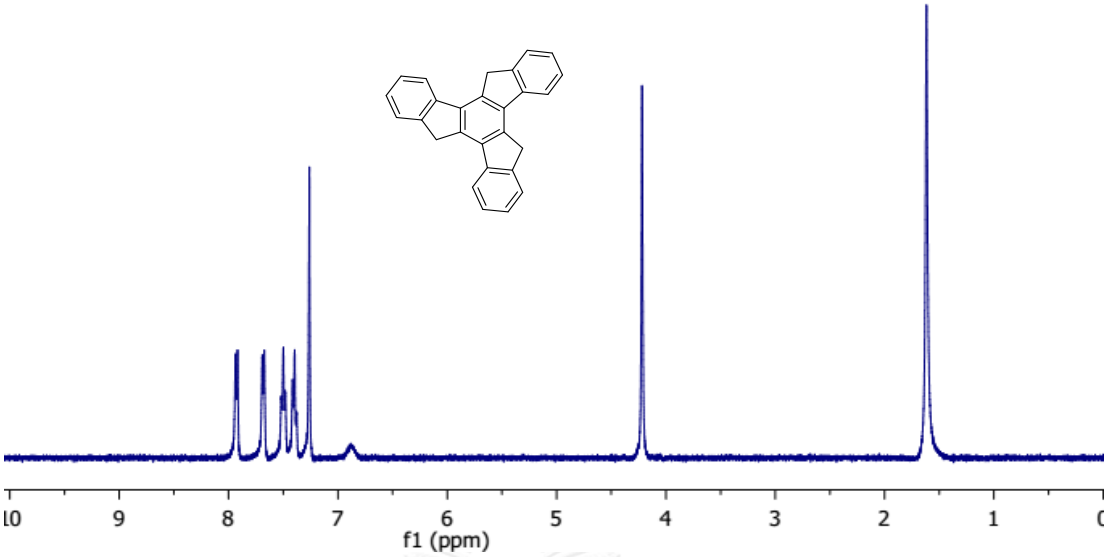

Figure A3. ^{1}H- NMR spectrum of truxene (**6**) in $CDCl_3$

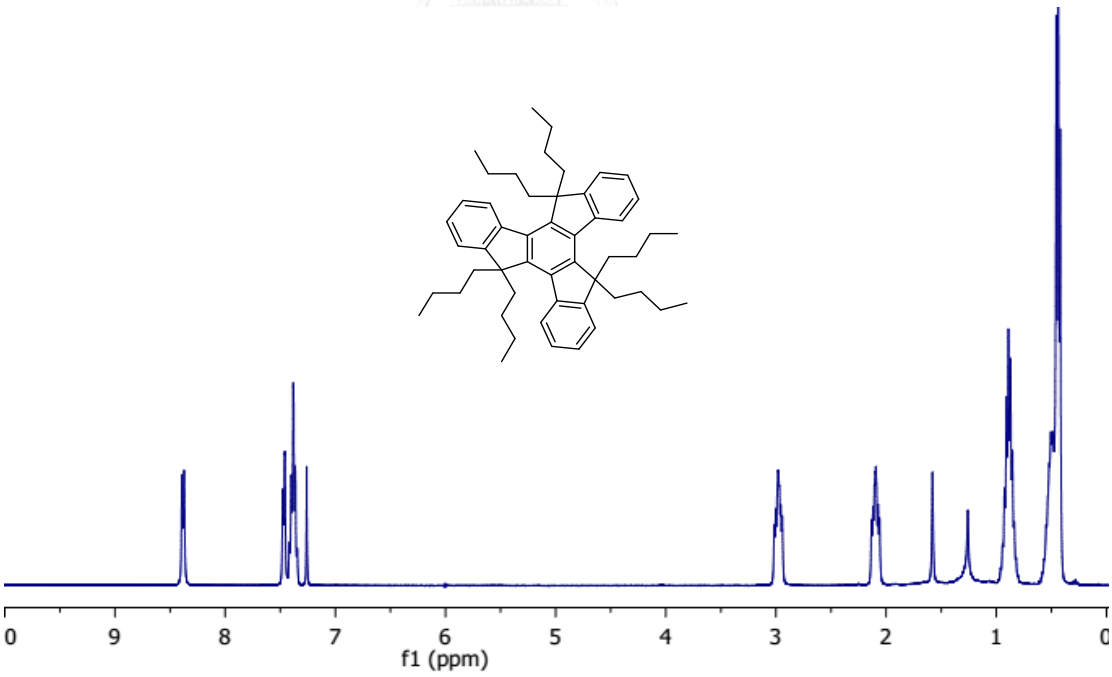

Figure A4. ^{1}H- NMR spectrum of 5,5,10,10,15,15-Hexabutyl-truxene (**7**) in $CDCl_3$

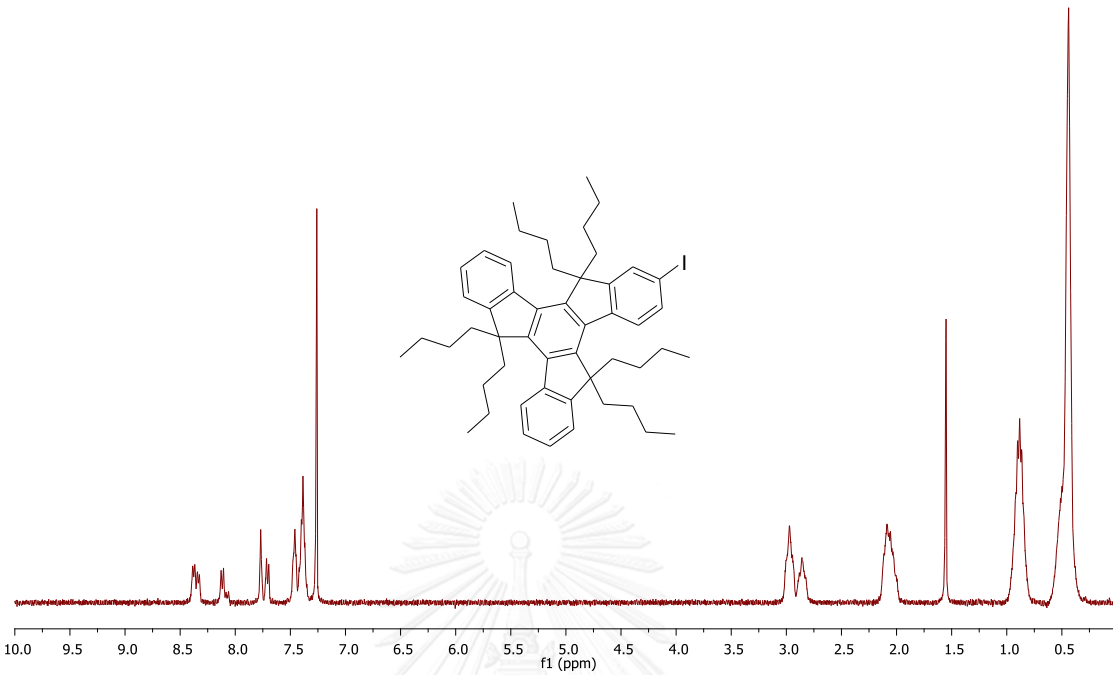

Figure A5. ^{1}H- NMR spectrum of 5,5,10,10,15,15-Hexabutyl-2-iodo-truxene (**8**) in $CDCl_3$

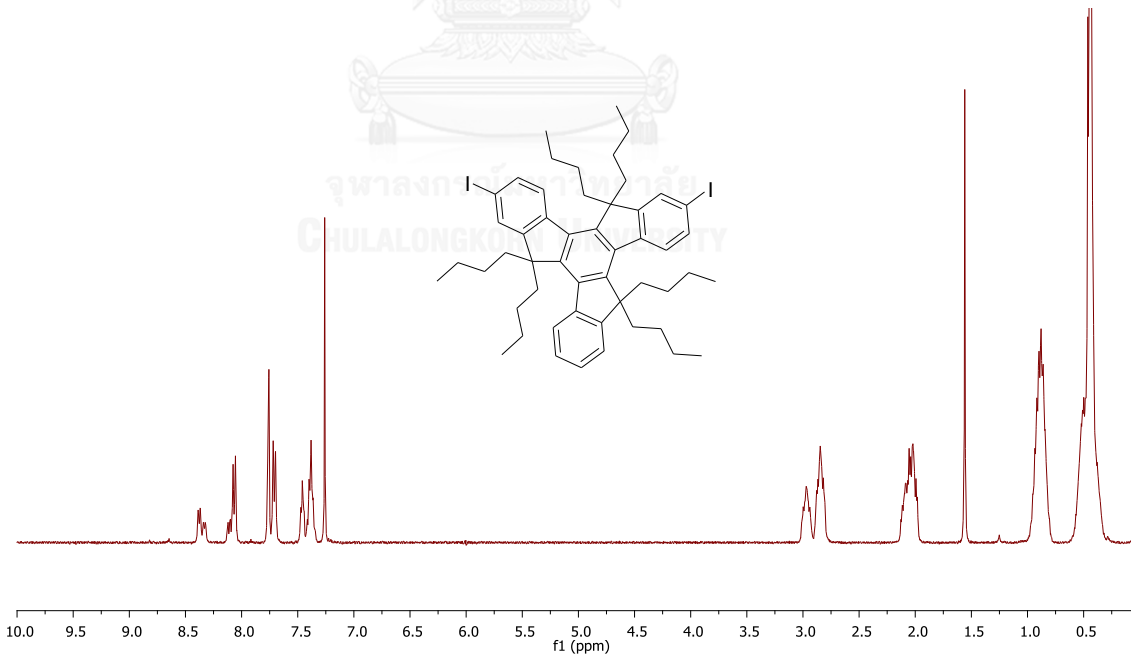

Figure A6. ^{1}H- NMR spectrum of 5,5,10,10,15,15-Hexabutyl-2,7-diiodo-truxene (**9**) in $CDCl_3$

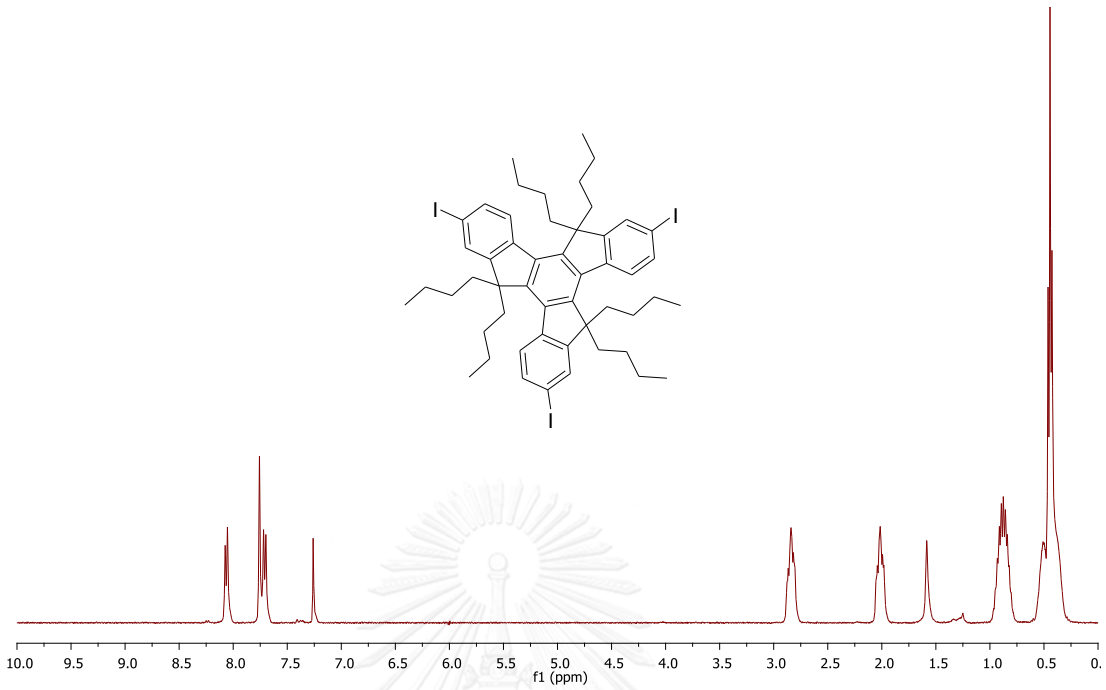

Figure A7. ^{1}H- NMR of 5,5,10,10,15,15-Hexabutyl-2,7,12-triiodo-truxene (**10**) in $CDCl_3$

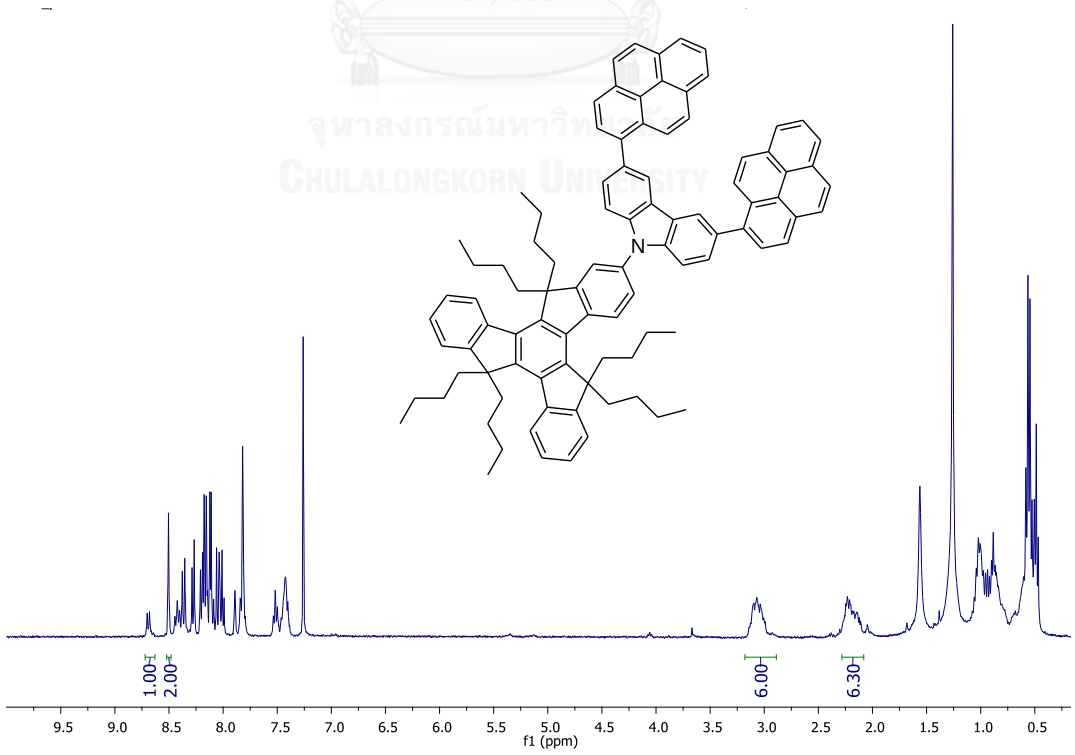

Figure A8. ^{1}H- NMR spectrum of compound **1** in $CDCl_3$

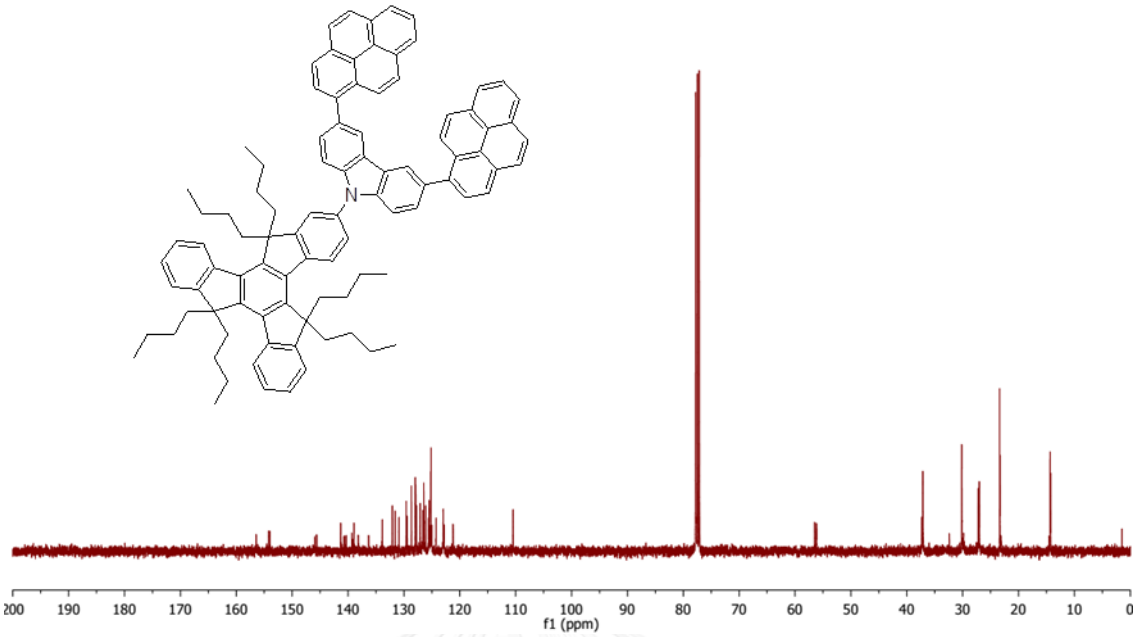

Figure A9. ^{13}C-NMR spectrum of compound **1** in $CDCl_3$

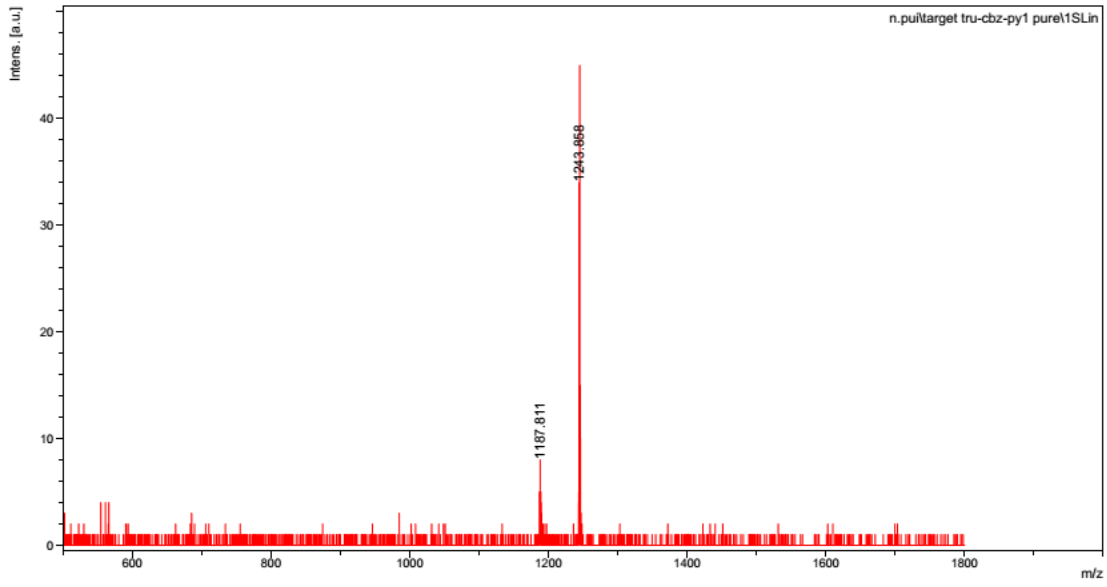

Figure A10. MALDI-TOF spectrum of compound **1**

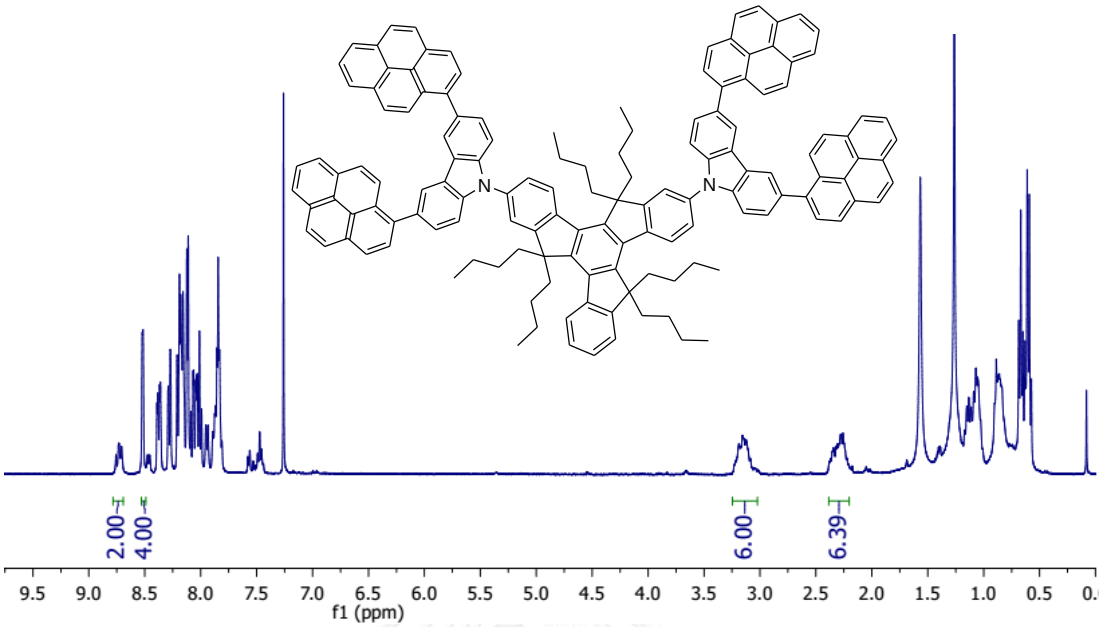

Figure A11. ^{1}H- NMR spectrum of compound **2** in $CDCl_3$

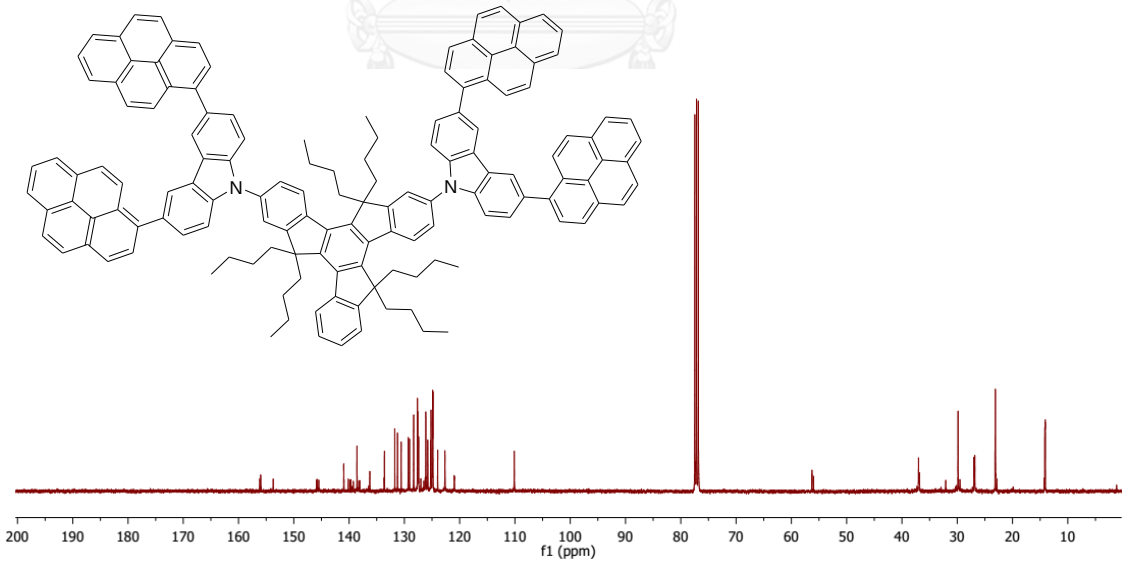

Figure A12. ^{13}C-NMR spectrum of compound **2** in $CDCl_3$

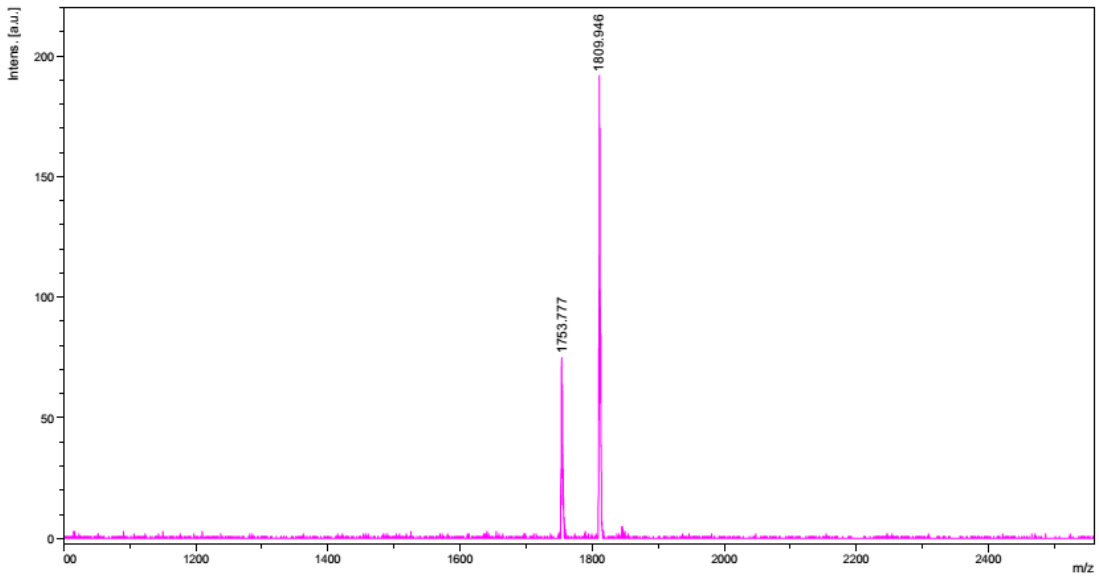

Figure A13. MALDI-TOF spectrum of compound **2**

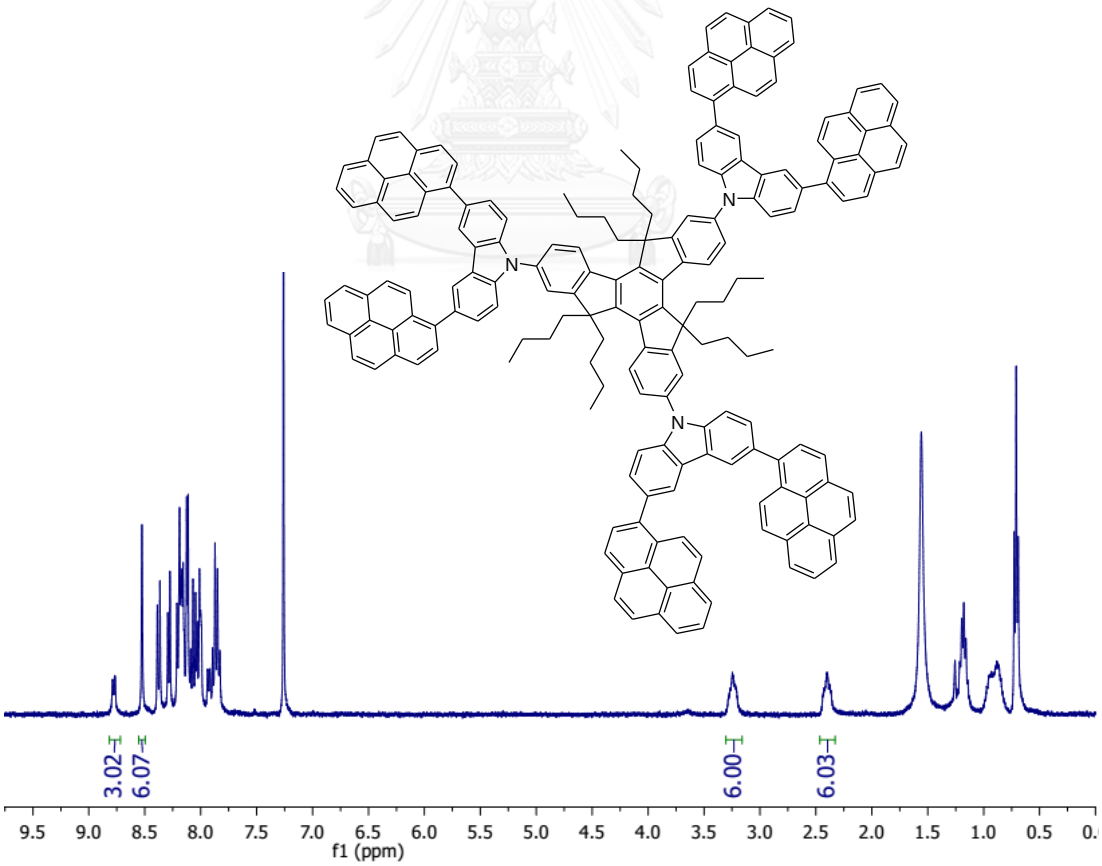

Figure A14. ^{1}H- NMR spectrum of compound **3** in $CDCl_3$

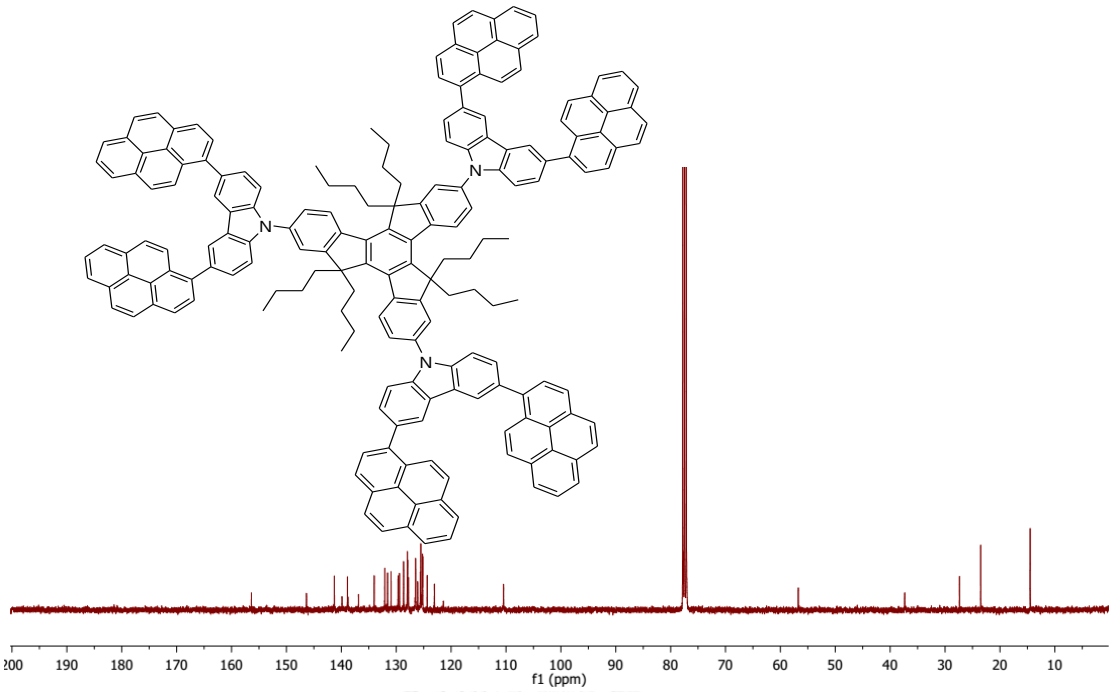

Figure A15. ^{13}C-NMR spectrum of compound **3** in $CDCl_3$

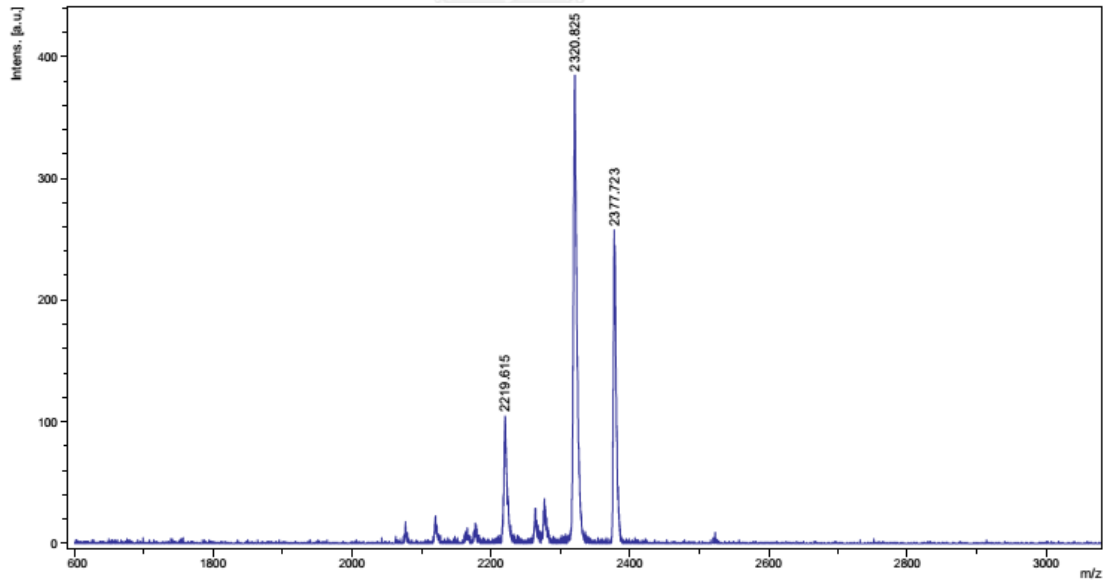

Figure A16. MALDI-TOF spectrum of compound **3**

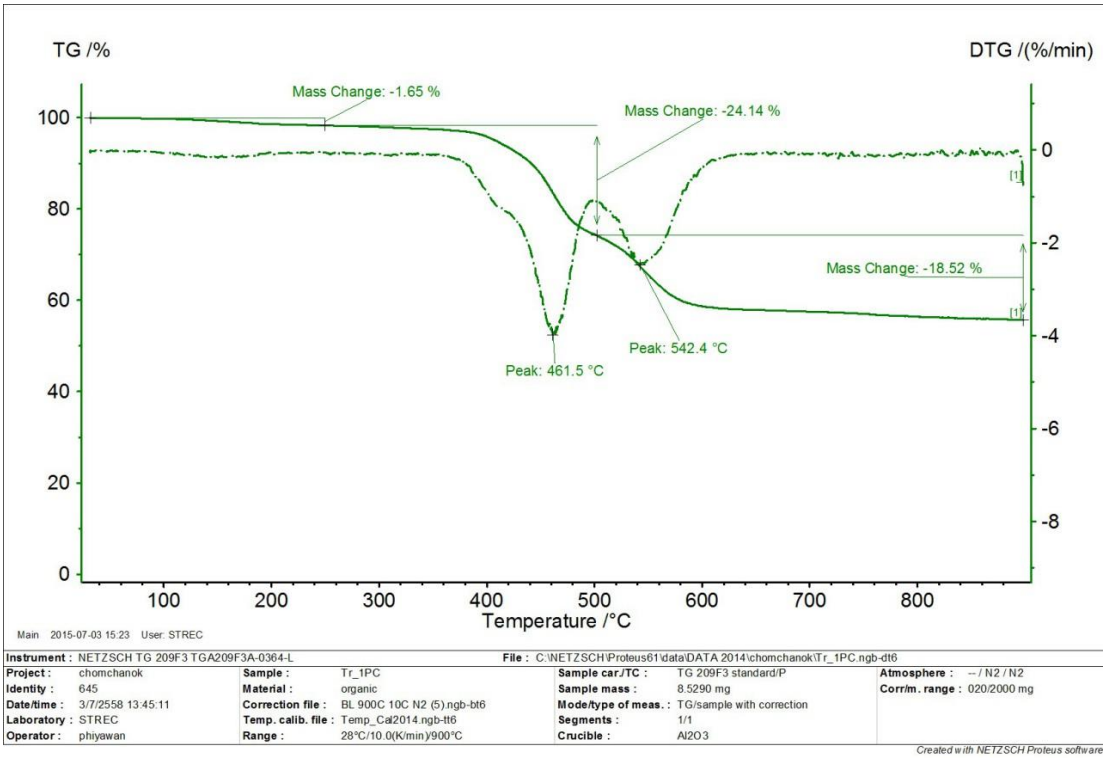

Figure A17. TGA spectrum of compound **1**

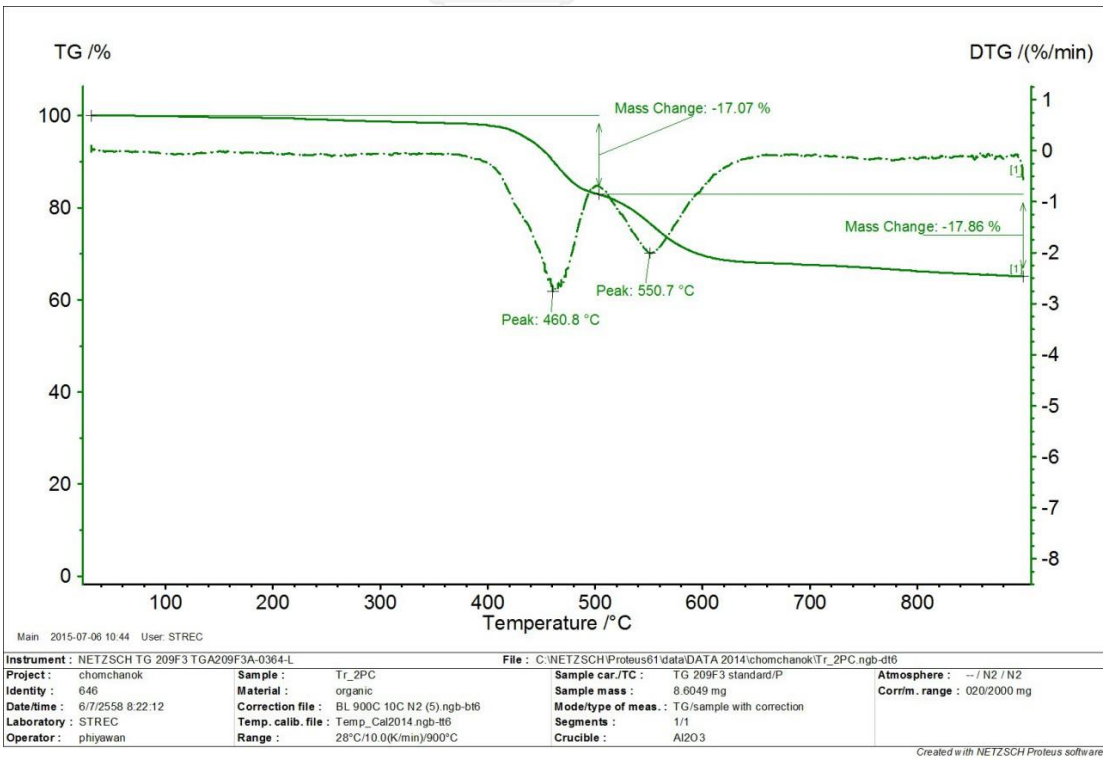

Figure A18. TGA spectrum of compound **2**

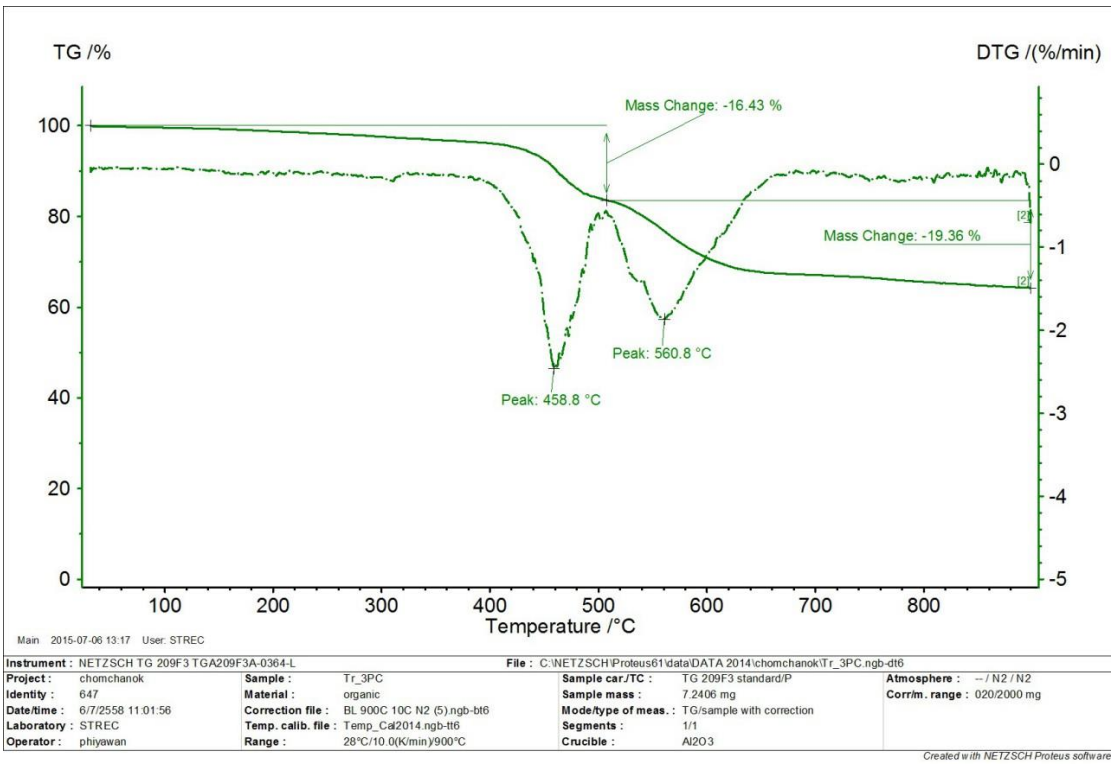

Figure A19. TGA spectrum of compound **3**

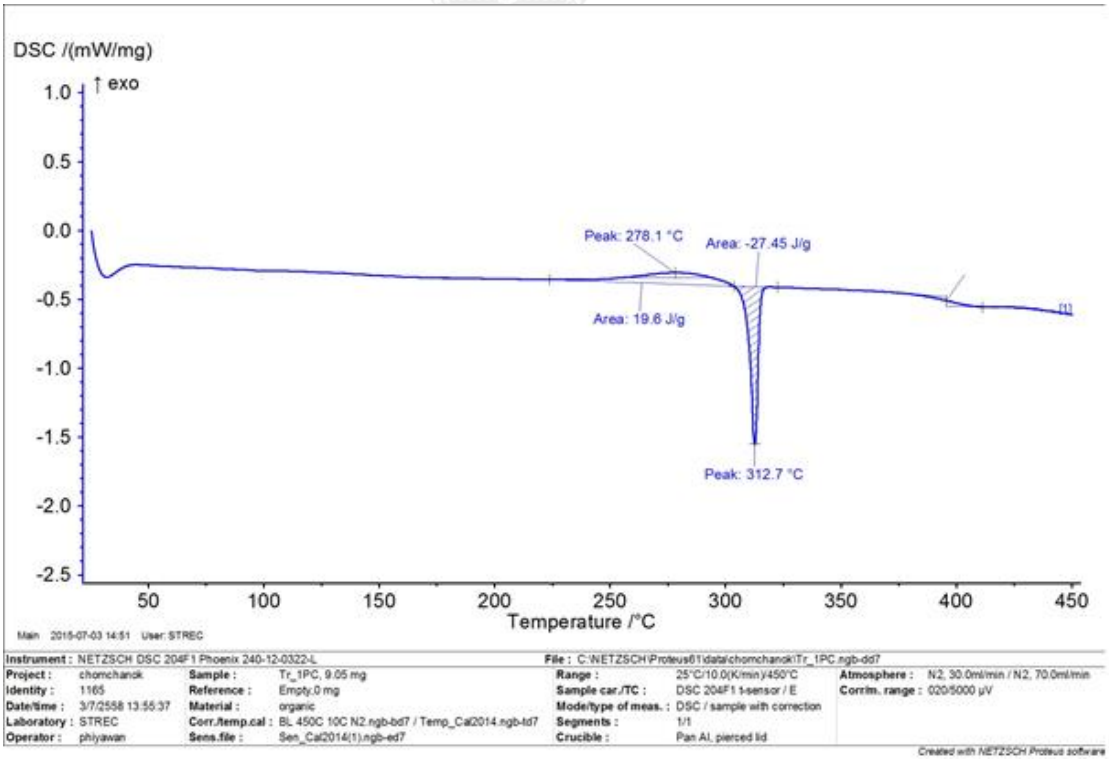

Figure A20. DSC spectrum of compound **1**

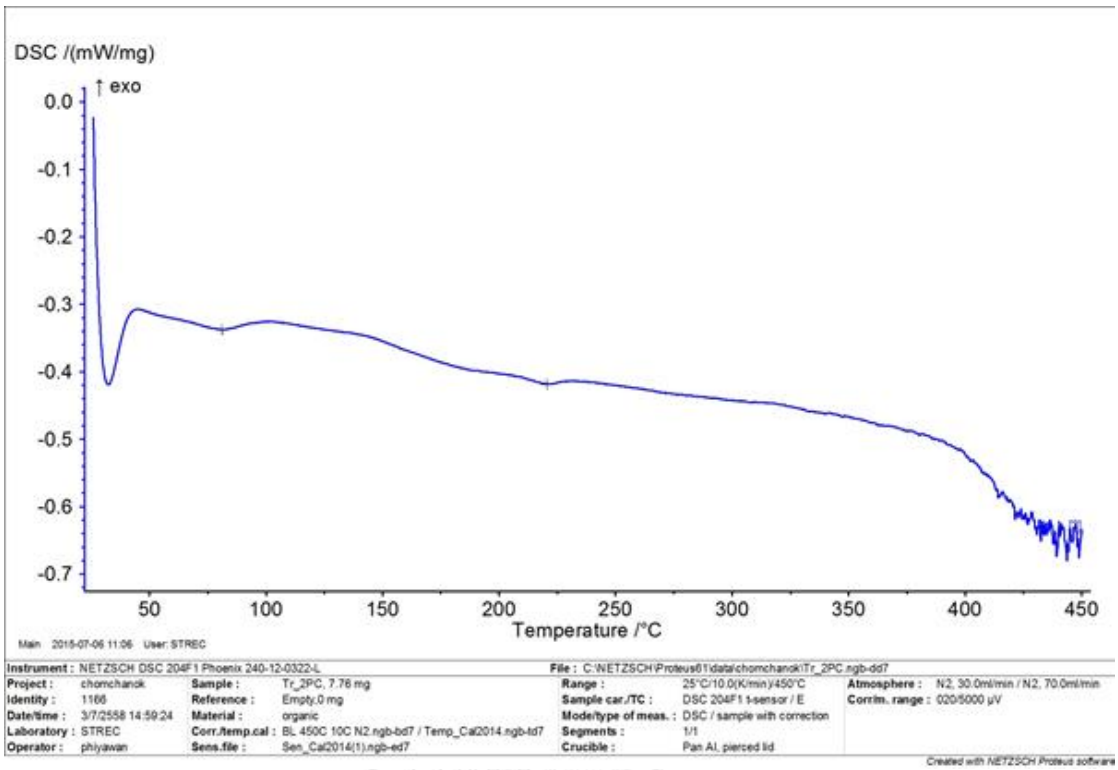

Figure A21. DSC spectrum of compound **2**

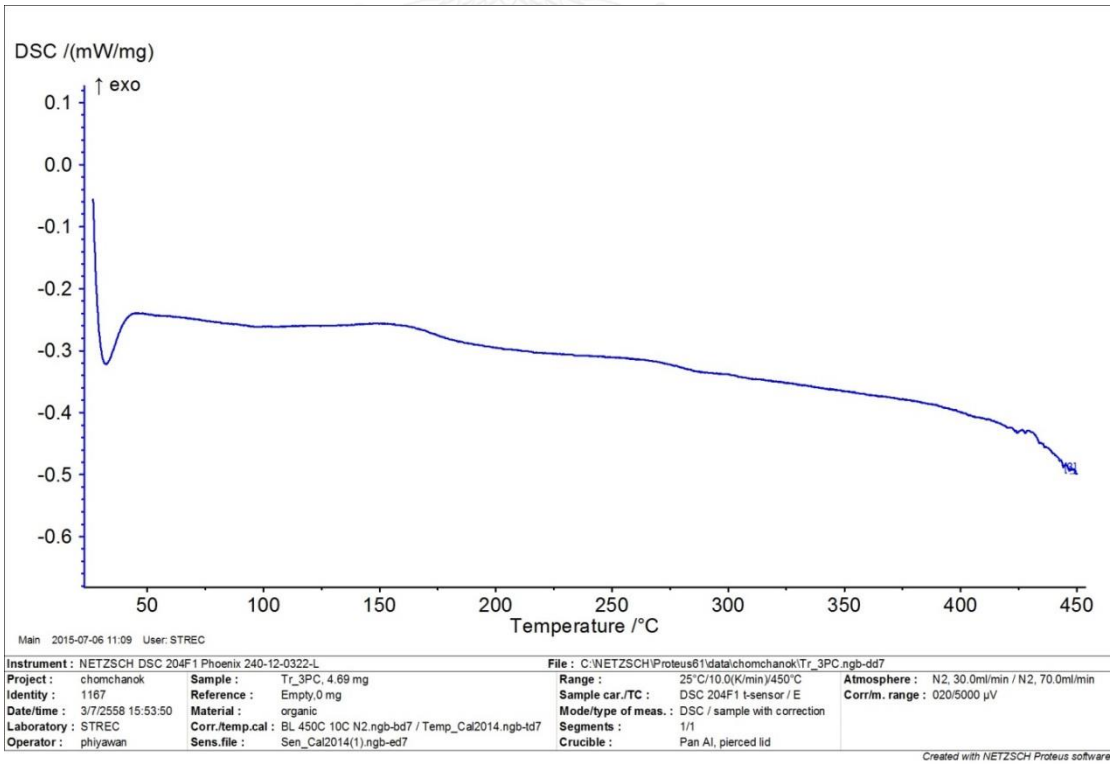

Figure A22. DSC spectrum of compound **3**

VITA

Miss Chomchanok Wongsilarat was born on August 7th, 1987 in Narathiwat province, Thailand. She was finished her high school from Debsirinromklao school at Bangkok in 2005. In 2009, she graduated her Bachelor's degree of Science, major of chemistry from King Mongkut's Institute of Technology Ladkrabang. In 2012, she continues her master's degree of Science Program of Petrochemistry and Polymer Science from Chulalongkorn University. During her master course, he joined Material Advancement and Proficient Synthesis (MAPS) GROUP under of supervision of Assoc. Prof. Dr. Paitoon Rashatasakhon. Her present address is 88/145 Onnuch 46 road, Suanluang, Bangkok, 10250. To contact her, please call 0804498877 or send e-mail: pui_14997@hotmail.com.